



**NATIONAL TECHNICAL UNIVERSITY OF ATHENS  
SCHOOL OF NAVAL ARCHITECTURE AND MARINE ENGINEERING  
DIVISION OF MARINE ENGINEERING**

## **Diploma Thesis**

**Dynamic intermediate bearing positioning for optimal shaft  
alignment under varying propeller hydrodynamic loads**

**Ioannidis Ioannis**

**Thesis Committee:**

**Supervisor: C. I. Papadopoulos, Associate Professor NTUA**

**Members: G. Dimopoulos, Associate Professor NTUA**

**G. Papalambrou, Associate Professor NTUA**

**Athens, June 2024**

## Table of contents

Table of contents.....	2
Acknowledgements.....	5
Abstract.....	6
List of tables.....	7
List of figures.....	8
1) Introduction.....	10
1.1) Shafting system description.....	10
1.2) Evolution of shaft alignment process.....	11
1.3) Current challenges associated with shaft alignment.....	11
2) Shaft alignment process (at design office).....	14
2.1) Chapters of Shaft Alignment Calculation Plan.....	15
2.2) Reaction Influence Numbers and Sensitivity Index.....	16
2.2.1) Reaction Influence Numbers.....	16
2.2.2) Sensitivity Index.....	16
2.3) Static and dynamic condition.....	17
2.4) Aft Stern Tube Bearing (ASTB).....	18
2.4.1) Supporting point.....	18
2.4.2) Misalignment angle.....	19
2.5) Crankshaft equivalent model.....	20
2.5.1) Number of modeled main engine bearings.....	20
2.5.2) Equivalent diameter of crankshaft bar.....	20
2.6) Class notations regarding the shafting system.....	21
2.6.1) TMON and TCM notations.....	21
2.6.2) ESA and Shaft Align notations.....	22
2.7) Propeller moment during running condition (dynamic).....	23
2.7.1) Shipyards' practice (from NTUA plan database).....	23
2.7.2) Statistical approach of research paper [25].....	27
3) Shaft alignment process (in shipyard).....	28
3.1) Gap & Sag values.....	29
3.2) Procedures of measuring bearing loads.....	30
3.2.1) Jack-up test.....	30
3.2.2) Strain gauge measurement.....	32

4) Shaft alignment related topics & Literature overview.....	34
4.1) Bearing damages.....	34
4.2) Propeller hydrodynamic loads .....	38
4.2.1) Propeller loads during straight ahead course .....	39
4.2.2) Propeller loads during maneuvering.....	40
4.2.3) Experimental and numerical studies of propeller hydrodynamic forces in relation to shafting system.....	42
4.2.4) Propeller loads during partial propeller immersion.....	45
5) Numerical modeling & utilized software .....	48
5.1) Shaft alignment tool.....	48
5.2) Bearing hydrodynamic lubrication theory and tool.....	50
5.2.1) Journal bearings .....	50
5.2.2) Principles of hydrodynamic lubrication .....	50
5.2.3) Operational and Performance Parameters.....	53
5.2.3) Bearing hydrodynamic lubrication tool.....	54
5.3) Hull deflection calculation tool .....	57
5.3.1) 1D FEM for calculating hull deflections in marine industry .....	57
5.3.2) 1D methods for calculating hull deflections .....	58
5.3.3) Solving the 1D equations .....	59
5.3.4) Hull deflection calculation model for case study ship & tool .....	62
6) Case study .....	71
6.1) Principal particulars of the studied vessel and operational conditions.....	71
6.2) Input data for Shaft Alignment Tool .....	73
6.2.1) Segment properties.....	73
6.2.2) External Loads .....	75
6.3) Shaft Alignment Booklet compared to Shaft Alignment Tool Software (NTUA).....	76
6.3.1) Influence factors .....	76
6.3.2) Bearing reactions .....	77
6.3.3) Shaft slope at ASTB .....	77
6.4) Need for intermediate bearing actuation.....	79
6.4 a) Designed draft running condition .....	80
6.4 b,c,d) Partially immersed propeller running conditions.....	82
6.4 e,f) Hull deflection max & min during running conditions.....	85
6.5) Implementation of intermediate bearing actuation.....	88

6.5.1) Search for ISB line of movement.....	88
6.5.2) Application of ISB line of movement.....	93
6.5.3) Extend of line of movement.....	97
6.6) Possible ISB actuation applications.....	98
6.6.1) ASTB temperature rise .....	98
6.6.2) Optimal static positioning depending the loading condition.....	99
6.7) Concept design of actuation mechanism for simulations on a scaled Test-rig.....	100
7) Conclusions and future work suggestions .....	102
Literature - References.....	104
Appendix A: Case study ship, resistance calculation for propeller partially immersion conditions	107
Appendix B: Tables of bearings loading ( $p/p_{\max}$ ), without and with ISB actuation for each examined scenario .....	110

## Acknowledgements

By completing my diploma thesis I would like to express my heartfelt gratitude to the following people:

First and foremost, I am deeply thankful to my family for their abundant love, caring and support throughout all these years, their sacrifices for educating me and for believing in me relentlessly.

I extend my sincere appreciation to my thesis advisor, Associate Professor Christos Papadopoulos, for the opportunity he gave me to explore the field of shaft alignment, which greatly interests me. His invaluable guidance, motivation and insightful comments have been instrumental in the completion of this work.

Special Thanks goes to PhD Candidate George Rossopoulos for his vital assistance, encouragement, thoughtful comments and exceptional cooperation during the entire thesis process.

Moreover, I would like to thank those remarkable people in the maritime industry for their advice, mentoring and opportunities they have provided me.

Last but surely not least, I express my deepest gratitude to my girlfriend for her unwavering support and encouragement and to my friends and fellow classmates for the shared experiences during the past five years.

## Abstract

As every mechanical system onboard a vessel, the shafting system has to be studied, optimized and verified according to existing rules. Shaft alignment is a process which at most cases refers to static conditions of the vessel, as per pertinent rules of classification societies. However, given that ship designs have changed over the last years, there are reported cases of vessels which, even though they meet current shaft alignment related requirements, may face unfavorable conditions, causing unacceptable load distribution on the bearings during their lifecycle. This is especially noticeable at shaft alignment sensitive ships (i.e. those with a single stern tube bearing), emphasizing the importance of considering also running conditions except from static conditions for a more comprehensive alignment evaluation. Recent literature emphasizes the substantial impact of propeller hydrodynamic forces on the shafting system, highlighting the necessity of their inclusion in elastic shaft alignment calculation, as is one of the major sources affecting shaft-bearing loading. For this reason, the primary goals of this thesis are to study the range of propeller hydrodynamic loads for a number of operational cases (straight ahead course at designed and ballast drafts, maneuvering) and evaluate the impact of extreme hull deflections due each loading condition and to determine how the shafting system responds to those loads. Furthermore, a motion control (actuation) mechanism is determined and examined for the intermediate shaft bearing for a case study ship, with focus on optimizing its position through specific adjustments, in order to completely eliminate bearing over or unloading and establish safe shafting system conditions, acceptable by IACS class rules. Moreover, hull deflections will be calculated through a simplified 1D calculation method. The concept of intermediate shaft bearing actuation is originated from the proposed future-works deriving from the i-MARINE [1] project.

## List of tables

Table 1: Hydrodynamic propeller loads based on results from CFD database.....	22
Table 2: Vertical bending moment expressed as % of nominal shaft torque from designs of NTUA database .....	23
Table 3: Data from plans containing information regarding propeller hydrodynamic loads .....	25
Table 4: Hydrodynamic loads (steady components) on single-screw ship propeller for shaft alignment and shaft vibration calculations as a percentage of the mean thrust $P_x$ and mean torque $M_x$ .....	27
Table 5: Common types and short description of bearing damages.....	35
Table 6: Mean values of hydrodynamic forces [18] .....	42
Table 7: Propeller Lateral forces and moments for starboard and port turn.....	43
Table 8: Relative and initial bearing offsets for examining intermediate bearing actuation .....	69
Table 9: Principal particulars of the case study vessel .....	71
Table 10: Shafting particulars of the case study vessel .....	71
Table 11: Longitudinal position and vertical offsets of bearings.....	72
Table 12: Operating conditions analyzed in booklet .....	73
Table 13: Geometric data of the propulsion shaft of case study vessel.....	73
Table 14: Propeller vertical load for immersion conditions .....	76
Table 15: Rest of vertical loads.....	76
Table 16: Comparison of influence factors (1/2).....	76
Table 17: Comparison of influence factors (2/2).....	76
Table 18: Comparison of bearing reaction forces .....	77
Table 19: Comparison of shaft slope .....	77
Table 20: Limits of propeller hydrodynamic load range.....	80
Table 21: Ballast conditions from Loading - Unloading Sequence booklet .....	82
Table 22: Results of Appendix A.....	83
Table 23: Conditions for ballast simulations .....	83
Table 24: Bearing Offsets calculated with Euler-Bernoulli method.....	85
Table 25: Relative Bearing Offsets calculated with Timoshenko method .....	87
Table 26: Legend for following diagrams .....	89
Table 27: Actual supporting position of ASTB for $M_z=211.746$ kNm, iterative process .....	93
Table 28: Length on line of movement for each condition .....	97
Table 29: Input parameters for resistance calculation method .....	107
Table 30: Hydrostatic characteristics of vessel for examined drafts .....	107
Table 31: Resistance components and EHP force .....	108
Table 32: Values for $M_z$ calculation.....	109

## List of figures

Figure 1: Typical propulsion system arrangement of a cargo vessel .....	10
Figure 2: Design with only one stern tube bearing [7] .....	12
Figure 3: Single and Multi bearing support of ASTB [9] .....	18
Figure 4: Realistic distribution of ASTB reaction force [14] .....	19
Figure 5: Misalignment angle (left) and double slope bearing (right) .....	19
Figure 6: FE model of crankshaft (a) and circular bar model (b) [21] .....	21
Figure 7: Percentages of positive bending moments of available plans.....	24
Figure 8: Assembly of shafting during second phase of alignment [20] .....	28
Figure 9: Flange arrangement in gap & sag analysis [20] .....	29
Figure 10 Shafting bearing jacking and schematic arrangement [22] .....	30
Figure 11: Typical bearing jacking diagram (plot of shaft lift versus jack load) [22] .....	31
Figure 12: Strain gauge technique for measuring bending moments [21] .....	33
Figure 13: Root cause investigation for Bulk Carriers and Containerships [29].....	34
Figure 14: Thermal wipe damage (left), fatigue damage (right) [22] .....	36
Figure 15: Propeller load components.....	38
Figure 16: Bending moment due to hydrodynamic propeller forces in the straight run condition [21] .....	39
Figure 17: Nominal wake distribution at the propeller disc during straight run [11] .....	39
Figure 18: Velocity triangle for a blade section .....	40
Figure 19: Nominal wake distribution at the propeller disc during port turn (left) and starboard turn (right) [11].....	41
Figure 20: Shaft line's deflection measurements in vertical plane [19].....	42
Figure 21: Shaft line's deflection measurements in transverse plane [36].....	43
Figure 22: Intermediate bearing load depending rudder angle and ME rpm [8] .....	44
Figure 23: Bearing loads redistribution during vessel maneuvering through reverse calculation [8] .....	45
Figure 24: Location of thrust eccentricity with respect to submergence ratio and advance coefficient [37] ..	47
Figure 25: Thrust and bending moment coefficient for different h/R and J values of POW test [37] .....	47
Figure 26: Shaft alignment tool workspace .....	48
Figure 27: Beam properties of a segment and Influence factors table .....	49
Figure 28: Analysis results.....	49
Figure 29: Cross section of a typical bearing geometry .....	50
Figure 30: Un-warped bearing geometry.....	51
Figure 31: Converging geometry of journal bearing .....	51
Figure 32: Boundary conditions for the oil film .....	53
Figure 33: Generated plots of pressure field (left) and film thickness (right).....	56
Figure 34: Hull deflections of stern section [20] .....	57
Figure 35: Cantilever loading and boundary conditions, simulating engine room and stern construction.....	62
Figure 36: User Interface of Inertia Calculator tool and required procedure [40] .....	63
Figure 37: Frame parts from the 3 construction plans .....	63
Figure 38: Process of measurement .....	64
Figure 39: Profile view of engine room of case study ship and frames measured .....	64
Figure 40: Measured second moment of area.....	65
Figure 41: Measured shear area .....	65
Figure 42: Shear Force points from Loading Manual interpolated by spline.....	66
Figure 43: First derivative of shear force spline giving distributed load .....	66
Figure 44: Hull deflection curves with Euler-Bernoulli method.....	67
Figure 45: Hull deflection curves with Timoshenko method .....	67
Figure 46: Relative hull deflections for I min, mean, max with Euler-Bernoulli method (up) and with Timoshenko method (down) .....	68

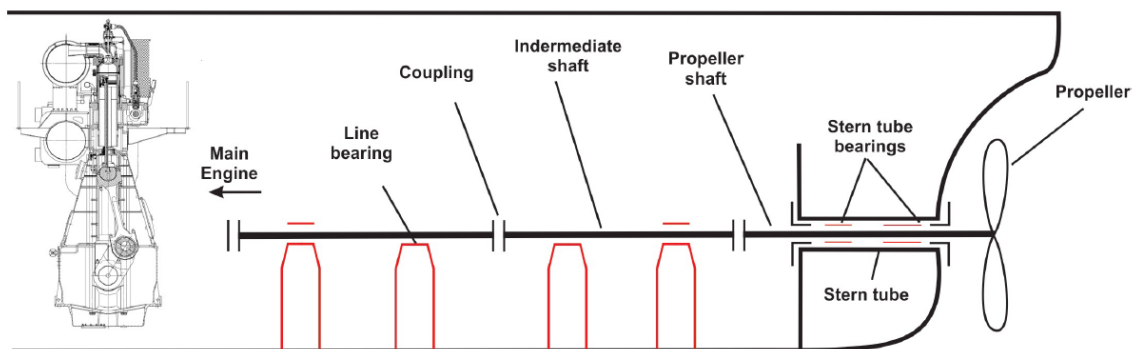


Figure 47: Calculated hull deflections envelope compared to available data .....	69
Figure 48: Relative and initial bearing offsets.....	70
Figure 49: Case study shaft equivalent 1D FEM model and shaft deflection curve for static condition .....	75
Figure 50: Allowable Propeller Loads Diagram for case study ship .....	78
Figure 51: Application of Mz in Shaft Alignment Tool .....	80
Figure 52: Behavior of shafting system under examined propeller hydrodynamic load range .....	81
Figure 53: Convention of propeller immersion ratio .....	82
Figure 54: Behavior of shafting system under examined propeller hydrodynamic load range, $T_M=3.476$ m... 84	84
Figure 55: Behavior of shafting system under examined propeller hydrodynamic load range, $T_M=4.8$ m..... 84	84
Figure 56: Shaft lines (running condition) for Euler-Bernoulli method's HD, min (up) max (bottom)..... 85	85
Figure 57: Behavior of shafting system under examined propeller hydrodynamic load range for HD min calculated with E-B method..... 86	86
Figure 58: Behavior of shafting system under examined propeller hydrodynamic load range for HD max calculated with E-B method..... 86	86
Figure 59: Shaft lines (running condition) for Timoshenko method's HD, min (up) max (bottom)..... 87	87
Figure 60: Behavior of shafting system under examined propeller hydrodynamic load range for HD min calculated with Timoshenko method .....	87
Figure 61: Behavior of shafting system under examined propeller hydrodynamic load range for HD max calculated with Timoshenko method .....	88
Figure 62: Selected area for examination.....	89
Figure 63: Possible positions of ISB for different Mz for achieving acceptable reaction forces..... 91	91
Figure 64: Plotted line of movement (Slope has been exaggerated for clarity) .....	92
Figure 65: Intersection of selected line with examined region, showing all acceptable and marginal positions .....	92
Figure 66: Behavior of shafting system under examined propeller hydrodynamic load range with ISB actuation.....	93
Figure 67: Shaft lines cases for varying propeller loads, while ISB placed optimally for each case on selected line .....	94
Figure 68: Behavior of shafting system under examined propeller hydrodynamic load range with ISB actuation $T_M=3.476$ m.....	95
Figure 69: Behavior of shafting system under examined propeller hydrodynamic load range with ISB actuation, $T_M=4.8$ m.....	95
Figure 70: Behavior of shafting system under examined propeller hydrodynamic load range with ISB actuation, HD max with Timoshenko method.....	96
Figure 71: Behavior of shafting system under examined propeller hydrodynamic load range with ISB actuation, HD min with Timoshenko method.....	96
Figure 72: Reaction forces while ISB moves on line of movement.....	9998
Figure 73: ISB optimal placement prior to departure depending the loading condition.....	99
Figure 74: Scaled Test-rig [1].....	100
Figure 75: Proposed configuration for ISB actuation for the testing rig.....	100

## 1) Introduction

### 1.1) Shafting system description

The primary objective of the shafting system (**Figure 1**) is to convert the rotative power output of the main engine (or engines) into thrust power, necessary for ship's propulsion. Except from the power transmission, the shafting system must also support the equipment's weight and loads, transmit thrust power to the ship's hull, operate vibration free, safely and reliably under all operating conditions with relatively low required maintenance [2] throughout the ship's lifecycle. It is also important to note that, unlike most onboard systems, a single-screw ship lacks redundancy in its mechanical system. Improper shaft alignment could lead to the lack of hydrodynamic lubrication and cause the rapid temperature rise, whipping or even melting the bearing liner material during maneuvering or other abnormal operations [3]. Furthermore, not achievement of aforementioned shaft alignment objectives can be manifested in the form of stern tube bearings, intermediate bearing or main engine bearing failures. In such instances, the ship may lose maneuverability, posing potential risks to the lives of the crew and causing disruptions to scheduled services, thereby impacting stakeholders. Therefore, the importance of conducting shaft alignment analysis is underscored by these considerations.



**Figure 1: Typical propulsion system arrangement of a cargo vessel**

The term *propulsion shafting* is given by ABS as:

*A system of revolving rods that transit torque and motion from the prime mover to the propeller. The shafting is supported by bearings, whose number and position is determined based on allowable bearing loads and lateral vibration (whirling) requirements. Static shafting alignment analysis criteria define the acceptable load distribution and contact condition between shafts and bearings.*

Bearings are classified into three types based on their application: journal bearings, ball bearings, and linear bearings. Journal bearings support the shaft designed to maintain the alignment of rotating parts and to transmit forces from these parts to the structure, so they are one of the most important parts of a ship's propulsion system. Therefore at the design stage, it is crucial to ensure that bearings and especially the aft stern tube bearing operate properly under the specified operational conditions.

There are five main factors that affect the propulsion system:

- Hull structure deflections, caused by loading condition and weather loads
- Thermal growth of the equipment and hull structures
- Excessive wear down of the stern tube bearing
- Propeller hydrodynamic loads due to thrust lateral and vertical eccentricity
- Tooth forces in case of geared installations (if applicable)

According to [4], the interaction between the main machinery and the environment is one of the most significant factors affecting the shafting system, potentially leading it to a failure.

### 1.2) Evolution of shaft alignment process

Before 1950, the straight alignment method involved aligning the centers of all support bearings along a single straight line when aligning shafts. This approach resulted in irregular load distribution among bearings. Since the late 1950s, the US Navy has recognized the significance of shaft alignment, prompting numerous studies in the late 1960s and early 1970s to establish practical guidelines for optimal bearing positioning. Notably, in 1959, based on extensive naval experience, a survey was conducted to evaluate design enhancements across various aspects, including fatigue, vibration, corrosion, and alignment of ship shafting systems. This survey underscored the critical role of shaft alignment in averting reduction gear damage attributable to misalignment.

Previous studies have highlighted the detrimental consequences of uneven bearing load distribution resulting from conventional straight alignment methods, which directly contribute to bearing damage such as overheating or excessive wear. However, research has shown that by appropriately adjusting vertically and axially the position of support bearings, a general trend in shaft alignment emerges. Specifically, studies indicate that as the number of support bearings decreases and consequently the distance between them increases, the impact of hull deformation on the shafting system diminishes, thereby enhancing system stability. These findings emphasize the efficiency and importance of curved alignment methods in achieving proper load distribution to shaft support bearings [5].

### 1.3) Current challenges associated with shaft alignment

Since the maritime industry is moving towards 2050 ships have to follow more efficient designs in order to align with the global goals of energy efficiency (i.e. EEDI) issued by International Maritime Organization (IMO). These new trends in design allow for increased cargo capacity by locating the main engine as aft as practicable to reduce engine room length and simultaneously make use of de-rated main engines running in lower RPMs matched with more efficient but heavier propellers combined usually with power energy saving devices [6]. At the same time scantling optimization and the use of high-tensile steel have made ship structure more flexible contributing to higher hull deflections while shafts' diameter and stiffness increases in order to meet the higher torque demands (higher power combined lower RPMs). All these trends have a substantial impact on one of the most crucial and complex mechanical system of a ship, the propulsion system.

Shipyards in a try to simplify shipbuilding concept and achieve higher shaft stability against hull deformation due to draft change, have adopted single stern tube bearing design (**Figure 2**)

(designs with only one stern tube bearing), meaning that forward stern tube bearing (FSTB) is removed [7], [8]. Consequently, particularly for modern oil tankers and bulk carriers, only the aft stern tube bearing is intended to support propulsion static and dynamic load and at the same time intermediate shaft bearing (ISB) is found to be sensitive to operational parameters. This design concept increases the risk of shaft and/or bearing damage due to the over-reliance on the aft stern tube bearing alone, which needs to support the overall weight of propeller and shafting system affected significantly by eccentric thrust forces as confirmed by several accident reports in recent years, associated with that issue [9], [8]. Large tank vessels as Suezmax and VLCC, large bulk carriers and large containerships are considered to be shaft alignment-sensitive vessels due to the lack of FSTB and their typical hull deflection profiles [10]. Additionally twin-screw ships which have a relatively higher propeller load compared to bearing capacity [11] and those with water lubricated bearings [8] fall also in that category.

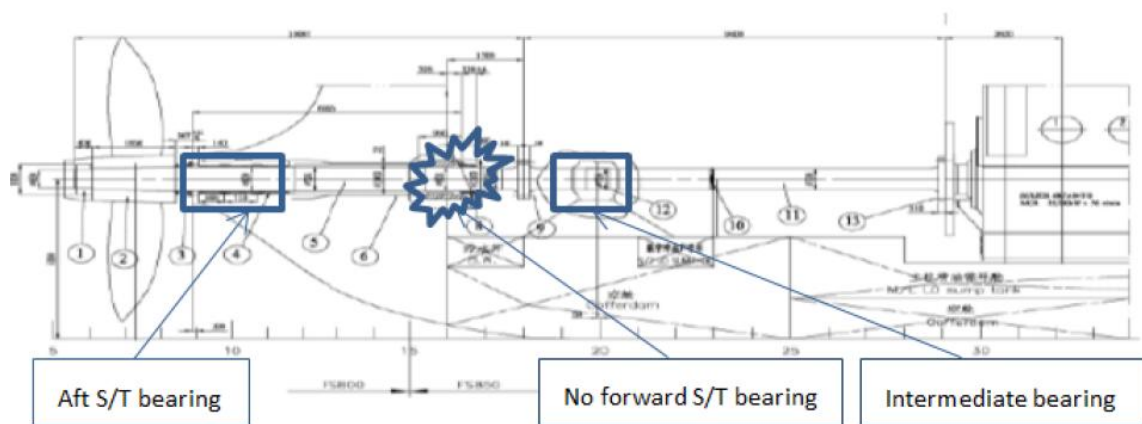


**Figure 2: Design with only one stern tube bearing [7]**

In 2018 it was stated by DNV [12] that: *“The industry has faced challenges with some of the more recent single stern tube bearing installations with respect to the reliability of the propeller shaft bearings. Extreme turns in the upper speed range have been observed as one of the predominant scenarios in which many of the failures have been reported.”*

In many shaft alignment calculations (which follow current pertinent rules of Classification Societies), propeller forces have either not been accounted for or in some have been calculated for a normal continuous running condition [7] (using approximations). In other words, a typical shaft alignment calculation process mainly focuses on achieving optimum alignment of the shaft in static conditions and effects influencing the alignment, such as propeller loads are not taken into consideration and this can be attributed to the relatively low number of related damages. However, since the 1990s, there has been an increase in the number of damages, particularly to aft stern tube bearings, caused mainly by larger hull deflections and increased propeller loads, whose magnitude and direction can alter significantly throughout the operational profile of the vessel [13]. Studies of the recent years, have examined the magnitude of these propeller loads and their impact on shafting system, [11], [13], [14], [15], [16], [17], [18], [19]. The prevailing consensus in most of them is that propeller forces should not be excluded from shafting analysis and that could contribute to safety and robustness of shafting systems’ performance enhancement. Another factor implying the need for examining these loads is the recent issuing of Class Notations regarding shafting system in relation to propeller loads (i.e. ESA and shaft align).

Concluding, in theory it is necessary to get the hydrodynamic propeller loads considered case by case in the shaft alignment design to quantify its effect on the bearing performance and according to [12], prediction of the propeller forces in turning conditions may be necessary to ensure safe operation of the propeller shaft bearing in all operating conditions.

## 2) Shaft alignment process (at design office)

During the design stage of a ship, regarding alignment of shafting system, produced plans are: Shaft Alignment Calculation Plan<sup>1</sup> and Torsional Vibration Calculation Plan. The first kind of plan will be analyzed below in detail.

Shaft alignment calculation (SAC) is executed for achieving the following objectives [20]:

- Bearing loads under all operating conditions are within the acceptable limits specified by the bearing manufacturer.
- All bearings remain always loaded, except as determined acceptable in accordance with Class rules requirements<sup>2</sup>.
- Shear forces and bending moments on propulsion equipment are within the limits specified by manufacturers.
- The designed relative misalignment slope between the shaft and the aft stern tube bearing is to be positive, and not to exceed 0.3 mrad.

Shaft alignment calculation is design specific and has to take under consideration parameters such as: design of shafting system, ship design, hull deflection and effect rules and regulations of Classification Societies. As every mechanical system modeling, SAC is subjected to certain simplifications and assumptions. Some of the most critical of them are listed below:

1. Hull deflection due to load distribution and temperature change can be taken into account or not. For the first case, it can be calculated by 1D FEM calibrated model or 3D FEM model.
2. Shaft is considered as beam under uniformly distributed load (shaft weight) and concentrated loads (e.g. propeller, cap, nut, turning wheel, moving masses, chain force)
3. Bearings can be considered as infinitely stiff, linear or nonlinear elastic.
4. Shaft-bearing interaction (hydrodynamic lubrication) may be taken into consideration.
5. The longitudinal position of support point in ASTB can be a percentage of the length or diameter of that bearing and can alter from static to dynamic condition. For rest of the bearings, support point is usually considered to be in the middle of their length.
6. Shaft can be considered not to be compressed due to thrust force.
7. When main engine is in operation, expands vertically by an amount provided by manufacturer due to thermal expansion.
8. Propeller hydrodynamic loads can be modeled or not. In case they are, usually they refer to straight run condition.
9. Buoyancy of propeller is considered and in some designs of cap and nut as well.
10. Crankshaft, which may be weightless, is modeled by a cylindrical beam and forces due to piston movement have a constant magnitude or follow a distribution.
11. Analysis is quasi-static.

---

<sup>1</sup> Accompanied by plans such as: Propulsion Shafting Arrangement, Stern Tube Assembly, Fairing Cap, Propeller Shaft, Intermediate Shaft, Stern Tube (and Forward) Bearing, Intermediate Shaft Bearing(s), Main Engine Data for Shaft Alignment etc.

<sup>2</sup> For the aft most bearing of 2-stroke diesel engine, zero bearing load (but no negative) can be accepted if agreed by engine manufacturer [21]

## 2.1) Chapters of Shaft Alignment Calculation Plan

A typical SAC plan consists of the following chapters:

**1) Short introduction and particulars of propulsion system:** general information are provided regarding the vessel, main engine, dimensions and material of shaft parts, propeller and PBCF (if applicable) and bearings.

**2) Assumptions and definitions:** reference line is defined, sign convention is stated, supporting positions, stiffness and permissible load range for all bearings is defined. Also slope boring criteria are checked.

**3) Model of shaft and input data for calculations:** shafting arrangement of whole modeled shafting system is depicted, including all necessary dimensions and applied loads as well as a table with finite elements data used for the beam model<sup>3</sup>. Also external loads such as propeller weight, flywheel, chain force, moving masses and propeller forces are presented. At some designs hull deflections are taken into account and the method of their calculation is included.

**4) Results of calculations:** matrix of reaction force influence (RIN) matrix is presented and bearing selected offsets and reaction loads with corresponding pressures for all examined conditions are included (e.g. cold 100%, hot 75%, hot 100% and dynamic). Moreover deflection curves, shear force and bending moment curves are presented for all examined conditions.

**5) Procedure of shafting system installation and alignment:** gap and sag values are calculated for specific propeller immersion conditions during shaft installation (and corresponding curves sometimes) as well as jack correction factors, the positions of jack forces and a procedure of that shafting system installation is proposed.

Requirements and range of limits are governed by class regulations since plans have to be reviewed by a recognized organization. Class regulations regarding shaft alignment of rotating machinery, such as the prime mover of a ship, are quite homogeneous between all major classes.

---

<sup>3</sup> Constructing the 3D model of shaft and modeling its interaction with bearings is a quite difficult process since a fluid-structure modeling is required. For this reason the customary method of shaft alignment analysis is the 1D finite element model of a continuous beam for calculating bending moments and reaction forces at all critical shaft locations.

## 2.2) Reaction Influence Numbers and Sensitivity Index

### 2.2.1) Reaction Influence Numbers

The reaction influence numbers (RIN), or coefficients, describe the relative change in bearing reactions due to a unit offset change of a particular bearing. These parameters are used to assess the shafting sensitivity to potential disturbances in bearing offsets, which can originate from hull deflections, thermal effects, and bearing offset adjustments [20]. High reaction influence number indicates high shaft sensitivity to misalignment and vice versa. All these numbers are tabulated into a square and symmetric matrix, where the number of rows and columns is equal to the number of bearings. The sum of each column and each row is zero, as the weight of the shaft remains constant in each case. Each column provides the change in bearing reactions corresponding to a unit rise ( $y_i$ ) at the respective bearing. The elements of this matrix ( $\sigma_{ij}$ ) are called influence numbers and are calculated as follows:

$$\sigma_{ij} = \frac{w_{ij} - w_j^0}{y_i}$$

Where:

$\sigma_{ij}$  : is the influence factor of bearing  $i$  on bearing  $j$

$w_{ij}$  : is the reaction force of bearing  $j$  when bearing  $i$  has moved vertically by an amount of  $y_i$

$w_j^0$  : is the reaction force of bearing  $j$  while all bearings have zero vertical offsets meaning they are in a straight line

$y_i$  : is the vertical offset of bearing  $i$

Given the  $\sigma_{ij}$  values are known, every bearing reaction force can be calculated for a set of vertical offsets as:

$$w_{ij} = \sigma_{ij} \cdot y_i + w_j^0$$

### 2.2.2) Sensitivity Index

Except from RIN matrix construction, these numbers can suggest an optimal longitudinal position of intermediate bearing through Sensitivity Index. The index is defined as [21]:

$$Sensitivity\ Index = \sum_{i=1}^N (\sigma_{mj})^2$$

Where:

$\sigma_{ij}$  : is the influence number of intermediate bearing on bearing  $j$

$N$  : number of total bearings taken into consideration according to designer's experience

$m$ : intermediate bearing number

With the help of this index the impact of intermediate bearing offset change (i.e. due to draft change) on stern tube and aft most main engine bearings can be reduced in a more balanced way. It is noteworthy that there has been a case of damage to the aft main engine bearing, attributed to the intermediate bearing longitudinal position being placed too close to the main engine.



### 2.3) Static and dynamic condition

Ensuring appropriate alignment of the shaft is crucial to accommodate all scenarios a ship might face during its whole operational profile. These scenarios typically fall into two main groups: static and running condition.

Shaft alignment in base of static considerations means that ship is stationary, shaft isn't rotating, propeller effects on shaft alignment are solely those caused by propeller weight acting in the vertical plane and no loads are acting in the horizontal plane. Moreover hydrodynamic lubrication is not active and at bearing locations shaft can move freely in the vertical direction, within a span of twice the radial clearance of each bearing. When ship is out of water, meaning the ship is in dry-dock, shaft experiences the "dry" weight. The difference with afloat ship case is that when propeller is immersed in water, the buoyancy force on the propeller acts in the opposite direction as the weight force, resulting a reduced effective weight. During that condition engine can be cold or hot and cases are examined for different propeller immersion conditions.

Running (stated also as dynamic) condition is a quasi-static approach for the seagoing condition of ship. At that case main engine operates at hot condition, modeled by an added vertical offset of all crankshaft bearing due to thermal expansion<sup>4</sup>, propeller produces thrust, resulting in propeller hydrodynamic loads applied at propeller node, supporting position of ASTB alters under selected considerations and hydrodynamic lubrication is active lifting the shaft off of the lower half of the bushing.

In the present study, the following assumptions have been made, regarding dynamic condition of case study vessel: (a) a uniform vertical offset of the crankshaft bearings due to thermal expansion and (b) shaft bending moments due to propeller vertical eccentric thrust have been considered, while (c) shaft vertical motion within bearing clearance governed by principles of hydrodynamic lubrication is neglected, while in some cases supporting point location of ASTB is calculated through hydrodynamic lubrication modeling.

---

<sup>4</sup> As main engine reaches working temperature, the expansion of the upper part of the engine is greater than the lower part and engine bed, creating a hogging distortion of the engine bed that must be taken into consideration. In shaft alignment studies, a uniform vertical thermal expansion of engine is considered for 'hot' cases. That number is given by engine manufacturers with typical values being between 0.2 and 0.5 mm.

## 2.4) Aft Stern Tube Bearing (ASTB)

The aft stern tube bearing is a particularly sensitive component of the shafting system, as it is significantly affected by both propeller gravitational and hydrodynamic loads. Additionally, it is challenging to inspect and replace. To address these issues, concepts such as slope boring and bearing inclination are widely implemented. These techniques regulate the contact area between the shaft and bearing, thereby helping to minimize edge loading. Furthermore, the length of the stern tube bearing is typically at least twice its diameter to control the peak oil film pressure and to provide damping for the shaft. [22].

### 2.4.1) Supporting point

Positioning of support point in ASTB (**Figure 3**) is based on practical experience and classes provide different recommendations [23]. This point represents the longitudinal position of assumed bearing reaction and there can be measured the misalignment slope between shaft and bearing. According to American Bureau of Shipping (ABS) when a single point support is to be considered, that point should be placed forwards from aft end of the bearing by  $1/3$  of bearing diameter ( $D/3$ ) for static condition and by  $1/3$  of bearing length ( $L/3$ ) in dynamic (running) condition. For double sloped bearings three support points should be used, at each bearing edge and at the transition point (knuckle). According to Bureau Veritas (BV) there should be considered at least five supporting points. The Nippon Kaiji Kyokai (NK) suggests that if a single support is considered, it has to be located at  $D/3$  or  $L/4$  from the aft end of bearing. When two support points are considered they should be located at each end of the bearing and for three support points and above, it may be decided by designer [21]. According to Det Norske Veritas (DNV), ships having a shaft diameter of 500 mm and above have to undergo a lubricity evaluation with at least two reaction force supporting positions of the aft stern tube bearing. The Society of Naval Architects and Marine Engineers recommend that when a single reaction force supporting position is considered, a point separated by  $D/2$  from the stern end should be the reaction force supporting position.

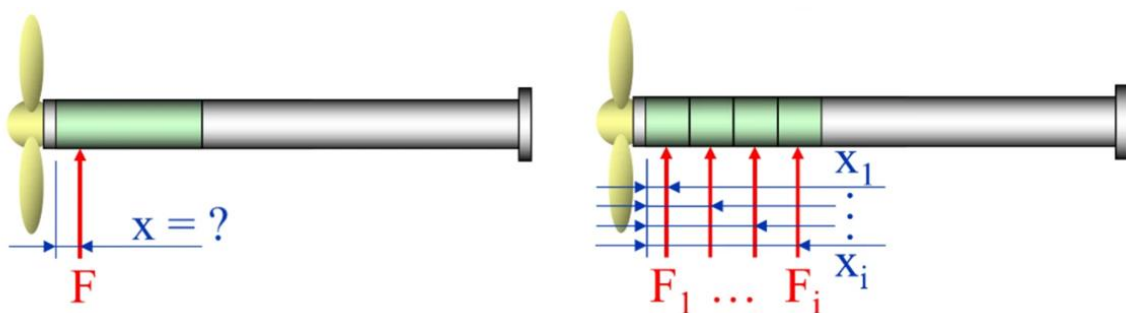


Figure 3: Single and Multi bearing support of ASTB [9]

The actual location of the support point can be determined using hydrodynamic lubrication software. By inputting basic geometric and operational parameters into a Reynolds equation solver, the pressure field is calculated (**Figure 4**), which provides the actual support location.

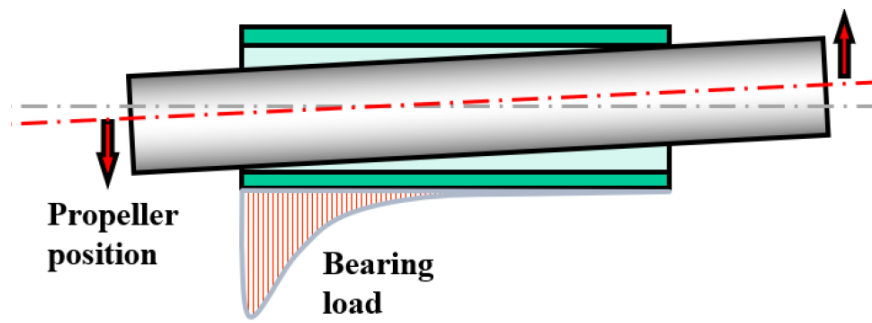


Figure 4: Realistic distribution of ASTB reaction force [14]

### 2.4.2) Misalignment angle

Another critical aspect of SAC is the relative slope of the propeller shaft against the aft stern bearing datum. This misalignment angle (**Figure 5**) directly influences bearing hydrodynamics, as it is crucial for maintaining proper lubrication conditions, avoiding load concentration at the aft end of the bearing, and ensuring better performance and longer bearing life. According to [20], the bearing slope significantly affects the phase of engine start-up in terms of bearing wear and friction, as well as the running condition during a starboard turn (for right-handed propellers), during which propeller hydrodynamic loads push the shaft downwards. During start-up, metal-to-metal friction occurs until an oil film is developed, while during that maneuvering case, oil film disruption can cause similar frictional issues.

A misalignment angle of 0.3 mm/m (0.3 mrad) for hot static conditions and additionally for hot running conditions, depending on the classification society, is specified as a practical guideline to ensure satisfactory hydrodynamic lubrication. This limit is widely accepted and applied as a marine industry practice, however the safety margin for this limit has not been completely explained and it should not be blindly applied. A dynamic fluid-structure interaction analysis can provide more accurate margins [20].

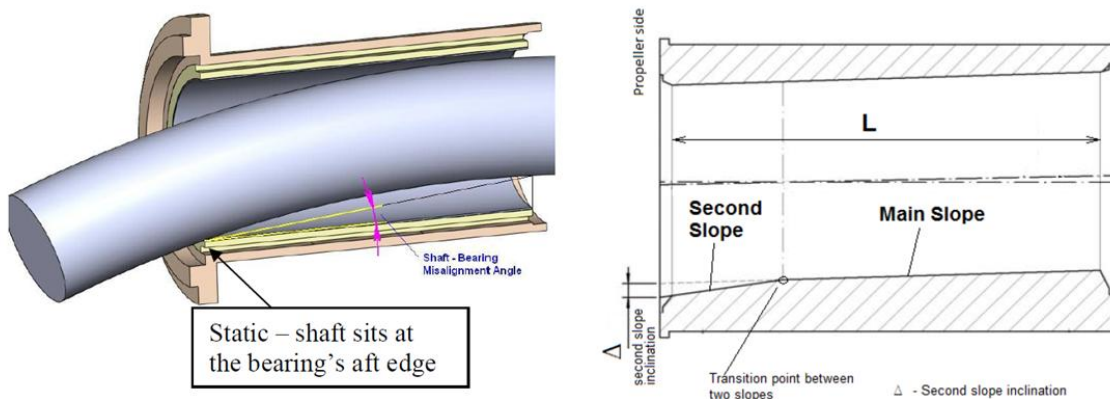


Figure 5: Misalignment angle (left) and double slope bearing (right)

When this limit is exceeded in the design, a reduction of the misalignment angle is to be considered either by slope boring or bearing inclination. Bearing slope is usually achieved by bearing outer surface machining, performed in shipyard.

In case of slope boring the angle  $\phi$  that has to be checked is: the relative slope of shaft against bearing datum minus the rake of stern tube bush resulted from slope machining of stern tube bearing.

## 2.5) Crankshaft equivalent model

The main engine crankshaft equivalent model used for shaft alignment calculation can be provided either by the engine manufacturer or determined by the shipyard's practice. However, if the manufacturer provides such a model, it is typically preferred for use [21]. The key parameters of this modeling include the number of bearings taken into account, the diameter of the circular bar representing the crankshaft and its weight. These parameters are essential for accurately simulating the behavior of the crankshaft in the shaft alignment calculation process.

### 2.5.1) Number of modeled main engine bearings

The number of modeled bearings has a negligible effect on the reaction forces of stern tube and intermediate bearings; however, it significantly impacts the reaction forces of main engine bearings. It's noted that to accurately calculate the reaction forces of three main engine bearings, two additional bearings should be included in the calculations. This means that for precise calculation of the reaction forces of the three aft most main engine bearings of a 6-cylinder engine, five main engine bearings should be included in the shaft alignment calculation. For directly coupled main engines, the three aft most main engine bearings are particularly susceptible to unloading and are most affected by the position of the intermediate bearing.

### 2.5.2) Equivalent diameter of crankshaft bar

To analyze the shafting system using 1D beam theory, an equivalent crankshaft model is required since the exact geometry of the crankshaft cannot be utilized. It's crucial in this procedure that the equivalent crankshaft possesses the same bending stiffness as the actual crankshaft. Therefore, the circular bar representing the equivalent crankshaft cannot have the same diameter as the crank journal due to the influence of webs. If the equivalent model is not provided the engine maker, it can be calculated either by numerical calculations using FEM or by approximate analytical expression [21]. In the numerical calculation approach, a detailed FE crankshaft model is constructed, wherein specific constrained nodes and enforced vertical displacements of bearing supporting points are selected. Additionally, a circular bar FE model is created with the same boundary conditions as before, but with a diameter adjusted to produce reaction forces equivalent to those of the crankshaft model. This adjustment is achieved by altering the diameter of the bar (**Figure 6**). In the analytical expression method, the assumption is made that the crankpin and crank journal have the same diameter. By utilizing certain dimensions of the crankshaft and the Poisson ratio of its material, an equivalent diameter is calculated. It's important to note that the equivalent model is independent of the angle of the crankshaft.

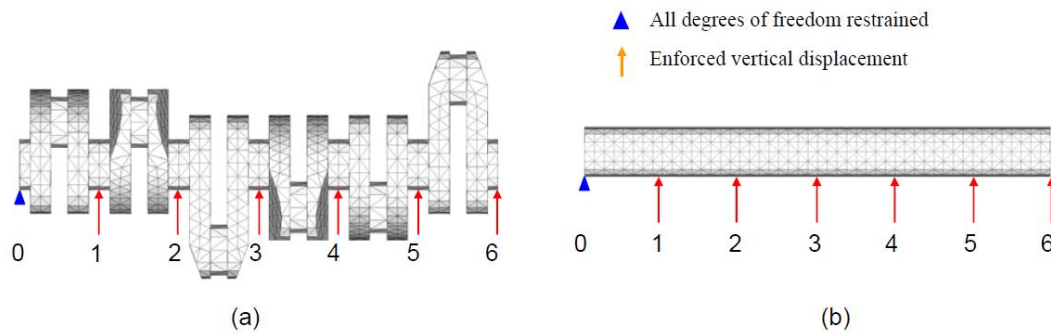


**Figure 6: FE model of crankshaft (a) and circular bar model (b) [21]**

## 2.6) Class notations regarding the shafting system

Class notations are symbols listed in the certificate of class of a vessel, indicating the standards according to which a ship is designed and built. The names of these notations may vary depending on the classification society. They encompass specific design criteria beyond generic class requirements, aimed at enhancing operating margins. Within the IACS classification societies, ABS has issued TCM notation, DNV has TMON and BV has ESA.

### 2.6.1) TMON and TCM notations

Tail shaft withdrawals for cargo vessels are typically required every five years by various ROs (Recognized Organizations). However, if a ship meets specific requirements, it may be eligible for an extension of this predetermined interval, reducing dry-dock time and expenses while minimizing the risk of damage to the system during withdrawal. The scope of the additional class notations such as TMON (tail shaft monitoring), issued by DNV [24] and TCM (tail shaft continuous monitoring) issued by ABS, add an extra level of safety related to the propeller shaft and propeller shaft bearing, including its lubrication by monitoring the temperature and lubricant condition of this equipment. They include a continuous recording of parameters under the responsibility of the ship's chief engineer. These class notations are applicable for vessels with oil or water lubricated propeller shafts. For oil lubricated propeller shafts for example, the requirement for propeller shaft withdrawal may be waived on a case-by-case basis, provided that documentation showing satisfactory condition of the stern tube arrangement is presented to the Society. The two notations have similar requirements. Specifically for TMON required documentation, covering the last three (3) years or since delivery or last propeller shaft survey shall include: monthly measurements of stern tube bearing temperatures (high and low) with corresponding sea water temperatures, oil consumption, water content in stern tube oil measured with onboard kit and analysis from accredited laboratory with conclusion at least every six months, bearing clearances from new building and wear down<sup>5</sup> measurements from last dry docking and seals (inboard and outboard) renewal dates.

<sup>5</sup> The bearing wear down measurement is the reduction in radial clearance between the bearing and the shaft due to abrasion and corrosion, measured by filler gauges, dial indicators or ultrasonic devices.

## 2.6.2) ESA and Shaft Align notations

ABS introduced the Enhanced Shaft Alignment (ESA, ESA+) notations in 2019, while DNV issued the Shaft align(1) and Shaft align(2) notations in 2018 for vessels assigned with TCM or TMON notations, respectively. These notations, among other things, place additional emphasis on the impact of transient hydrodynamic propeller forces and moments acting on the shafting system, particularly during extreme turning conditions in the upper speed range, as well as the impact of hull deflections due to draft changes [24]. A turning condition is defined as the condition which the ship is performing a steady state full rudder turn to port or starboard, commencing from a straight course at a ballast or full scantling draft at MCR condition [10].

Some benefits for owners having such shaft notation on their ships are the following [6]:

- Greater confidence in the standard of shaft alignment calculation and processes calculations.
- Tailored solutions to shaft alignment sensitive vessels.
- Potentially improved shafting system integrity during life of the vessel.
- Complete shaft alignment tracking records in case of an accident.

To obtain the mentioned notations for a ship, specific requirements must be met. Focusing on the spectrum of propeller loads for which is defined either by results from CFD database (for ESA and Shaft align(1)<sup>6</sup>), or are design-specific using CFD software (for ESA+ and Shaft align(2)). In ESA notation it is stated that the empirical formulae which have to be used for the running condition calculations are those in the following table:

**Table 1: Hydrodynamic propeller loads based on results from CFD database [10]**

	Straight Ahead Condition	Turning Condition
For single screw vessel	$\pm 5\% Q$	$\pm 30\% Q$
For twin screw vessel	$\pm 20\% Q$	$\pm 30\% Q$

Where:

Q is the torque at MCR

Positive sign (+) implies a moment that is pushing the propeller downward about the transverse axis, whereas the negative sign (-) implies a moment that is pushing the propeller upward about the transverse axis

In Shaft align(1) notation (DNV) it is stated that it is required an increased propeller bending moment ranging from -30% to +30% MCR torque in the aft bearing loading criteria.

---

<sup>6</sup> Shaft align (1) is intended for propulsion systems installed on vessels with conventional hull forms and incorporates enhanced aft bearing performance during running and turning operating conditions. Shaft align (2) is intended for propulsion systems requiring additional calculations to estimate additional propeller hydrodynamic propeller loads during turning conditions. Typical installations are vessels with non-conventional hull forms such as asymmetric stern, twin skeg, etc.

## 2.7) Propeller moment during running (dynamic) condition

### 2.7.1) Shipyards' practice (from NTUA plan database)

During the design stage, it is imperative to analyze and define the interaction between the rotating propeller and the wake field, as it generates forces and moments that affect the shafting system. Upon examining various designs, the following approaches to address this issue were identified:

1. **No Modeling of Dynamic Loads:** Static conditions are exclusively examined, neglecting the dynamic effects of propeller-wake interaction.
2. **Application of Vertical Bending Moment:** A vertical bending moment is applied to the propeller node, representing the thrust vertical eccentricity. This approach assumes that this bending moment adequately captures the effect of propeller-wake interaction.
3. **Modeling of Vertical and Lateral Forces and Moments:** Both vertical and lateral forces and bending moments are applied, aiming to capture the effect of propeller-wake interaction more realistically.
4. **Differentiation for Ballast and Laden Conditions:** The above modeling approach is distinguished for different ship conditions, such as ballast versus laden.
5. **Differentiation for Operational Speeds:** Similar to the previous approach, but distinguishing between different operational speeds, such as dead slow versus full speed.

To analyze these approaches, the NTUA database of (SAC) plans was thoroughly examined to assess how the propeller vertical bending moment due to thrust eccentricity is accounted for. A fleet consisting of bulk carriers, tankers, LNG carriers, and containerships built between 2008 and 2019 was studied. The way of modeling propeller hydrodynamic loads can be related to:

- Shaft torque while engine operates in MCR
- Propeller thrust and eccentricity of thrust estimations
- Propeller weight

Since the exact calculation method for these loads is not always explained in detail in SAC plans, in order for a comparison to be possible, all bending moments of studied plans will be expressed as a percentage of shaft torque while main engine operates at MCR condition. A positive percentage means that bending moment lifts the propeller cantilever upwards. Designs that had had simulated a dynamic condition (also called running condition) are enlisted in the following table.

**Table 2: Vertical bending moment expressed as percentage of nominal shaft torque from designs of NTUA database**

Type of ship	Size	Year	Shipyard	MCR Power [kW]	MCR [rpm]	Propeller			Mz [kNm]	Percentage of nominal shaft torque
						Diameter [m]	Weight in air [t]	Blades [#]		
	DWT									
Bulk Carrier	58,000	2013	STX	8,500	115	6	14.7	4	105	15%
	82,000	2011	DSME	10,170	91	7	25.3	4	365	34.2%
	82,000	2010	N/A	11,620	127	6.2	16.8	4	117	13.4%
	180,000	2008	STX	18,660	91	8.2	40.8	4	296	15.1%
	210,000	2013	BSHI	17,500	82.6	8.8	40.9	4		40% and -15%

	DWT									
Tanker	11,000	N/A	MaWei Shipbuilding Industries	3,575	142	4.5	4.83	4	51	21.21%
	23,500	2018	Fujian Mawei Shipbuilding	5,220	167	4.20	5.935	5	61	20.54%
	50,000	2014	SAMSUNG	7,260	99	6.6	6.6	4	175	25.02%
	115,000	2011	SAMSUNG	13,560	105	7.25	7.25	4	157	12.80%
	113,000	2012	Hyundai HI	18,660	91	8.2	8.2	4	293	15.00%
	320,000	2012	DSME	24,380	63	10.6	7.56	4	885	23.95%
	CBM									
LNG Carrier	38,000	2013	Hyundai HI	7,889	108	N/A	15.8	N/A	151	21.77%
	84,000	2013	Hyundai HI	12,400	92.2	N/A	27.8	4	264	20.56%
	174,000	2019	Hyundai HI	12,113	77.1	twin screw 8.4	35.2	3	792	59.65%
	TEU									
Containership	1,800	2015	Hyundai HI	12,050	105	6.5	19.73	6	210	19.19%
	2,800	2016	Hyundai HI	24,260	91	7.8	38.4	6	389	15.28%
	3,100	2014	DSEC	25,191	104	7.35	40.118	5	500	21.62%
	3,800	2017	Hyundai HI	19,620	91	7.9	34.29	4		15% and 30%
	4,500	2012	Hyundai HI	23,000	73.9	8.6	64.438	5	1082	36.41%
	6,800	2014	Hanjin HI	26,700	84	8.7	57.384	5	455	15.00%
	9,200	2012	DSME	51,070	84	9.2	N/A	6	626	10.78%
	14,000	2016	Hyundai HI	54,960	80	N/A	101	N/A	1143	17.42%
	18,270	2013	DSME	23,310	72	9.4	71.8	4	1078	34.87%

Percentages for positive bending moments of the table above are plotted in the following chart:

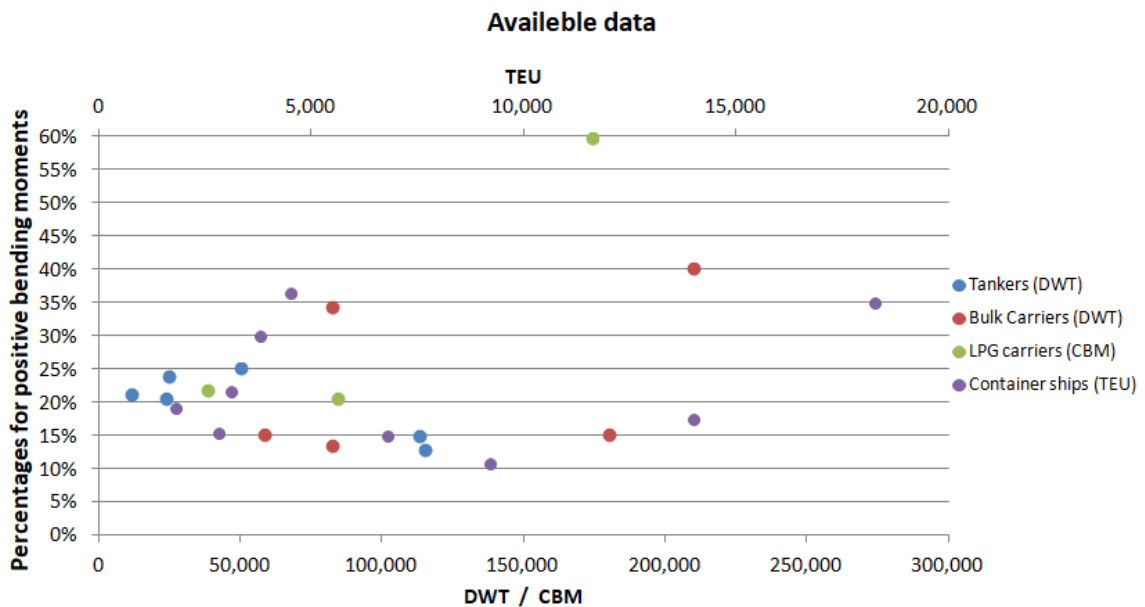


Figure 7: Percentages of positive bending moments of available plans

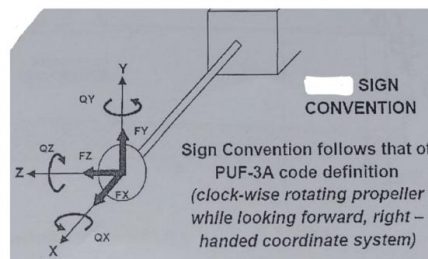
The value of  $M_z$  moment acting on propeller node seems to be according to each shipyard's practice, which may be ship type and size dependant and alter through the years through accumulated experience. Roughly half of available SAC plans have not taken into account propeller



hydrodynamic loads, or maybe they did but it is not stated. For single screw ships it can be seen that this percentage lies between 10% and 40%. Classification societies suggest a value for that moment. Specifically DNV suggests +40% (acting upwards)<sup>7</sup> and at minimum -5% (acting downwards) of full torque to estimate hydrodynamic propeller loads during running condition, while ABS uses 15% (acting upwards). Consequently, since above factors imply that selection of that percentage is strongly related to shipyard's practice and a creation of a statistical formula would not be a useful tool. Another reason for this is that a fleet of ships can be constructed according to one SAC plan, so that formula would be biased by the numbers of ships built according to each.

However the table above could be helpful during preliminary design of shafting system for ships similar to those listed in the table, as one more condition can be examined increasing robustness of the system. Although it may be uncertain that percentage it is surely better to be used for examining a running condition than not to. Few of the plans contained information regarding propeller hydrodynamic loads in vertical and horizontal directions and are presented below:

**Table 3: Data from plans containing information regarding propeller hydrodynamic loads**



<b>Bulk Carrier, 82k DWT, MCR 10,170 kW 91 rpm, Propelled diam. 7 m</b>		
Loads in vertical direction	Force Fy	13 kN (upward)
	Moment Qz	365 kNm (upward)
Load in horizontal direction	Force Fz	23 kN (port)
	Moment Qy	118 kNm (starboard)

<b>Tanker, 320k DWT, MCR 24,380 kW 63 rpm, Propelled diam. 10.6 m</b>		
Thrust Force		2740 kN
Loads in vertical direction	Force Fy	108 kN (upward)
	Moment Qz	885 kNm (upward)
Load in horizontal direction	Force Fz	61 kN (port)
	Moment Qy	900 kNm (starboard)

<b>LNG carrier, 174k CBM, MCR 12,130 kW 77.1 rpm, Propelled diam. 8.4 m twin screw</b>					
Force (kN)		Dead slow		MCR	
Moment (kNm)		Ballast Draft	Full Draft	Ballast Draft	Full Draft
Fx	Thrust Force	-67.589	-67.912	-1004.439	-1009,242
Mx	Torque	89.544	89.401	1330.713	1328.590
Fy	Horizontal Force	8.484	7.298	126.145	108.449
My	Horizontal Moment	38.913	53.345	578.294	792.765

<sup>7</sup> Percentage of 40% is considered as simple and conservative estimation. Calculation of shafts in marine applications, DNV Class Guideline, August 2021 Edition

Fz	Vertical Force	-1.280	1.968	-18.370	29.240
Mz	Vertical Moment	-7.192	13.908	-106.882	206.685

<b>Containership, 18.27k TEU, MCR 23,310 kW 72 rpm, Propelled diam. 9.4 m</b>			
Loads in vertical direction	Ballast Draft	Force Fy	4 kN (upward)
		Moment Qz	1172 kNm (upward)
	Design Draft	Force Fy	66 kN (upward)
		Moment Qz	1078 kNm (upward)
Load in horizontal direction	Ballast Draft	Force Fz	159 kN (port)
		Moment Qy	97 kNm (starboard)
	Design Draft	Force Fz	143 kN (port)
		Moment Qy	554 kNm (starboard)

<b>Containership, 2.8k TEU, MCR 24,260 kW 91 rpm, Propelled diam. 7.8 m</b>		
Thrust Force	Force Fx	-108 kN

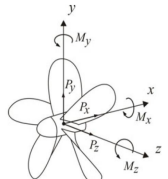
<b>Containership, 3.1k TEU, MCR 25,191 kW 104 rpm, Propelled diam. 7.35 m</b>		
Loads in vertical direction	Force Fy	71 kN (upward)
	Moment Qz	500 kNm (upward)
Load in horizontal direction	Force Fz	52 kN (port)
	Moment Qy	401 kNm (starboard)

<b>Containership, 9.2k TEU, MCR 51,070 kW 84 rpm, Propelled diam. 9.2 m</b>		
Loads in vertical direction	Force Fy	105 kN (upward)
	Moment Qz	626 kNm (upward)
Load in horizontal direction	Force Fz	42 kN (port)
	Moment Qy	726 kNm (starboard)

### 2.7.2) Statistical approach of research paper [25]

In that work a fleet of 25 ships was examined and validated with two other studies [Krylov Institute 1973] and [Carlton 2007], however according to the author, improvements can be done by using recent propeller load theoretical and experimental studies. The steady and fluctuating components found, are presented in (Table 4). It is observed that the steady component of the vertical bending moment is independent of the propeller blades' number and equals -35% of full torque. It's important to note that the negative sign indicates that the moment pushes the propeller cantilever downwards. Additionally, data are available for calculating the fluctuating components of these loads, which are a function of blade frequency (mZ) and propeller rotation angle ( $\theta$ ). These coefficients are dependent on the number of propeller blades.

**Table 4: Hydrodynamic loads (steady components) on single-screw ship propeller for shaft alignment and shaft vibration calculations as a percentage of the mean thrust  $P_x$  and mean torque  $M_x$**

Number of blades	Z	Z = 4,5,6		Sign convention
		Mean value	Deviation ( $\pm$ )	
Vertical force	$P_y$	4.8	3.1	
Horizontal force	$P_z$	-5.0	2.0	
Horizontal moment	$M_y$	28.4	7.8	
Vertical moment	$M_z$	-35.0	10.0	

Modeling propeller hydrodynamic loads solely based on thrust and torque has its drawbacks. It limits the representation of the vessel's operational profile to primarily straight runs and fails to encompass more generic scenarios such as maneuvering and varying draft conditions during ballast voyages. Additionally, relying on older data for thrust estimations introduces uncertainty into the results. Despite these limitations, this method can still be valuable for examining specific running conditions within an SAC plan. **The nature of propeller hydrodynamic loads and their modeling in this thesis is thoroughly explained in paragraph 4.2.**

### 3) Shaft alignment process (in shipyard)

The calculation of shaft alignment is typically handled by a design office, which may offer an installation procedure for the shafting system. However, it falls upon the shipyard to execute the installation and alignment, drawing upon their accumulated experience. The alignment process for ships equipped with fixed pitch propellers, as delineated in references [20] and [26], comprises two major phases: the dry-dock phase (before launching) and the afloat phase (after launching). Application of shaft alignment is not expected to start before the vessel stern blocks are fully welded and all of the heavy structures are in place. The common practice in new-building vessels is to start the alignment procedure from the aft and working its way forward. Specifically during the first phase, boring of stern tube is executed (if needed), stern tube bearing is placed, reference line is set<sup>8</sup> and a preliminary alignment of bearings, temporary supports, shaft parts and main engine is done (**Figure 8**). Firstly, propeller shaft (including cap and nut) has to be installed and be aligned carefully in relation to the stern tube bearing and the exact placement of propeller shaft is ensured by clearances in both vertical and horizontal axis according to shaft alignment plan. For designs with forward stern tube bearing, then that bearing must have a positive reaction force, while if only ASTB exists, then a temporary support is placed at a position according to the shaft alignment calculation. In both cases maybe a jack down force (typically in the range of 5-15 tons) at the forward end of the propeller shaft is required to achieve positive reaction force. Afterwards stern seals are placed and ship can become afloat and start the second phase of alignment.

The second phase can start given that ship hull is completed, superstructure is placed, most of welding work is completed and main engine is completely assembled. Intermediate shaft is then supported by its bearing and by one or two temporary supports. As reference for propeller with intermediate flange coupling are gap & sag values, defined in shaft alignment calculation plan and are attained by bearing and temporary support height adjustment. The same process is followed for any subsequent intermediate shafts until main engine where gap & sag values between forward flange of foremost intermediate shaft flange and crankshaft aft flange have to be achieved by adjusting the height of main engine with the jacking screws.

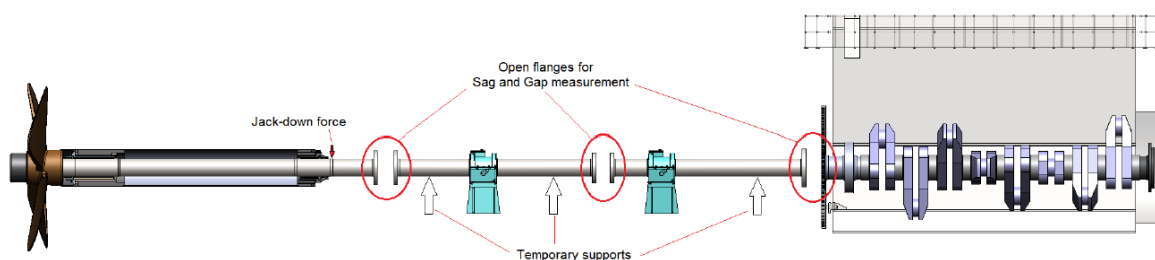


**Figure 8: Assembly of shafting during second phase of alignment [20]**

After gap & sag values of all shafts are attained then flanges will be coupled with bolts tightened at defined torque, temporary supports and jack down force can be removed. Consequently alignment measurements are taken (jack up tests at intermediate and 3 main engine aft most bearings or strain gauge tests, crankshaft deflections, main engine bedplate sag) while factors

---

<sup>8</sup> Process of sighting (reference line) is conducted by one of the following methods: piano-wire, optical telescope or laser. Each of them has advantages and disadvantages regarding cost, required experience, accuracy and set up process.

which can affect the results have to be controlled. This means that draught and trim have to be constant, no ballast operations and movement of heavy parts can be done and heat sources have to be eliminated several hours prior to measurements such as tank heating and welding works near the propulsion system.

Commonly when corrections in alignment are required, intermediate bearing offset is fine-tuned to achieve the prescribed values of shaft alignment plan. Afterwards chocking of main engine and intermediate bearing is performed. In older constructions metal chocks were used, while nowadays epoxy resin chocks (chock fast) are preferred. Finally shaft bearings are chocked as well and engine holding down bolts have to be tightened. In case loads lie outside their limits, intermediate bearing is adjusted by chock scraping or by inserting shim plates. It's worth noting that any significant alterations required after sea trials can lead to considerable cost escalation [27]. While the shipyard bears overall responsibility for the entire process, many aspects of the procedure must be conducted under the attendance of both the classification society and the owner.

### 3.1) Gap & Sag values

Gap & sag measurements are usually executed prior to shaft assembly and is simultaneously performed on all open mating flanges of the shafting system while ship is on dry-dock condition. They are also calculated with the same beam theory model as the shafting system [20]. In case ship is afloat, then analysis may be in question since hull deflections can affect the results. Gap & sag values can have tolerance of  $\pm 0.05$  mm and  $\pm 0.10$  mm respectively [26]. The gap (angular offset) is the horizontal distance and sag (radial offset) is the vertical distance between two disconnected flanges which can be seen in (Figure 9).

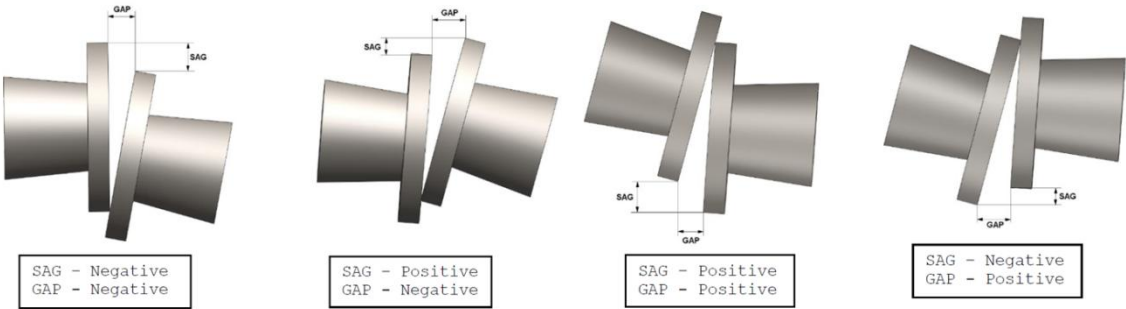


Figure 9: Flange arrangement in gap & sag analysis [20]

### 3.2) Procedures of measuring bearing loads

After completing the shaft alignment process and coupling the shafts while removing temporary supports, it becomes vital to measure the actual bearing reaction forces at the support points. Common methods for conducting these measurements are:

- Jack-up test
- Strain gauge measurement

#### 3.2.1) Jack-up test

During the shaft alignment procedure, it's essential to measure the static loads of the intermediate and forward stern tube bearings (if applicable) to ensure that they produce satisfactory reactions. In addition a jack up for the two or three aft most main engine bearings is desirable. However, in some cases, it may not be feasible to conduct such measurements directly. In such instances, alternative methods like crank web deflections or the strain gauge method are implemented to verify that manufacturer's restrictions are met [21]. Bearing jacking measurements involve a direct and continuous series of measurements facilitated by an arrangement of sensors and measuring instruments (**Figure 10**). This method offers several advantages, including its relative ease of implementation in shaft positions where jacks can be installed without requiring dismantling of the shaft. However, measurements near stern tube bearings may pose challenges. The equipment utilized in this process typically includes:

- Hydraulic jack
- Displacement sensor
- Strain gauge or load cell and
- Analog to digital device for simultaneous measurements and data logging to computer

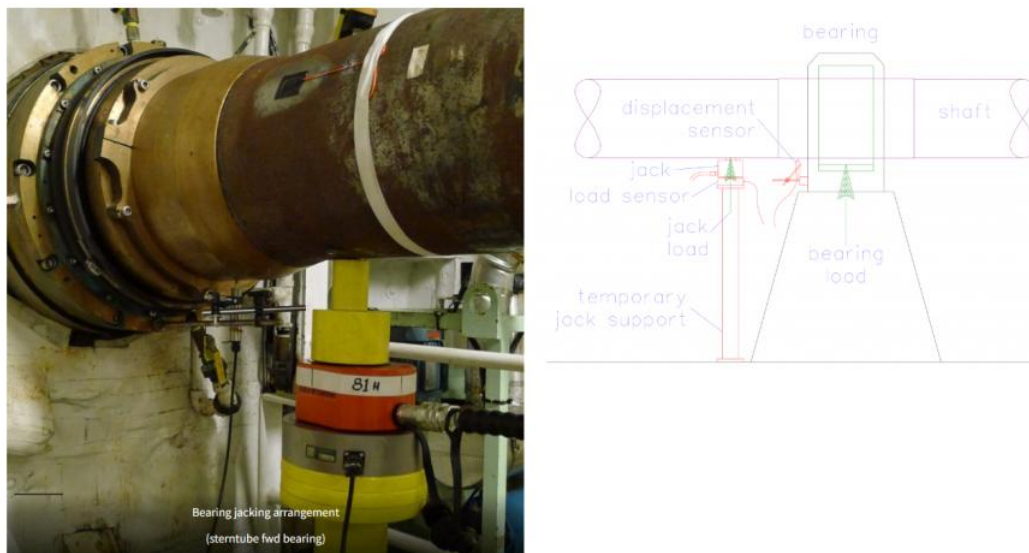


**Figure 10 Shafting bearing jacking and schematic arrangement [22]**

The procedure commences by placing the aforementioned equipment adjacent to the bearing under examination. It's crucial to ensure that the displacement sensor is properly positioned to avoid being influenced by floor plate deformation or bearing rise. As the oil pressure in the hydraulic jack increases, the shaft begins to move upwards until it makes contact with the upper

shell of the bearing. Upon pressure release, the shaft moves downward again. During this process, a set of points, comprising jack lift and jack force, is simultaneously collected. Multiple jacking tests are typically conducted to obtain a more accurate averaged value of the load, thereby reducing systematic measurement errors. Subsequently, the collected data points are plotted (Figure 11). The plotted curve reveals certain key characteristics of the procedure. Initially, both the bearing and the hydraulic jack bear the load, leading to a relatively flat curve segment. This occurs because both components undergo elastic deformation. However, as the shaft moves upwards, contact with the bearing is lost, and the load is solely carried by the hydraulic jack, resulting in a change in the curve gradient. The reverse sequence takes place during the jack-down phase. This transition point is referred to as the breaking point. The resulting curve exhibits a hysteresis phenomenon, meaning that for a given external load, pressure is higher in the jack up than in jack down process due to the unavoidable friction between the cylinder and the rod. Moreover in case of lifting the shaft higher than needed, jack load can suddenly increase (gradient becomes higher) as it will come in contact with the upper shell of the bearing or another bearing maybe is going to be unloaded.

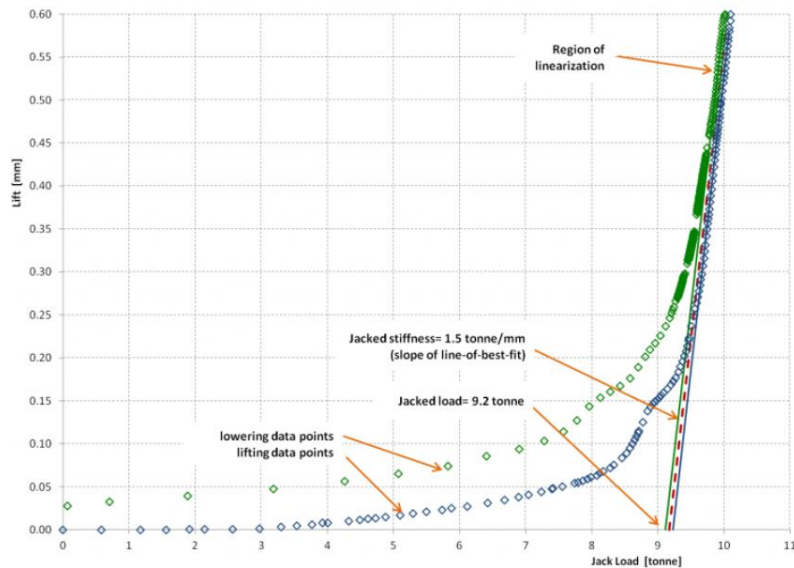


Figure 11: Typical bearing jacking diagram (plot of shaft lift versus jack load) [22]

Since the measurements are done, two steps are needed to calculate the reaction force of bearing in question.

a) From the bearing jacking up diagram, both curves parts above the breaking points are fitted with linear curves, which are then extrapolated downwards until they intersect the horizontal axis. The average of these two loads gives the jack load  $R_J$ . This jack load can be considered as the load of the jack for zero elevation, while the bearing in question has been removed.

b) The bearing load  $R_B$  and jack load  $R_J$  are linked by the correction factor  $C_f$ , thus:

$$R_B = C_f \cdot R_J$$

Correction factor is calculated as:  $C_f = -\frac{I_{BB}}{I_{BH}}$ , where:

$I_{BB}$  : is the bearing's influence number, while jack is considered as supporting point

$I_{BJ}$  : is the influence number of the bearing to jack supporting point

The relations above have arisen from jack up test, considering the following procedure is performed: hydraulic jack is set next to the bearing without carrying any load and then moves upwards by an amount  $\delta$  until shaft-bearing contact is lost. At that moment jack carries the load  $R_J$  and bearing is supposed to be removed and afterwards jack lowers by the amount  $\delta$ . During that part bearing support point is lowered by an amount of  $h$ . Bearing support point is then set again and moves upwards by amount  $h$ , until jack load becomes zero. At this point, the bearing load is denoted as  $R_B$ .

In shaft alignment terms, during the process above, the part of hydraulic jack unloading due to bearing move is (1) and the part of bearing loading is (2):

$$R_J + I_{BJ} \cdot h = 0 \quad (1) \quad R_B - I_{BB} \cdot h = 0 \quad (2)$$

By eliminating term  $h$ :

$$R_B = -\frac{I_{BB}}{I_{BJ}} \cdot R_J$$

### 3.2.2) Strain gauge measurement

In situations where not all bearings are accessible for the jack-up test, such as bearings in the stern tube, the strain gauge method is employed to obtain the axial strain from bending moments of the shaft. This is achieved by utilizing the moment equilibrium equation. While this method offers advantages such as the ability to take strain measurements in both static and dynamic conditions, its main disadvantage lies in the time-consuming installation and calibration of equipment. In contrast to jack-up test, strain measurements can be taken both in static and dynamic condition. Additionally, the validity of measurements obtained through this method can be verified by comparing results with those obtained through the jack-up test. Despite its advantages, it's worth noting that this method is not widely adopted, as only a few shipyards utilize it.

#### Wheatstone bridge concept

The Wheatstone Bridge (**Figure 12**) is a classic electrical circuit commonly used in measurement applications. It comprises four resistors arranged in a diamond shape. When used in strain measurements, one of these resistors ( $G_1$  or  $G_3$ ) is replaced by strain gauge. The bridge is connected to a voltage source ( $V_{in}$ ), and a galvanometer is connected between the bridge's midpoints (13 and 24). Strain gauges are sensors that exhibit changes in their electrical resistance in response to applied mechanical strain. When placed on a shaft, these strain gauges can detect deformations or alterations in the shaft caused by applied loads or external forces. As the shaft undergoes deformation due to applied strain, the resistance of the strain gauge changes, leading to an imbalance in the bridge. This imbalance results in a voltage difference ( $V_{out}$ ), which can be measured and correlated to the amount of strain experienced by the shaft



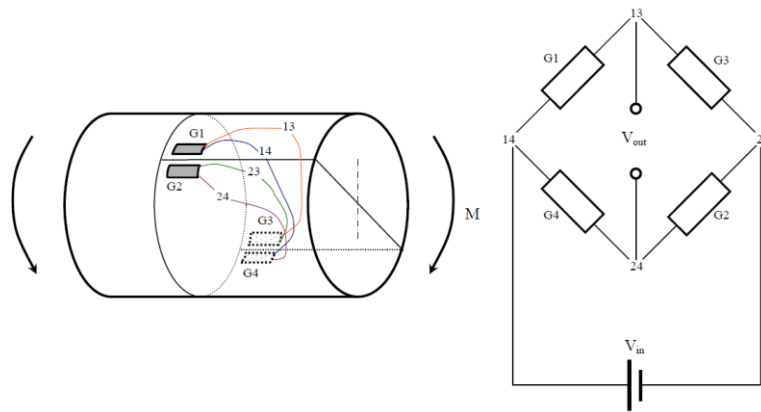


Figure 12: Strain gauge technique for measuring bending moments [21]

Equation of bending moment is below:

$$B = E \cdot \pi \cdot \frac{D_{out}^4 - D_{in}^4}{32 \cdot D_{in}} \cdot \frac{V_{out}}{V_{in}} \cdot \frac{2}{k}$$

where:

- E: Young elasticity modulus of shaft
- $D_{in}, D_{out}$ : inner and outer diameter of shaft
- k: strain gauge constant

## 4) Shaft alignment related topics & Literature overview

### 4.1) Bearing damages

Damages and failures of ship's components can lead to severe consequences for ship, transported cargo and people, accompanied by delays for repair time in dry-dock and economic losses (repair costs, cargo degradation, claims etc.). For these reasons nature of damages must be examined and measures have to be taken to mitigate their root cause. Some of the most usual ship-born equipment damages can be classified in the following four general categories:

1. Ship structure damages
2. Deck equipment and machinery damages
3. Propulsion machinery and diesel generator damages
4. Auxiliary machinery damages

Among these, the shafting system, like any mechanical system on a ship, is susceptible to damage from various sources, both internal and external. According to [28], between 1998 and 2008, one-third of ship problems by cost were attributed to machinery issues, with propulsion claims ranking second after main engine claims. Recent data from article [27] indicate that between 2013 and 2017, approximately 200 ship owners reported shaft bearing failures to ABS. Moreover, an increase in stern tube bearing damages has been noted by insurance group Gard [29], which conducted a thorough examination of frequencies and causes of such damages over the 2013-2022 period (**Figure 13**). During this period, stern tube-related claims primarily involved bulk carriers (27%) and container ships (26%), followed by crude oil tankers and general cargo ships (7% each). The root cause analysis conducted for bulk carriers and container ships is presented in the figure below, shedding light on the factors contributing to these damages and the associated implications for ship operators and insurers.

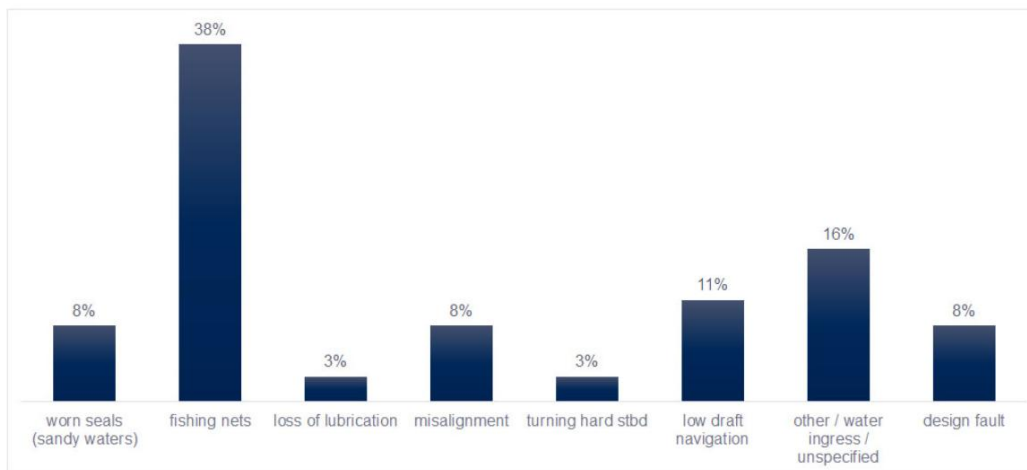


**Figure 13: Root cause investigation for Bulk Carriers and Containerships [29]**

In the event of a ship experiencing such a failure, a series of steps must be taken to address the issue effectively. The vessel needs to be towed to the nearest berth, where the shaft will be disassembled, and orders for new parts will need to be placed. Subsequently, the shaft can be reassembled according to the new shaft alignment plan. However, from a financial perspective, the importance and necessity of proper design, monitoring, and maintenance of the shafting

system become evident due to the high costs associated with repair work after damage. For a small vessel, a failure of the aft stern tube bearing due to misalignment, leading to emergency dry-docking, can result in costs exceeding \$250,000. In contrast, for a large vessel, damage involving a bent shaft requiring replacement can cost in excess of \$1 million [30]. According to [31] the majority of damages occur within a short period from a few minutes to an hour under the respective operating conditions.

Regulations for Environmentally acceptable lubricants (EALs) have also contributed to ASTB damages [7] as there have been reported ASTB overheating cases during mooring trial or at sea trial due to application of the EALs in stern tube. It is noteworthy that at some vessels, such bearing overheating incident disappeared simply after changing the lubricant to mineral oil from EALs.

The following table summarizes the most common types of bearing damages along with brief descriptions, based on references [22], [31], [32], [33], [34] and [35]. Despite the challenge of establishing separate categories due to their interconnected nature, the prevalent bearing damages found in bearings are as follows:

**Table 5: Common types and short description of bearing damages**

Type of bearing damage	Short description
<b>Abrasion:</b>	Very common type, caused by debris rotating along with oil in the lubricant film or insufficient lubrication. These solid particles possibly become embedded in one of the sliding surfaces.
<b>Fatigue: (Figure 14)</b>	Caused by excessive dynamic loads and high levels of vibration, with overheating decreasing white-metal's fatigue strength. Can be avoided by using stronger bearing linings and cautious design.
<b>Scoring / Erosion:</b>	Contaminant particles larger than minimum film thickness embedded into the white-metal layer. Erosion is caused by large quantities of particles in the lubricant smaller than film thickness. Proper filtration and clean lubricant are required.
<b>Wiping: (Figure 14)</b>	One of most common damage type of ASTB (usually at aft region), occurring in any kind of lining material if insufficient lubrication or cooling of the oil takes place, indicating partial or complete loss of hydrodynamic oil film. Then circumferential movement of white-metal takes place whose deposits re-solidificate in oil grooves. Moreover the physical contact of the shaft with the bearing material is reflected by an elevated bearing temperature and in most cases at an exponential rate of rise.
<b>Cavitation:</b>	This kind of damage affects the entire bearing area characterized by cavities, often located in low-pressure zones such as oil grooves or oil holes induced by the implosion of gas or air bubbles released from a lubricating oil film under specific conditions reaching locally pressures up to 220 bar. The risk of cavitation increases with rising of bearing speeds and loads. Sufficient viscosity should be ensured.
<b>Fretting:</b>	Fretting wear takes place when two contacting solid surfaces are subjected to relatively small amplitude oscillatory motion in the order of a few microns. Occurs due to insufficient contact pressure, local welding and tearing having taken place between the bearing back and housing bore.

<b>Design Faults:</b>	Can be avoided had pre-production testing taken place.
<b>Incorrect Assembly:</b>	Typical cases are: incorrect positioning of oil feed connections or incorrect tension of the housing bolts.
<b>Static Fretting:</b>	This can be caused during assembly of the shafting system.
<b>Misalignment:</b>	Causes can be taper-shaped in the housing or journal surface and debris may be trapped between shell and housing. Load concentration on one area of the bearing can cause localized severe wear and high temperature creating that pattern on the surface.
<b>Production Factors:</b>	Geometric inaccuracies may cause damages in regions of the bush. A metallurgical imperfection in the bearing lining.
<b>Electrical Pitting:</b>	A damaged on both shaft and bearing due to poor insulation allowing electrostatic arcing between the two surfaces. It is observed in areas with lowest oil film thickness, which are the least insulated since pose the least resistance. Insulation and grounding of bearings has to be checked.
<b>Thermal Ratcheting :</b>	Caused by the cyclic process of alternate cooling and heating of the bearing, thermal cycling leads to bearing deformation and can be indicated by increased bearing temperature.
<b>Chemical Corrosion:</b>	Sliding area becomes rough and porous and loaded area becomes decolorized. Wear, cavitation and erosion contribute to this phenomenon as well as aggressive oil additives, contaminated oil and high operational temperatures accelerate the chemical process. Corroded bearings have to be changed, and quality oils have to be used.

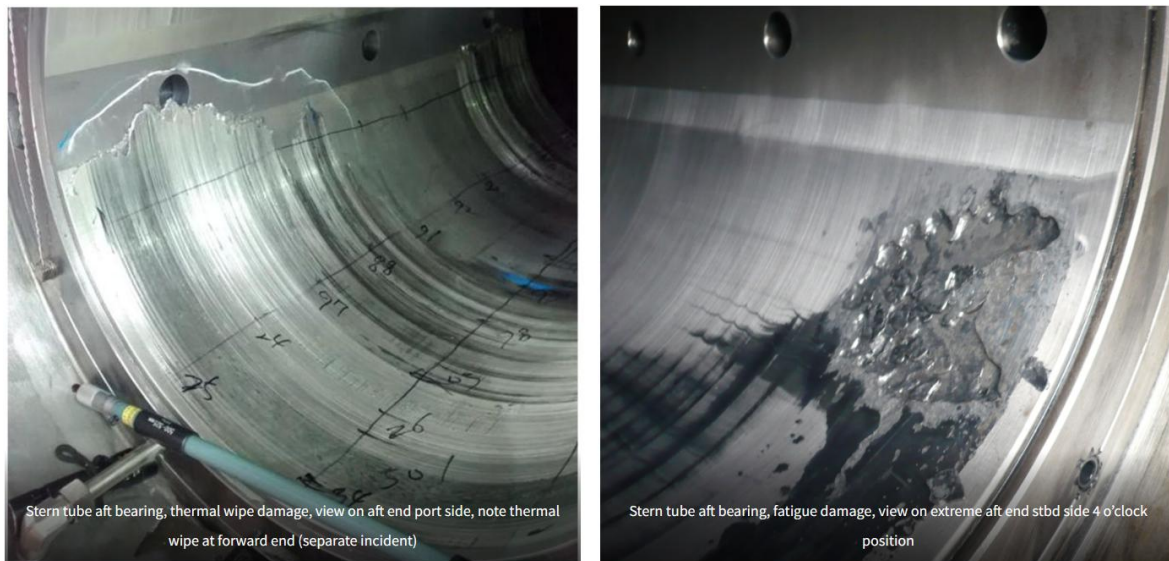


**Figure 14: Thermal wipe damage (left), fatigue damage (right) [22]**

Some of the aforementioned factors contributing to shafting system failures stem from unfavorable bearing load distribution. When one bearing unloads, the load on adjacent bearing(s) increases, potentially leading to dynamic instability of the system [20]. This redistribution of load can result from various factors such as hull deflection and propeller loads, which vary depending on the speed and course of the ship as water flow changes at the propeller disc, especially during transient turning conditions. These propeller loads are induced to the shafting system and influence the magnitude of bearing reaction forces potentially resulting in an exponential increase in local pressures and thermal loading. During these conditions (combination of mixed and

boundary lubrication), sufficient hydrodynamic oil film thickness is difficult to be retained causing an abrupt overheating mainly in the aft most part of the ASTB [31]. According to [16] in the last few years some stern tube bearings of passenger vessels were severely damaged, which often occurred following a sharp course change when sailing in high speeds.

Ships equipped with right-handed propellers are particularly vulnerable to ASTB overheating during starboard turns<sup>9</sup> in the upper speed range, where bearing load and misalignment angle increase. As for main engine bearings [5], damage to the aft most engine bearing during running conditions is primarily caused by wiping due to overload, while damage to the aft most crankshaft bearing is typically related to hammering caused by under-loading. Additionally, static unloading of the second aft most main engine bearing is critical for the engine's performance and may lead to bearing failure due to crankshaft pounding load from cylinder combustion forces [20].

---

<sup>9</sup> Explained in paragraph 4.2.2

## 4.2) Propeller hydrodynamic loads

Aside from the bending moments caused by the weights of the propeller and shaft, propeller lateral forces and moments result from the wake field, which is the circumferentially non-uniform velocity of the water inflow to the propeller, and propeller interaction. These propeller hydrodynamic loads depend on several factors, including hull geometry, ship draught, propeller geometry, engine speed, ship speed, sea state, direction of ship motion, and type of motion path [17]. Quantifying these propeller hydrodynamic forces requires either Computational Fluid Dynamics (CFD) simulations or tank tests for all operating conditions of the vessel. However, performing calculations using advanced CFD is both expensive and time-consuming and it can be challenging to obtain results with sufficient accuracy, leading to uncertainty in the model. As stated in [8], propeller loads, especially during transient phases like vessel turning, are difficult and time-consuming to predict accurately even with the most advanced CFD calculations. Given these challenges and considering the scope of this thesis, a different approach will be followed. While propeller load calculations are essential, they belong to a different scientific field of naval architecture and fall outside the scope of this thesis.

The coordinate system for propeller load components is shown in (Figure 15), where propeller is viewed by stern, meaning that positive x-axis is looking to the stem of the ship, z-axis is looking at the starboard side and y-axis is looking to the deck.

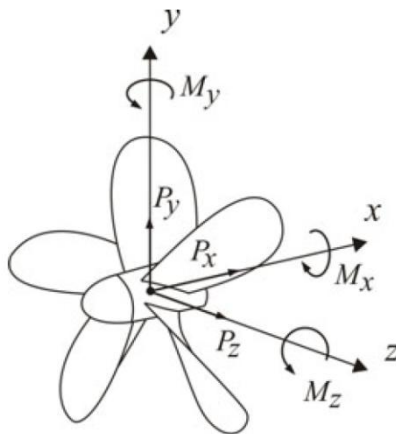
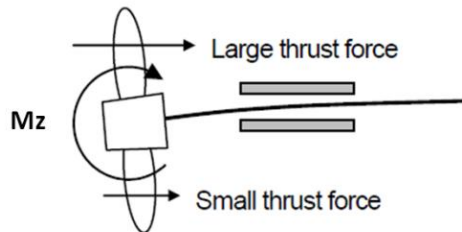


Figure 15: Propeller load components [28]

Among the various operating conditions of a ship, three are particularly significant: the straight ahead course, port turn, and starboard turn. Each of these conditions induces changes in the wake field of the propeller, resulting in varying propeller hydrodynamic forces that exert forces and moments on the shafting system. **According to China Classification Society experience [7], propeller hydrodynamic loads can be simply simulated by application of the moment  $M_z$  as  $\pm 30\%$  of the nominal propeller torque ( $Q$ ).** It is also stated that this assumption is based on several successful solutions to bearing failure cases and is valid for conventional tankers, bulk carriers and container ships letting the designer be on the safe side of calculations. Furthermore, it is important to note that there is no universally recognized method for computing propeller loads specifically for shaft alignment calculations [4].

### 4.2.1) Propeller loads during straight ahead course

The center of propeller mean thrust force is different from the actual center of the propeller due to the non-uniformity of distribution of the ship's wake. When propeller blade rotates in the wake field, generates a larger thrust force in the upper side of the propeller center than in the lower side. This leads to the generation of an eccentric thrust that acts on the propeller, resulting in the generation of a vertical bending moment,  $M_z$  with a direction as illustrated below:



**Figure 16: Bending moment due to hydrodynamic propeller forces in the straight run condition [21]**

In general the bending moment,  $M_z$ , can be said to be a kind of “safety enhancing” moment, because acts so that edge loading on the aft portion of aft most bearing may be reduced. According to NK Class [21] it is acceptable to take this upward moment by eccentric thrust force into account when performing calculations for the hot condition.

A typical wake field of a 10,000 TEU containership with conventional single propeller in straight ahead condition has a pattern as in (Figure 17), where it can be observed that axial velocity in the upper part of disc is slower (blocked flow by hull), so greater thrust is developed when blade is in the upper part of its orbit. Except from the axial part of velocity, tangential velocity also contributes to the resultant force. When blade of a clockwise rotating propeller moves in the starboard side of the disc, greater thrust is developed, since blade moves against the tangential velocity. That generation of forces can be approached by the propeller blade foil velocity triangle (Figure 18).

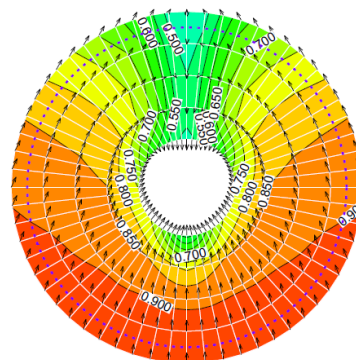


**Figure 17: Nominal<sup>10</sup> wake distribution at the propeller disc during straight run [11]**

<sup>10</sup> The nominal wake field is the wake field that would be measured at the propeller plane without the presence or influence of the propeller modifying the flow at the stern of the ship. If this field is altered by the presence of propeller is called effective wake.

The inflow angle for the propeller blade section is  $\theta - \beta$ , where:

$$\theta = \tan^{-1} \frac{P(r)}{2\pi r} \quad \beta = \tan^{-1} \frac{V}{\omega r}$$

Since  $\theta$  does not change and for constant  $\omega r$ , reduction of  $\beta$  results higher produced lift by that blade section. Except from produced lift creating thrust, drag of each section contributes to vertical and horizontal hydrodynamic forces end moments.

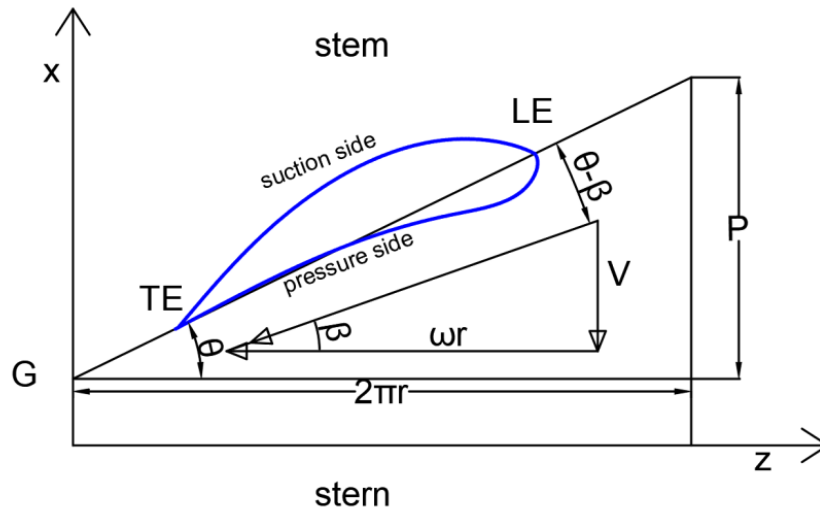


Figure 18: Velocity triangle for a blade section

#### 4.2.2) Propeller loads during maneuvering

When propeller operates in uniform flow in the direction of circumference, only thrust and torque are generated. In reality propeller faces a non-uniform flow due to the presence of the hull in front and for that reason, besides thrust and torque, forces and moments are developed [15]. Alternation of speed or course of ship can influence the propeller hydrodynamic loads, particularly on the aft stern tube bearing, as water flow changes [16]. For shaft alignment-sensitive ships, such as those without a forward stern tube bearing, these forces and moments have a more evident effect on the ISB loading when compared with traditional shafting systems with two stern tube bearings, mainly because of the longer bearing span [8].

During starboard turning the centre of effective thrust shifts lower in the propeller disc causing downward bending at the end of the propeller shaft that has same direction as that generated by propeller weight. By examining the matter in a hydrodynamic view, this effect is mainly created by the cross flow (the tangential component of flow) which is directed from portside to the clockwise rotating propeller (and is free from the effect of the skeg). The cross flow locally increases the circumferential flow component at the propeller blades in the lower and port part of the propeller disc (where blades move counter to the cross flow direction) and decreases in the upper part of the disc (where blades move in the same direction as the flow) [16], [11]. During port turn the sign of the eccentric thrust load is the same as in the straight ahead course (above disc center), meaning it is opposite to the moment produced by propeller weight. In this case the tangential



component of flow has the opposite direction of the propeller rotation in the upper and starboard side, so there is the highest angle of attack according to the direction of the tangential flow. For left-handed propellers, apply the same as right-handed for straight ahead course, while the opposite for turning conditions in respect to vertical bending moments due to thrust vertical eccentricity.

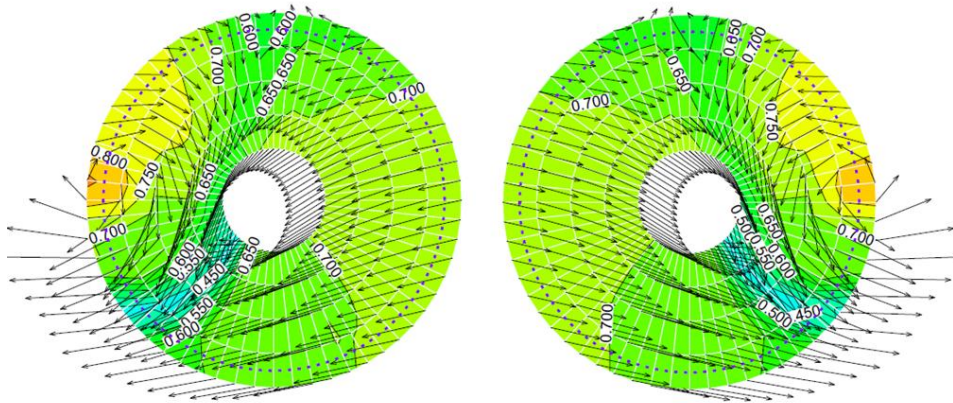


**Figure 19: Nominal wake distribution at the propeller disc during port turn (left) and starboard turn (right) [11]**

The effect of rudder turn can be shown in the position of aft stern tube bearing loading. During starboard turns, meaning propeller is pushed downwards, the contact of shaft and aft stern tube bearing is at its aft part. During port turns, meaning propeller is pushed upwards, that contact moves towards the forward part of the bearing [19].

**The consideration of propeller bending moment  $M_z$  as  $\pm 30\%$  of the nominal propeller torque will be involving all three cases (straight ahead course and turns). However a value of  $M_z$  cannot be matched to an exact condition. However straight ahead values correspond to negative percentages, while positives value to starboard turns.**

### 4.2.3) Experimental and numerical studies of propeller hydrodynamic forces in relation to shafting system

Technical paper [19]

In order to get a view of that phenomenon, a diagram from a Bureau Veritas [19] technical paper is presented (**Figure 20**). Through quasi-static and dynamic behavior analysis, they examined a vessel with 33,000 kW propulsive power, a 50-ton propeller and a 700mm shaft diameter. Sensors were strategically placed along the shafting system to capture shaft line deflections during different operating conditions. Sensors were placed at key positions of the shafting system for obtaining the shaft line during straight ahead in full power and 10° deg starboard and port turn in 90% of full power. Shaft line's deflections in vertical plane, for the aforementioned conditions, are presented below:

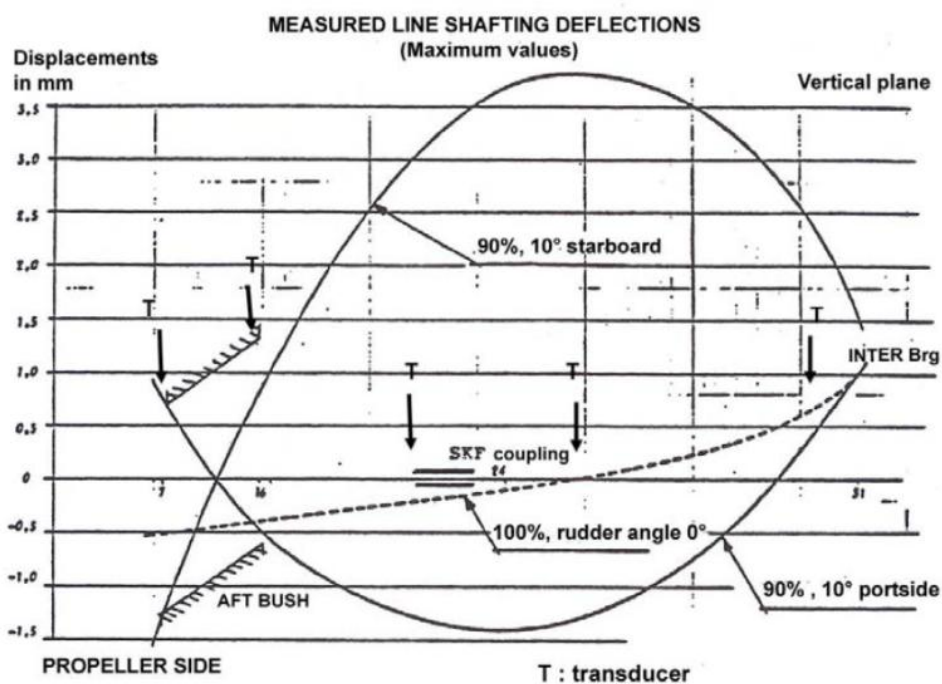


Figure 20: Shaft line's deflection measurements in vertical plane [19]

It is clear how the shafting line deflects during the 3 examined quasi-static cases. Hydrodynamic forces found are below:

Table 6: Mean values of hydrodynamic forces [19]

Rudder angle	0°	10° port	10° starboard
% of output	100	90	90
Fz (t)	-7	0	20
Fy (t)	3	35	15
Qz (t.m)	67	153	-270
Qy (t.m)	73	0	-15

Propeller hydrodynamic loads affect the shafting system in transverse direction as well (**Figure 21**).

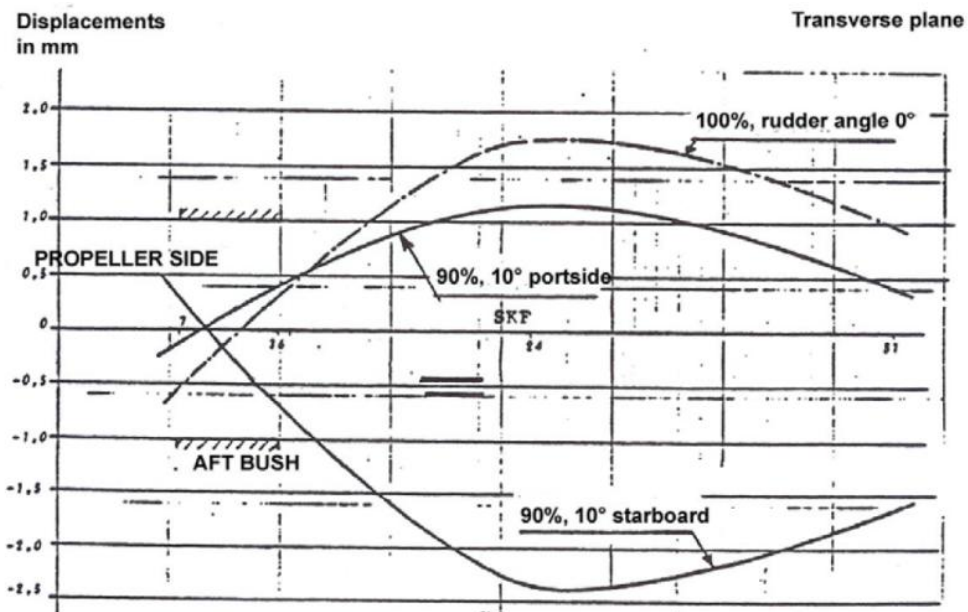
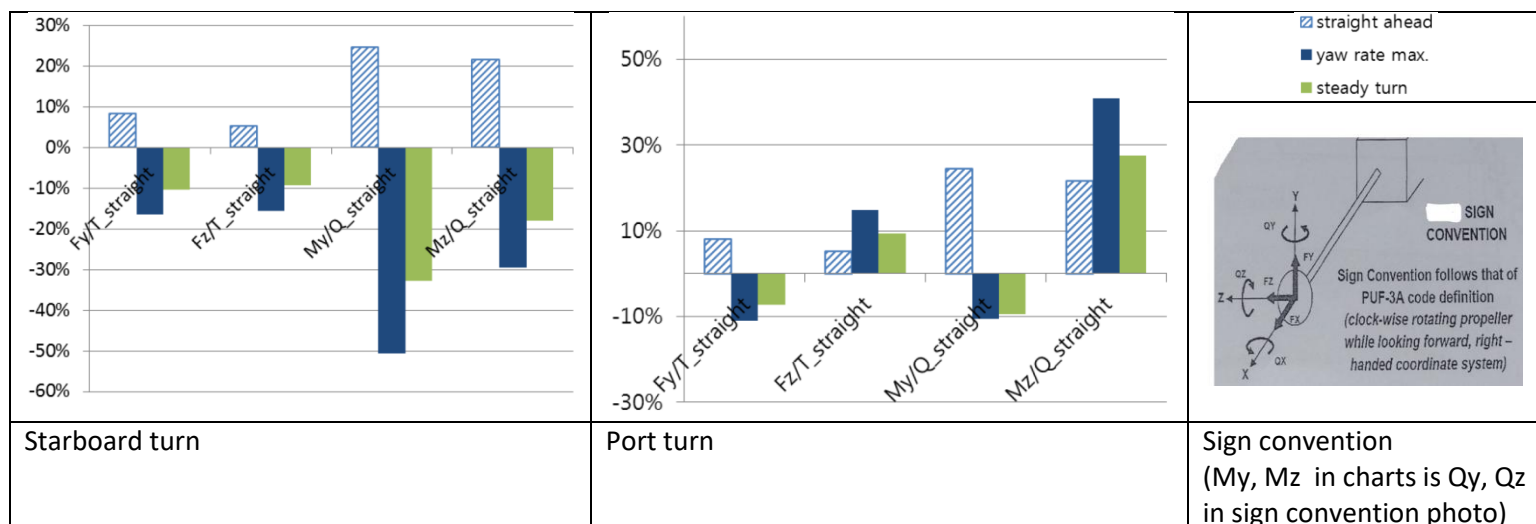


Figure 21: Shaft line's deflection measurements in transverse plane [36]

### Technical paper [11]

One more insightful study is [11], where propeller hydrodynamic forces of a 10,000 TEU container ship were calculated using numerical modeling (STAR-CCM+). The propeller shaft forces during the turning test were calculated in the flow field reproduced by the maneuvering simulation, based on the sea trial data of similar vessel, using the quasi-steady approach of Kuroiwa et al (2007) to capture the flow angle against the propeller plane at a specific instant during turning. The velocity inlets were introduced as boundary conditions of the side planes to consider the oblique flow into the propeller during turning. Results are presented below:

Table 7: Propeller Lateral forces and moments for starboard and port turn



Regarding vertical bending moment  $M_z$ , from diagrams above, the following is observed:

- When ship is in straight run,  $M_z$  pushes propeller cantilever upwards.

- When ship turns to port, Mz keep sign as straight ahead and increases.
- When ship turns to starboard, Mz changes sign and pushes propeller cantilever downwards

### Technical paper [8]

There has been an innovative experimental study (Smart Bearing Sensor) [8] on the shafting system of a 36,700 t DWT Chemical/Product Carrier with MCR of 9480 kW at 127 rpm in which strain gauges and displacement sensors were placed on intermediate bearing, capable of measuring bearing's house deformations while shaft was in static and in dynamic operational condition (steady and transient), thus converting it in a weighting machine. Data from sensors were collected and through a reverse calculation analysis, bearing loads and stern tube bearing-shaft misalignment angle could be calculated. Ship performed a series of maneuvers in a range of propeller rpm. Results are presented below:

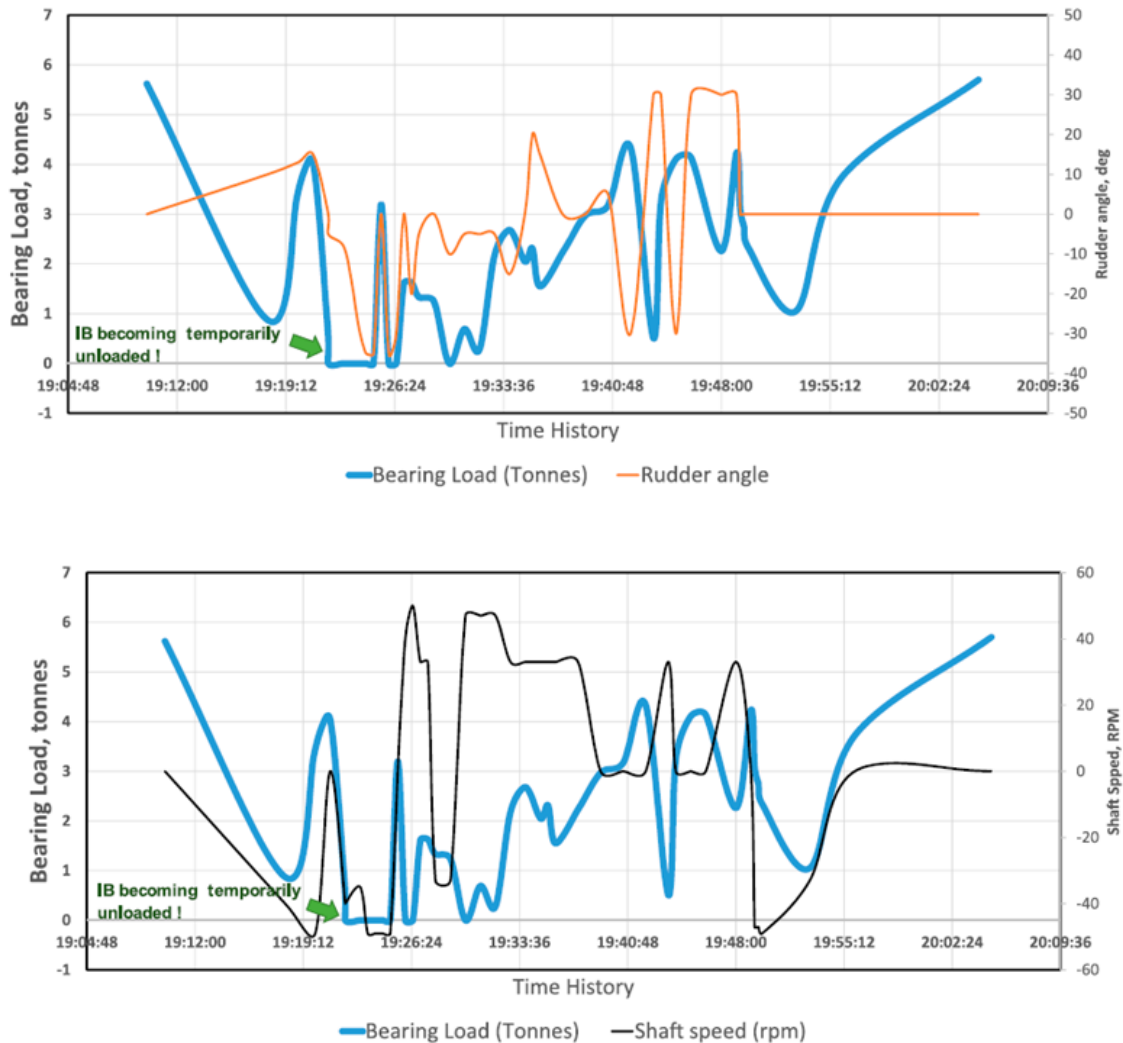


Figure 22: Intermediate bearing load depending rudder angle and ME rpm [8]

The experiment's results reveal that the intermediate bearing experienced temporary unloading three times during the sea trial. This occurrence coincided with a propeller moment of 232 kNm, exerting a downward force on the propeller (**Figure 22**). Moreover misalignment angle in stern tube bearing during vessel maneuvering was 0.550 mrad while in hot static condition was 0.297 mrad (typical upper limit is 0.3 mrad).

By examining bearing forces the following observations can be made:

- Propeller hydrodynamic forces are modeled solely with a vertical bending moment.
- The bending moment during unloading (232kNm) is equal to 32% of shaft torque when M/E operates at MCR.
- Propeller hydrodynamic forces affect ASTB, ISB and two aft most main engine bearings, while the rest bearing reactions practically are not affected.

	Bearing Reactions [Tonnes]		Redistributed Weight [Tonnes]
	Hot Static condition - Shaft Alignment Calculations Model	Unloaded Intermediate Bearing - During Vessel Manoeuvering	
PROPELLER MOMENT	0	232kNm	
aft sterntube bearing	62.55	66.46	3.9
intermediate bearing	5.26	0.00	-5.3
Aftmost Main Engine bearing	8.43	13.47	5.0
Main Engine bearing 7	9.66	5.90	-3.8
Main Engine bearing 6	27.39	27.49	0.1

**Figure 23: Bearing loads redistribution during vessel maneuvering through reverse calculation [8]**

#### 4.2.4) Propeller loads during partial propeller immersion

Occasionally ships have to operate with their propeller partially immersed or with propeller being quite close to free surface which is an off-design condition. Such cases are [36]:

- Vessel going in/out of dry-dock<sup>11</sup>
- Low cargo load
- Phasing in/out trading areas with limiting factor (e.g. port restrictions, minimum water depth)
- Rough sea condition

Aforementioned operations cannot always be avoided and can pose an additional risk for the shafting system, especially when suitable precautionary measures of power limitation and rudder angle are not taken. Under such exceptional operating condition, an excessive thrust force creates downward bending moment on the shaft, resulting in edge loading on ASTB, increased misalignment angle, torsional vibrations and possibly bearing unloading. A conventional screw

<sup>11</sup> Many shipyards (especially in China) are located in shallow waters compelling large vessels to sail for substantial distances at very light ballast draught before entering deep waters.

propeller has been designed to operate far from the free surface in order free surface effects to be minimized, otherwise that interaction causes ventilation. Specifically MARPOL defines propeller tip to be 600 mm beneath free surface during all loading cases included in vessel's loading manual. As per ABS [20], it is suggested to operate vessels with a propeller partially immersed at low speeds, limiting maneuvering to the minimum rudder angles required for safe navigation and use of tugs. The additional bending moment generated is a function of the degree of lack of immersion, RPM and shaft power. In other words is proportional to thrust force, so it is proportional to square of RPMs. The literature addressing that phenomenon and its effect on shaft alignment is relatively more limited compared to straight ahead and turning conditions and there is no generic statistical formula for loads acting on the shaft. Nonetheless, it is possible to make logical assumptions to construct a simplified model of hydrodynamic propeller loads during the partial immersion of the propeller.

Valuable information can be derived from article [37] where results from open-water tests for a four-blade right-handed propeller are presented and analyzed. This is a model of a modified KP458 propeller used in a KVLCC2 where a six-component dynamometer was placed to acquire forces during test for different advance coefficients and submergence ratios. The way to define a specific condition of propeller position is the submergence ratio parameter:  $h/R$ , where  $h$  is the vertical distance between free surface and propeller shaft center and  $R$  is the propeller radius. So when propeller is immersed and tip touches free surface  $h/R=1$ , when not immersed and tip touches free surface  $h/R=-1$  and when propeller is semi immersed  $h/R=0$ . It is used a right handed coordinate system for propeller forces, where the bow direction is positive x-direction, starboard direction was positive y-direction and downward direction was positive z-direction.

From dynamometer measurements it was found that propeller undergoes a disparity in thrust between its lower and upper part. Evidently, only the submerged part is capable of generating thrust, thereby there is an eccentricity resulting in moment  $M_y$  about the transverse axis. This thrust eccentricity denotes the distance by which the thrust line is away in the radial direction from the center of shaft axis within the propeller plane. According to the article, the specific location of thrust eccentricity is illustrated in **(Figure 24)**. Vertical eccentricity of thrust is calculated as  $ecc_{vertical} = -M_y/F_x$ , where  $F_x$  represents the thrust produced by propeller. There is also transverse thrust eccentricity, which does not affect the degree to which shaft bends in the vertical plane in 1D FEM model.

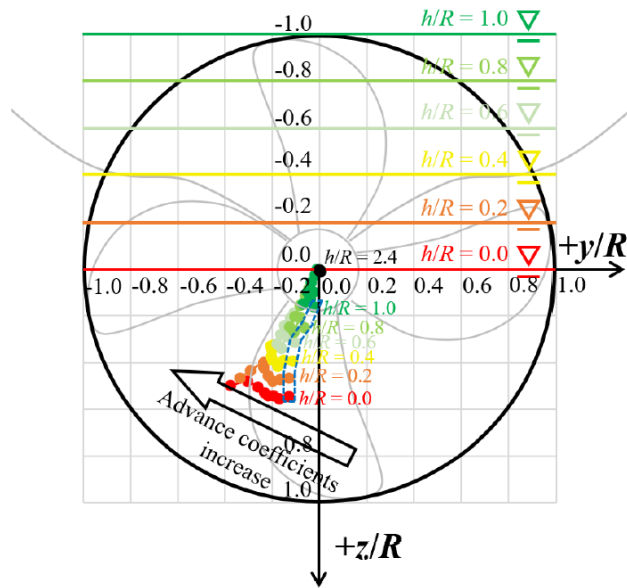


Figure 24: Location of thrust eccentricity with respect to submergence ratio and advance coefficient [37]

It is evident from diagrams of (Figure 25) that as the ratio  $h/R$  decreases,  $K_{my}$  reaches higher values until it starts to drop below  $h/R=0.4$ . Despite the greater difference in submerged area at the lowest  $h/R$  values, the largest  $K_{my}$  occurs at  $h/R=0.4$ . This phenomenon is attributed to the Wanger effect, suggesting that when a blade in the air abruptly enters the water, only half of the original lift is momentarily generated, and the lift gradually recovers with time. The decline in  $K_{my}$  below  $h/R=0.4$  is attributed to a reduction in thrust due to the decreased submerged area.  $K_{my}$  is defined as y-direction propeller bending moment coefficient and equal to  $M_y/\rho n^2 D^5$ , where  $\rho$  is water density,  $n$  propeller's rate of revolution and  $D$  propeller diameter.

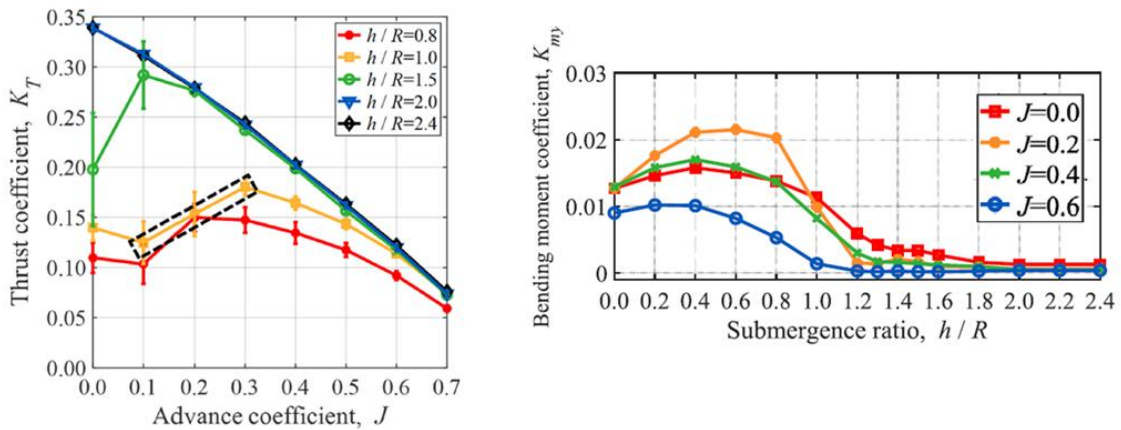


Figure 25: Thrust and bending moment coefficient for different  $h/R$  and  $J$  values of POW test [37]

Except from the difference in propeller hydrodynamic loads, partially submerged propeller means less submerged volume, resulting in less buoyancy force. Consequently propeller will seem heavier for the shafting system.

## 5) Numerical modeling & utilized software

### 5.1) Shaft alignment tool

The Shaft Alignment Tool (*shaftAlignment\_bending\_moment.exe*) is a simple program utilized to calculate bearing reaction forces and compute influence factors for a given shaft under specific vertical loads and moments applied at nodes. The software is created and developed in the department of Marine Engineering of School of Naval Architecture and Marine Engineering of National Technical University of Athens (NTUA) and its workspace is shown in figure (Figure 26).

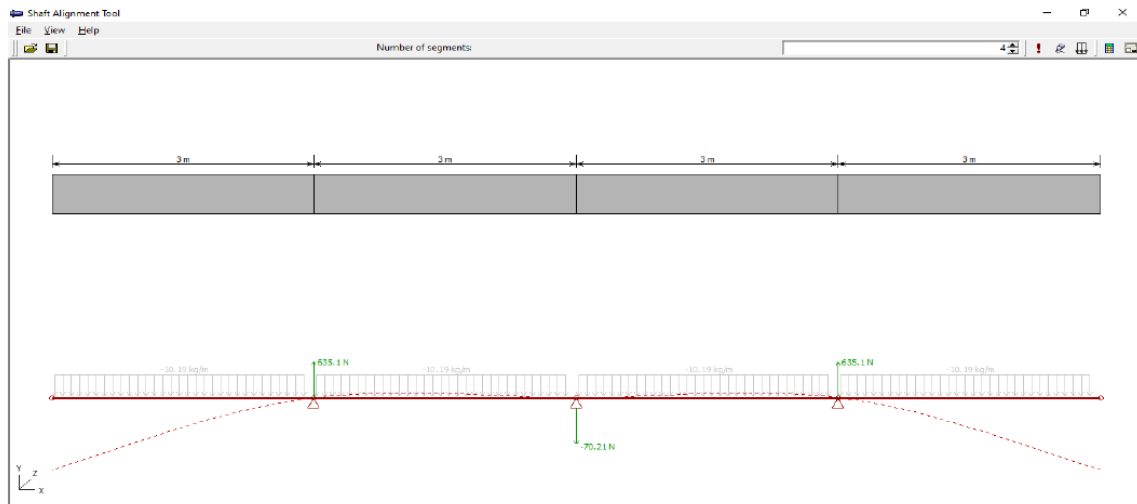


Figure 26: Shaft alignment tool workspace

In this program user is able to define the number and properties of shaft segments (length, distributed load, moment of inertia, Young modulus) (Figure 27) and set nodes between them to be constrained at a specific offset or to be free. A constrained node represents the vertical position of a bearing. External loads (forces and moments) are applied on nodes. All these input data are enough to construct the stiffness matrix and load vector of system. Then results can be found at a specific tab of the workspace including: RIN (Figure 27), bearing reactions, nodes displacements and slope (Figure 28).

For the purpose of this thesis, a Matlab code was developed, able to read any .sft file in an automated way<sup>12</sup>, perform desired changes such as node movement and external load application, run the program, read results file (Figure 29), storing necessary outputs of each iteration and presenting them altogether in a suitable form.

<sup>12</sup> Input file of Shaft Alignment Tool is a txt file including key words and numbers which is saved as .sft file.



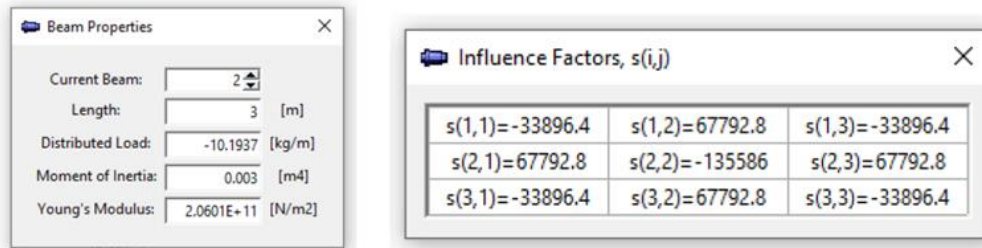


Figure 27: Beam properties of a segment and Influence factors table

Shaft Model - Analysis Results

Model Data						
Nodes						
Node No	Coord. X (m)	Coord. Y (m)	Coord. Z (m)			
1	0	0	0			
2	3	0	0			
3	6	0	0			
4	9	0	0			
5	12	0	0			
Beam Members						
Member No	Length (m)	Distr. Weight (kg/m)	Total Weight (kg)	Moment of Inertia (m4)	Young's Modulus (N/m2)	
1	3	-100	-300	0.003	2.0601E+11	
2	3	-100	-300	0.003	2.0601E+11	
3	3	-100	-300	0.003	2.0601E+11	
4	3	-100	-300	0.003	2.0601E+11	
Forces						
Node No	Fx (N)	Fy (N)	Fz (N)	Mx (Nm)	My (Nm)	Mz (Nm)
1	0	-1.16529E-12	0	0	0	9.37916E-13
2	0	635.105	0	0	0	3.41061E-13
3	0	-70.2098	0	0	0	1.7053E-13
4	0	635.105	0	0	0	-3.41061E-13
5	0	-5.68434E-14	0	0	0	-2.27374E-13
Displacements						
Node No	Ux (m)	Uy (m)	Uz (m)	Rx (rad)	Ry (rad)	Rz (rad)
1	0	-3.08408E-06	0	0	0	1.20063E-06

Figure 28: Analysis results

## 5.2) Bearing hydrodynamic lubrication theory and tool

Before the presentation of the Reynolds solver, a short description of journal bearings and their interaction with rotating shaft will be given.

### 5.2.1) Journal bearings

Journal bearings are the simplest type of radial bearings, widely used in maritime industry. Their main advantages are: simple and high precision constructions, increased robustness and lifespan due to beneficiary hydrodynamic lubrication and high load capacity combined with good absorption and damping characteristics. In these bearings, the stator is a plain hollow cylinder, while the rotor (shaft) lies on the inner surface of the bearing. Between the stator and the rotor, there is a small clearance, usually filled with lubricant and a cross section of a typical journal bearing is in (Figure 29). The principles governing hydrodynamic lubrication phenomenon of journal bearings are:

1. The rotor begins to rotate within the stator, therefore lubricant is dragged along the perimeter of the shaft.
2. Lubricant is forced to enter a converging (wedge-like) geometry between the stator and the rotor.
3. Given the fact that the lubricant is incompressible, it develops pressure, thus lifts the shaft over the bearing, preventing a “dry-friction” situation caused by metal to metal contact.

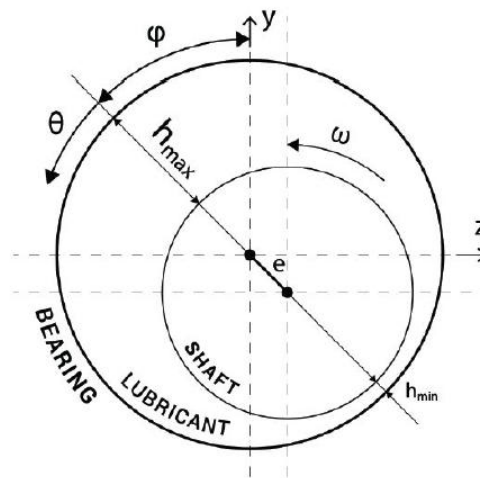


Figure 29: Cross section of a typical bearing geometry

### 5.2.2) Principles of hydrodynamic lubrication

For examining hydrodynamic lubrication principles, firstly a problem similar to that of a shaft within a journal bearing has to be defined. A **shaft of diameter (d)** is rotating inside the inner surface of a **hollow cylinder of diameter (D)**, where  $D > d$  and the quantity  $D - d$  is **bearing clearance (c)**. Furthermore, the space between the two surfaces is filled with sufficient amount of lubricant with defined properties. As illustrated in (Figure 30), during steady state operation (constant rpm), shaft rests slightly off center in comparison to the bearing. There is a point along the circumference where distance between the two surfaces becomes minimum. This offset is interpreted using three variables:

- **Attitude angle ( $\phi$ ):** The angle where minimal distance between the two surfaces occurs.
- **Eccentricity ( $e$ ):** The off-center distance along the radius at attitude angle.
- **Eccentricity ratio ( $k$ ):** The ratio of eccentricity over the radial clearance.

When  $k=0$ , journal and the bearing are concentric, while when  $k=1$  there is journal-bearing metal contact.

To further simplify the analysis of the problem, the inner bearing surface can be considered as if it had been cut along its length and un-warped on a flat surface (**Figure 30**). In the same fashion the same mental abstraction can be made for the shaft, preserving the distance between stator and rotor. Consequently, there are two surfaces facing each other and forming a converging geometry (**Figure 31**). In this converging region, the shaft and bearing distance decreases as the circumferential coordinate increases, until it reaches its minimum at the **attitude angle ( $\phi$ )**. Beyond this point, a diverging region is formed where the exact opposite takes place. Since the gap between the two surfaces is filled with lubricant, the minimum distance point corresponds to the minimum oil film thickness.

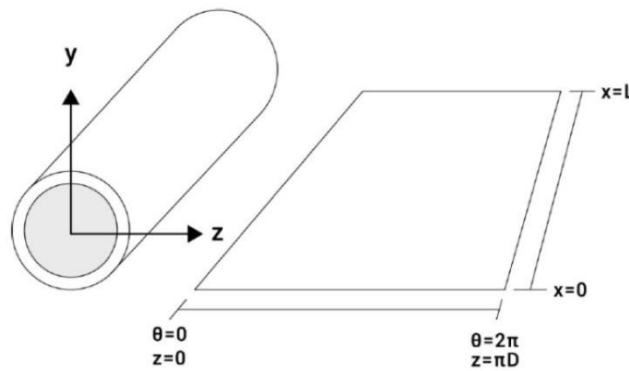


**Figure 30: Un-warped bearing geometry**

In journal bearings, pressure is developed by means of hydrodynamic lubrication, where the build-up pressure of the lubricant, initially separates and then, keeps the two surfaces apart.

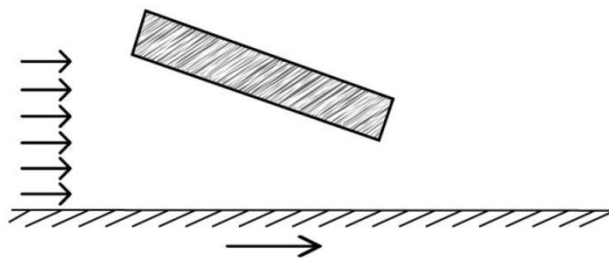


**Figure 31: Converging geometry of journal bearing**

The phenomenon was examined by Reynolds, who made the following assumptions:

- Gravitational forces can be ignored in comparison with the viscous forces
- The pressure is constant through the thickness of the film
- The curvature of the surfaces is large compared with film thickness
- There is no slip between the fluid and the solid surface
- The lubricant is a Newtonian viscous fluid
- Lubricant flow is laminar (steady-state condition is assumed)
- Inertia induced forces can be neglected compared to viscous forces
- Lubricant viscosity remains spatially constant (iso-viscous condition)

The mathematical expression governing hydrodynamic lubrication is called the Reynolds equation, derived from the Navier-Stokes equations with the application of the aforementioned assumptions. In order for hydrodynamic lubrication to come into effect, relative angular velocity must not be zero. The reason why oil builds pressure is the converging (wedge-like) geometry. Reynolds' equation also describes the geometry's influence on the spatial gradient of the pressure and is the following:

$$\frac{U}{2} \cdot \frac{\partial h}{\partial z} = \frac{1}{\mu} \left[ \frac{\partial}{\partial z} \left( \frac{h^3}{12} \cdot \frac{\partial p}{\partial z} \right) + \frac{\partial}{\partial x} \left( \frac{h^3}{12} \cdot \frac{\partial p}{\partial x} \right) \right]$$

Where,

- U: is the tangential velocity of the shaft
- $\mu$ : is the lubricant dynamic viscosity
- h: is a function that describes the oil film thickness in 3D space
- p: is the pressure distribution in 3D space

As shaft rotates, oil is dragged into the wedge volume. In order for mass to be conserved along the flow direction, as the wedge converges, a gradient of pressure is generated. Pressure increases at the beginning of the wedge, restricting flow. On other hand, pressure decreases near the end of the wedge, thus boosting outflow. The existence of a pressure gradient causes the fluid velocity profile to bend inwards at the entrance and to bend outwards at the exit. Boundary conditions are required to solve Reynolds' equation. In the case of a journal bearing, the boundary condition at an end of the bearing is simply that the oil film pressure is equal to ambient air pressure, because the boundary of the oil film at the end of the bearing is clear-cut. Of all the boundary conditions proposed, the most notable are:

- **Sommerfeld's boundary condition** assumes that pressure is equal to zero at the edges of the un-warped bearing geometry. The converging section of the geometry develops positive pressure distribution, while the diverging section develops a similar negative pressure distribution. The above analysis concludes that total pressure is equal to zero, thus the lubricant is not capable of supporting any weight. This condition is unrealistic.
- **Gümbel's boundary condition** (also known also as half Sommerfeld's condition) assumes that pressure distribution at the converging section is identical to the one given by Sommerfeld condition. In contrast, pressure distribution at the diverging section is equal to zero. This boundary condition leads to inaccurate results, because it is violating mass conservation in the diverging part of the bearing.

- **Reynolds' boundary condition** (also known as Swift–Stieber's condition), assumes that the oil film terminates at a certain position ( $\phi = \pi + \delta$ ) at which both the pressure and pressure gradient are zero, simultaneously. This condition eliminates a discontinuity of oil flow at  $\phi = \pi$ , a physical contradiction involved in Gümbel's condition.

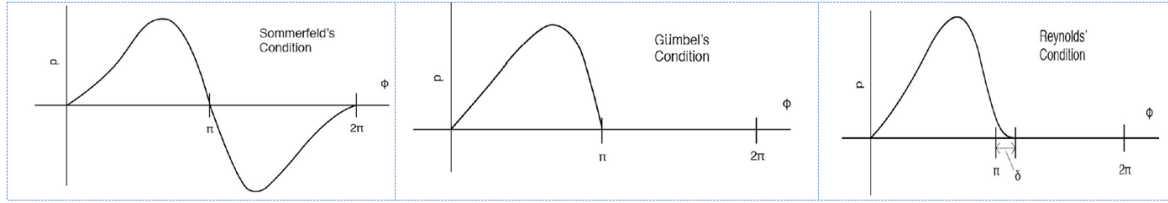


**Figure 32: Boundary conditions for the oil film**

**Reynolds' boundary condition gives more accurate results than the two other boundary conditions.**

### 5.2.3) Operational and Performance Parameters

#### Load Capacity

The hydrodynamic load carried by the oil film can be calculated by integration of the lubricant pressure along the circumference and length of the outer shaft surface and can be further broken down into a pair of vertical ( $W_y$ ) and horizontal ( $W_z$ ) components, where are calculated as:

$$W_y = \int_0^{2\pi L} \int_0^L p \cdot \sin\left(\varphi + \theta - \frac{\pi}{2}\right) \cdot R \cdot dx \cdot d\theta$$

$$W_z = \int_0^{2\pi L} \int_0^L p \cdot \cos\left(\varphi + \theta - \frac{\pi}{2}\right) \cdot R \cdot dx \cdot d\theta$$

$$W = \sqrt{W_y^2 + W_z^2}$$

#### Sommerfeld Number

The Sommerfeld number is a non-dimensional characteristic bearing parameter and is a dimensionless quantity, as long as consistent units are used (i.e. S.I.). It comprises both design ( $R$ ,  $c$ ,  $L$ ,  $D$ ) and operating ( $\mu$ ,  $\omega$ ,  $W$ ) parameters. For a given bearing, the larger value of Sommerfeld number is, the less severe is the loading of the bearing and vice versa. All bearings operating at the same Sommerfeld number have same operational characteristics and equal non-dimensional parameter values. Sommerfeld number is given by the following formula:

$$S = \left(\frac{R}{c}\right)^2 \cdot \frac{\mu \cdot \omega \cdot L \cdot D}{W}$$

Where,

- $R$ : is the shaft radius
- $c$ : is the radial bearing clearance
- $\mu$ : is the dynamic viscosity of the lubricant
- $\omega$ : is the rotational speed of the shaft

- L: is the bearing length
- D: is the bearing diameter
- W: is the total, externally applied, load

#### Friction Force and Friction Coefficient

One of Reynolds' assumptions demanded that the lubricant is a Newtonian viscous fluid, whose viscosity cannot be neglected. An implication of this assumption is that shear stresses are present at the shaft-lubricant interface. The integral of these shear stresses gives the total friction force.

$$F = \int_0^2 \int_0^{\pi D} \left( \frac{2y-h}{2} \cdot \frac{\partial p}{\partial z} + \frac{U}{h} \right) \cdot dx \cdot d\theta$$

**Friction coefficient ( $f^*$ )** can be defined as a ratio of friction force over total bearing load:

$$f^* = \frac{F}{W}$$

#### Power Loss

As a consequence, friction forces produce power losses. If shaft was able to transmit the full amount of power available to the propeller, there wouldn't be any power losses. That is not the case though. Some of the transmitted power is taken away by friction in each support bearing. Friction power loss of a bearing can be calculated using the following formula:

$$P_{loss} = F \cdot U = W \cdot f^* \cdot \omega \cdot R$$

### 5.2.3) Bearing hydrodynamic lubrication tool

For shaft-bearing interaction an in-house Reynolds solver was utilized, created in a previous diploma thesis [38] and was further developed by Laboratory of Marine Engineering of NTUA. A short program description will be given [32]. Input values for the algorithm are geometric parameters of the journal bearing (L, D, c, rpm, misalignment angles etc.), solver parameters (grid meshing, solver selection, convergence criteria etc.) and applied bearing vertical and horizontal loads, all included in an input file.

```

2_Test_journal_bearing_REYNOLDS_open_with_notepad.brg - Σημειωματάριο
Αρχείο Επεξεργασία Μορφή Προβολή Βοήθεια
Solution type: 1: STEADY, 2: Transient (solveInTime()), 3: SIMPLE SOLVE , 4-100: Test case mode
1
Thermal Analysis: 1: Isothermal, 2: Isoviscous Thermal, 3: THD
1
Parallelization type 1: SINGLE CORE, 2: OPEN MP (add also number of cores), 3: CUDA
1 4
Equilibrium type 1: EQUILIBRIUM_ESTIM, 2: EQUILIBRIUM_ESTIM_AND_SOLVE, 3: EQUILIBRIUM_ESTIM_AND_CALC, 4: EQUILIBRIUM_CALC
4
Calculate stiffness/damping: 1: NO, 2: STIFFNESS ONLY, 3: STIFFNESS AND DAMPING
2
Vertical Load - Horizontal load (Applies to Steady-State solution only)
-194002 0
Bearing geometry: Diameter, Length, Radial clearance,
0.510 1.020 0.00045
Lubricant viscosity (isothermal analysis)
0.07
Lubricant properties : Feeding oil temperature (K), oil density (kg/m3), specific heat capacity (J/kg.K), thermal conductivity (W/m.K)
303.15 1025 1500 0.25 3.38942 8.64526 0.6
Rotational speed (RPM)
115.
Divisions along circumference / length (Ddiv/Ldiv)
181 121
Number of Cycles, Number of points per cycle
1 360
Solver type (1 Reynolds, 2 Reynolds slip, 3 Elrod, 4 Elrod slip)
1
Misalignment angle X, Misalignment angle Z
0.092 0.
Guess Eccentricity, attitude angle
0.75 -25.0
Newton Raphson load accuracy, attAngle accuracy (deg), relaxation factor
0.01 0.5 1.1
Include time derivatives (1 true, 0 false)
0
Convergence criterion (1 maximum difference, 2 mean difference)
2
Boundary Conditions: Pressure along length (Pa), Pressure along circumference (Pa)
10. 10.
Symmetry in Y Direction(1 true, 0 false)
0
Reynolds Parameters: omega, max GaussSeidel iterations
1.9 100000 1.e-7
ELROD Parameters: SOR omega, max GaussSeidel iterations, max GaussSeidel difference, Elrod Bulk value, Factor Switch algorithm (1 or
1.05 300000 1.e-9 1.e9 2 0.72 0.99995
Continuity along X Direction(1 true, 0 false)
0
First line: Number of Oil grooves. Consecutive lines: Oil inlet groove: start angle (from y axis), end angle, start length (%), end l
1
-10. 10. 0.45 0.55 200100. 1
Output Iteration list
4
0 450 600 700
First Line:Stator. Second line: Rotor. Include slip (True/False), Slip start angle, slip end angle,Slip start y, Slip end y, bstar
0 90.36 199.27 0.15 0.85 1
0 30 160 0.2 0.8 0.1
Number of overlaid textures. Include texture (True/False), Texture parameters (startx, endx, number of dimple cells, density x direct
0
0 20 220 5 0.7 0.15 0.85 5 0.7 0.000015
Transient Load CA, Px, Pz

```

Given the input parameters, the algorithm meshes the unwrapped journal bearing into small divisions. At first, an initial assumption is made for eccentricity  $'e_0'$  and attitude angle  $'\phi_0'$  and by using an equation for film thickness, the film thickness geometry  $'h_0'$  is calculated. Afterwards, the Reynolds equation is solved numerically according to the Gauss-Seidel iterative method and the pressure field is calculated. The hydrodynamic force components in axis z, x are derived by integration of the pressure field on the bearing surface. If the initial assumptions for eccentricity  $'e_0'$  and attitude angle  $'\phi_0'$  are correct, force equilibrium is attained. Usually, proper values of the  $'e_0'$  and  $'\phi_0'$  need to be re-estimated by means of a Newton-Raphson method for two variables, until force equilibrium is reached. At the end, all the bearing operational parameters of interest are calculated (friction force  $'F'$ , maximum pressure  $'p_{max}'$ , mean pressure  $'p_{mean}'$ , etc.) and printed to an output file.

```

results0.txt - Σημειωματάριο
Αρχείο Επεξεργασία Μορφή Προβολή Βοήθεια
Input Data
0.51 Journal Diameter [m]
1.02 Bearing Length [m]
0.00045 Clearance [m]
115 Rotational speed [RPM]
-194002 Vertical Load [N]
0 Horizontal Load [N]
0 Total Load [N]
0.07 Lubricant viscosity [Pa s]
-0.092 Non-dimensional misalignment angle yz (psiX)
0 Non-dimensional misalignment angle xy (psiZ)
181 Divisions in the circumferential direction
121 Divisions in the axial direction

Parallelization Type : Single Processor

0.115522 Sommerfeld Number
0.429398 Eccentricity ratio
60.8968 Attitude angle
0.147144 Non-dimensional Load Capacity
2.66989 Normalized friction Coefficient
197863 Vertical Load [N]
-6.17263 Horizontal Load [N]
746056 Maximum Pressure [Pa]
16.8968 Angle of maximum pressure [deg]
-0.0109914 Distance of actual support location from bearing center [m]
3585.67 Misalignment Moment Mx [N m]
0.000233595 Minimum film thickness [m]
45.507 1.07616 Inlet Flow rate [lt/min], Non-dimensional value
20.0989 0.475304 Side Flow rate (leakage [lt/min], Non-dimensional value)
2.86284 Power loss [kW]
0.237723 Friction torque [kN m]
0.697486 Stiffness Coefficient Kz [x 10^9 N/m2]
-0.810913 Stiffness Coefficient Kx [x 10^9 N/m2]
0.717283 Stiffness Coefficient Kzx [x 10^9 N/m2]
1.24602 Stiffness Coefficient Kxz [x 10^9 N/m2]
337 Iterations
101.786 Runtime of the last iteration [s]
0 Total Runtime [s]

Simulation Parameters
STEADY SOLUTION
SYMMETRY_Y_DIRECTION DISABLED
CONTINUITY_X_DIRECTION DISABLED
TIME DERIVATIVES NOT INCLUDED
CONVERGENCE CRITERION: MAX DIFFERENCE
KHONSARI FACTOR SWITCH ALGORITHM

```

Moreover plots are created of pressure field and film thickness (Figure 34).

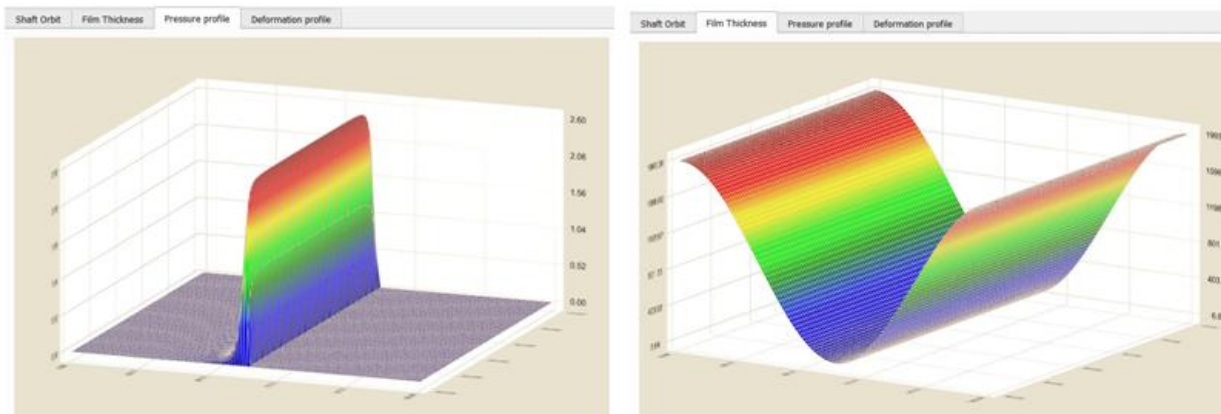


Figure 33: Generated plots of pressure field (left) and film thickness (right)

The solver will be utilized in this thesis to calculate the actual support point of ASTB for specific cases.



## 5.3) Hull deflection calculation tool

### 5.3.1) 1D FEM for calculating hull deflections in marine industry

Considering hull flexibility and the resulting hull deflections in shaft alignment calculations can significantly enhance the robustness of the calculations. Hull deflections alter the relative offsets of bearings, thereby causing load redistribution among the bearings. However, in the majority of available (SAC) plans, the hull is assumed to be rigid and thus hull deflections are not accounted for varying drafts. Ship loading conditions play a crucial role in bearing reactions, and they can vary depending on factors such as whether the ship is ballasted or fully loaded (**Figure 34**).

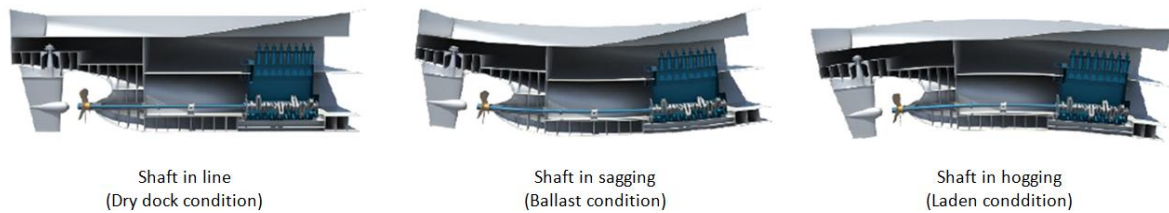


**Figure 34: Hull deflections of stern section [20]**

Incorporating hull deflections into shaft alignment calculations can be approached through either measurement-based methods or analytical techniques, such as numerical models. While developing a full 3D Finite Element Method (FEM) model of a ship is complex and time-consuming, simpler 1D calculation methods based on Euler-Bernoulli and Timoshenko beam theory can be employed. These methods offer a quick and cost-effective way to account for hull deflections, requiring inputs such as external loads, second moment of area, shear area of frames, and material properties.

This calculation method is described in i-MARINE [1] D2.3 report Chapter 4.1 and is also proposed by Intellectual Maritime Technologies [39]. The author of the latter states that hull deflection calculations are overlooked in many articles and reports by shaft designers with possible reasons to be:

- they may not see the need to study them
- they believe hull is so stiff, so hull deflections is not worth considering
- they may not be able to perform such calculations

In general hull deflections studies are outside the scope of shaft alignment calculations, with 1D methods being inexpensive (taking few days) but simplistic (not exact and results of measurements or full FEM for similar ship are desired to be available). Nevertheless one should consider that: "It is far better to foresee even without certainty than not to foresee at all" and an early robust approximation of hull deflections can be obtained using broadly available information with minimum pre-processing effort by the user [40].

Moreover in Tanseef Rules<sup>13</sup> in chapter of *Alternative hull deflection calculation* is stated that:

---

<sup>13</sup> Tanseef Rules, Emirates Classification Society, Guide for Optimized Shaft Alignment, Effective from 15 February 2024

Hull deflection calculation carried out with programs using simple beam theory or other programs related to the vessel's stability and loading calculations may be accepted provided that: sufficient information in terms of data and calculations demonstrating that the obtained hull deflection values are reliable are included in the report.

### 5.3.2) 1D methods for calculating hull deflections

#### Euler- Bernoulli method

In Euler-Bernoulli (E-B) theory, deformations are caused only by bending moments and is described by the following fourth-order ordinary differential equation:

$$\frac{d^2}{dx^2} \left( EI \frac{d^2 u}{dx^2} \right) = q$$

Where:

- $u(x)$ : is the deflection of the beam at some longitudinal position  $x$
- $q(x)$ : is the distributed force per unit length acting in the vertical direction  $y$
- $E$ : is the modulus of elasticity of material under consideration
- $I(x)$ : is the second moment of area calculated with respect to the axis which passes through the centroid of the cross-section and is perpendicular to the applied load

Since  $\frac{dV}{dx} = -q$  and  $\frac{dM}{dx} = V$ , equation can be written for every finite element as:

$$EI(x) \frac{d^2 u(x)}{dx^2} = M(x)$$

Assumptions of this theory are [1]:

- Plane sections perpendicular to the neutral axis (NA) before deformation stay plane and perpendicular to the NA after deformation
- The deformations are small
- The beam is essentially prismatic (no openings or discontinuities)
- The material is homogenous and elastic

#### Timoshenko method

Timoshenko beam theory is a general case of E-B method, in which shear deformation and rotational bending effects are also taken into account, by effectively reducing the beam stiffness.

The governing coupled differential equations are the following:

$$\frac{d^2}{dx^2} (EI \frac{d\varphi}{dx}) = q$$

$$\frac{du}{dx} = \varphi - \frac{1}{G \cdot A_s} \frac{d}{dx} (EI \frac{d\varphi}{dx})$$

Where:

- $A_s$ : shear area
- $G$ : shear modulus
- $V$ : shear force
- $\phi$ : is the angle of rotation of the normal to the mid-surface of the beam, defines as:

$$\phi = \frac{du}{dx} - \gamma$$

$$\gamma(x) = \frac{V(x)}{G \cdot A_s(x)}$$

Assumptions of this theory are [1]:

- The longitudinal axis of the unloaded unreformed beam is straight.
- All loads applied to the beam act transverse to the longitudinal axis
- The total slope ( $x$ ) of the centerline results from the effects of bending deformation and shears deformation and can be expressed as the sum of the rotations due to shear deformation and the rotation due to bending deformation.
- The material is considered linear elastic, homogeneous and isotropic. Hence, the generalized Hooke's stress-strain laws are valid.
- The deformations and strains are considered so small and the strain-displacement equations of infinitesimal elasticity are used.
- Plane sections perpendicular to the NA before deformation stay plane but not necessarily perpendicular to the NA after deformation.

### 5.3.3) Solving the 1D equations

#### Finite Element Method (FEM)

Finite element method is based on discretization a beam into a set of elements, which are connected to other elements through nodes. External applied load is applied to these nodes in form of forces and bending moments. This method is approximating the solution using piecewise polynomial functions over the examined elements.

General displacement function  $v(x) = c_1 + c_2x + c_3x^2 + c_4x^3$  gives pretty accurate approximations for purposes of finite element methods and it has four constants as the numbers of degrees of freedom (DOF). Transverse displacement  $v(x)$  describes the way element is moving in terms of pure bending and transverse displacement, while  $\phi(x) = \frac{dv(x)}{dx}$  describes the slope at each point. The four unknown coefficients will be found from boundary conditions (BC). Specifically:

Node 1 ( $x=0$ )	Node 2 ( $x=L$ )
$v(0) = v1$	$v(L) = v2$
$\phi(0) = \phi1$	$\phi(L) = \phi2$



By expressing the four constants in terms of  $v_1, \phi_1, v_2, \phi_2$ , replacing them into the general displacement function and rearranging then:

$$v = N_1 v_1 + N_2 \phi_1 + N_3 v_2 + N_4 \phi_2$$

$$\text{Where: } N_1 = \frac{L^3 - 2Lx^2 + x^3}{L^3}, \quad N_2 = \frac{L^2 x - 2Lx^2 + x^3}{L^3}, \quad N_3 = \frac{3Lx^2 - 2x^3}{L^3}, \quad N_4 = \frac{x^3 - Lx^2}{L^3}$$

Coefficients above are called shape functions and are equal to the numbers of degrees of freedom (DOF) in the system. Using the total potential energy equation, the beam element stiffness matrix is derived as:

$$k^e = \int_0^L (B^T EI(x) B) dx$$

Where:

$$B = \left[ \frac{dN_1}{dx}, \frac{dN_2}{dx}, \frac{dN_3}{dx}, \frac{dN_4}{dx} \right]$$

$$\text{And finally for E-B theory: } k^e = \frac{EI(x)}{L^3} \begin{bmatrix} 12 & 6L & -12 & 6L \\ 6L & 4L^2 & -6L & 2L^2 \\ -12 & -6L & 12 & -6L \\ 6L & 2L^2 & -6L & 4L^2 \end{bmatrix}$$

Load vector for uniform distributed transverse loading  $q_e$  is:

$$F_{ext} = \frac{q_e L}{2} \begin{bmatrix} 1 \\ L/6 \\ 1 \\ -L/6 \end{bmatrix}$$

Stiffness matrix is calculated for every element (local), as well as its loading vector, which afterwards will construct the stiffness matrix of the whole structure (global) and the corresponding loading vector. Finally the system  $\mathbf{F}=\mathbf{K}\mathbf{u}$  is created, boundary conditions are applied and the displacement and slope at every node can be calculated.

For Timoshenko method beam element stiffness matrix is:

$$k^e = \frac{EI(x)}{L^3(1+\varphi)} \begin{bmatrix} 12 & 6L & -12 & 6L \\ 6L & (4+\varphi)L^2 & -6L & (2-\varphi)L^2 \\ -12 & -6L & 12 & -6L \\ 6L & (2-\varphi)L^2 & -6L & (4+\varphi)L^2 \end{bmatrix}$$

Where:

$$\varphi = \frac{12 EI(x)}{G A_s(x) L^2}$$

## Finite Difference Method (FDM)

Finite difference method shares many things in common with FEM. It is a way to solve differential equations using Taylor's series for converting them into algebraic equations which are solved for the points of examined grid.

For E-B equation in the below form, central differences will be used for derivatives calculation over the grid.

$$EI(x) \frac{d^2u(x)}{dx^2} = M(x)$$

$$\frac{d^2u(x)}{dx^2} = \frac{u(x - \Delta x) - 2u(x) + u(x + \Delta x)}{\Delta x^2} + O(\Delta x^2)$$

So the equations for constructing the matrix, valid for the internal points  $x$  of grid is:

$$\frac{u(x - \Delta x) - 2u(x) + u(x + \Delta x)}{\Delta x^2} = \frac{M(x)}{EI(x)}$$

Boundary conditions will restrict the solution. Specifically for a cantilever beam with left end free and right end clamped, the following BC are assigned.

Point	Condition
<i>free end</i>	$M(x) = 0$
<i>clamped end</i>	$u(x) = 0$ & $\frac{du(x)}{dx} = 0$

For node at free end  $u(1)$  no equation is used and the deflection value will be derived from the solution of the system. For node at clamped end deflection value is set as  $u(n)=0$  and the governing equation will be as below:

$$\frac{u(n - 1) - 2u(n) + u(n + 1)}{\Delta x^2} = \frac{M(x)}{EI(x)}$$

Given that  $u(n)=0$  and  $u(n-1)=u(n+1)$  then it can be written as:

$$\frac{2u(n - 1)}{\Delta x^2} = \frac{M(n)}{EI(x)}$$

For point  $u(n-1)$  the governing equation can be written as

$$\frac{u(n - 2) - 2u(n - 1)}{\Delta x^2} = \frac{M(n - 1)}{EI(n - 1)}$$

For the given (BC) the resulting stiffness matrix **A**, deflection vector **u** and load vector **M** are:

$$\begin{bmatrix} 1 & -2 & 1 & 0 & 0 & \dots & 0 & 0 & 0 \\ 0 & 1 & -2 & 1 & 0 & \dots & 0 & 0 & 0 \\ \vdots & \ddots & \ddots & \ddots & \ddots & \ddots & \ddots & \vdots & \\ 0 & 0 & 0 & 0 & \dots & 0 & 1 & -2 & 1 \\ 0 & 0 & 0 & 0 & \dots & 0 & 0 & 1 & -2 \\ 0 & 0 & 0 & 0 & \dots & 0 & 0 & 0 & 2 \end{bmatrix} \times \begin{bmatrix} u(1) \\ u(2) \\ \vdots \\ u(n-3) \\ u(n-2) \\ u(n-1) \end{bmatrix} = \begin{bmatrix} M(1) \cdot \Delta x^2 / (E \cdot I(1)) \\ M(2) \cdot \Delta x^2 / (E \cdot I(2)) \\ \vdots \\ M(n-3) \cdot \Delta x^2 / (E \cdot I(n-3)) \\ M(n-2) \cdot \Delta x^2 / (E \cdot I(n-2)) \\ M(n-1) \cdot \Delta x^2 / (E \cdot I(n-1)) \end{bmatrix}$$

$u(n)=0$ .

The two solving methods obviously give the same results, with their divergence to decrease as the mesh gets finer. FEM method will be used and the first derivative of shear curve from Loading Manual will build the load vector.

### 5.3.4) Hull deflection calculation model for case study ship & tool

In order to calculate the influence of draft and loading change in shaft alignment of the case study ship Euler-Bernoulli and Timoshenko beam theory will be used. For shaft alignment purposes, there is no need for examining the ship over its entire length [20], since deflections from forward bulkhead of engine room (Figure 40) and aft are enough (frame -5 to frame 35 for the case study ship).

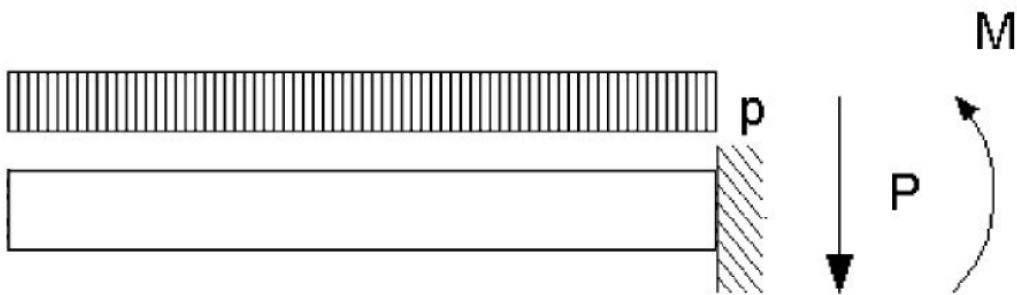


Figure 35: Cantilever loading and boundary conditions, simulating engine room and stern construction

Second moment of area ( $I$ ), loading conditions (Shear Force curves), elasticity modulus ( $E$ ), shear area ( $A_s$ ) and shear modulus ( $G$ )<sup>14</sup>, are necessary data for the calculation. Specifically they can be obtained and calculated by the following booklets:

#### Second moment area, shear area (through measurements on frames) and elasticity modulus:

- Structural details for hull construction
- Engine room construction (main deck)
- Engine room construction (upper platform)
- Double bottom construction in engine room
- Stern construction
- Engine bedplate scantlings if were available, would increase accuracy

<sup>14</sup> For Timoshenko beam theory

## Loading conditions (through diagrams digitizing)

- Final Loading manual Typical Loading

For second moment of area, a Graphical User Interface (GUI) program called Inertia Calculator was utilized, which calculates section properties of any vessels' frames. It is a tool of Laboratory of Marine Engineering of NTUA developed during a diploma thesis in 2022 [40]. Input data is a frame, which after being imported, scale has to be defined and user manually selects the plates and stiffeners that are taken into account in the calculation. After that process, app returns values of: second moment of area, neutral axis position and shear area of a frame. Environment and procedure are shown in (Figure 36).

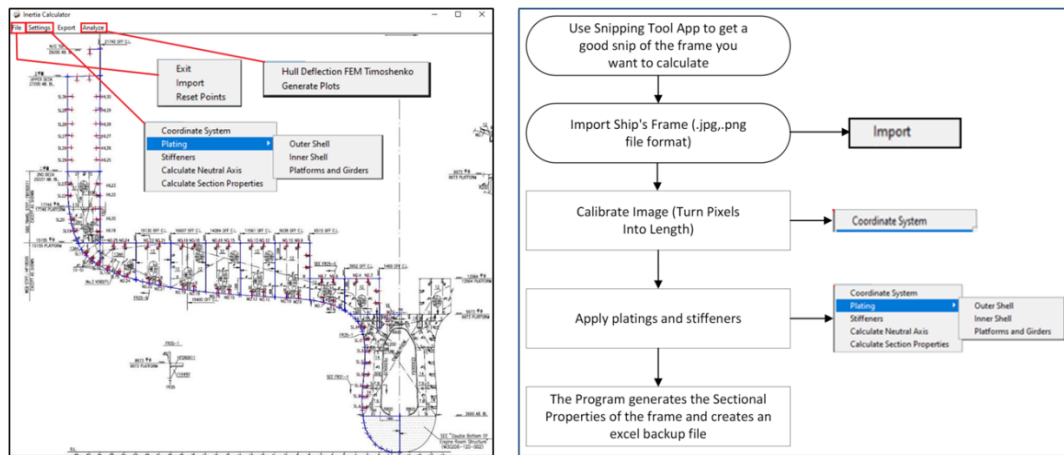


Figure 36: User Interface of Inertia Calculator tool and required procedure [40]

Case study ship's frames for engine room were divided in 3 parts (double bottom, upper platform and main deck) and for this reason they had to be suitably scaled and merged (Figure 37) in order to be imported in the tool. Afterwards using the GUI program measurements were taken (Figure 38).

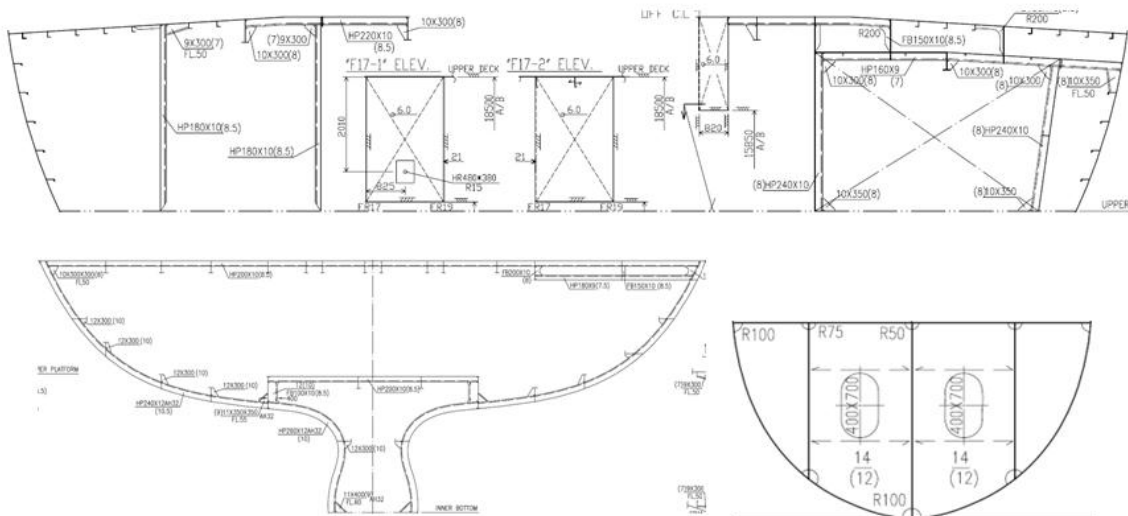


Figure 37: Frame parts from the 3 construction plans

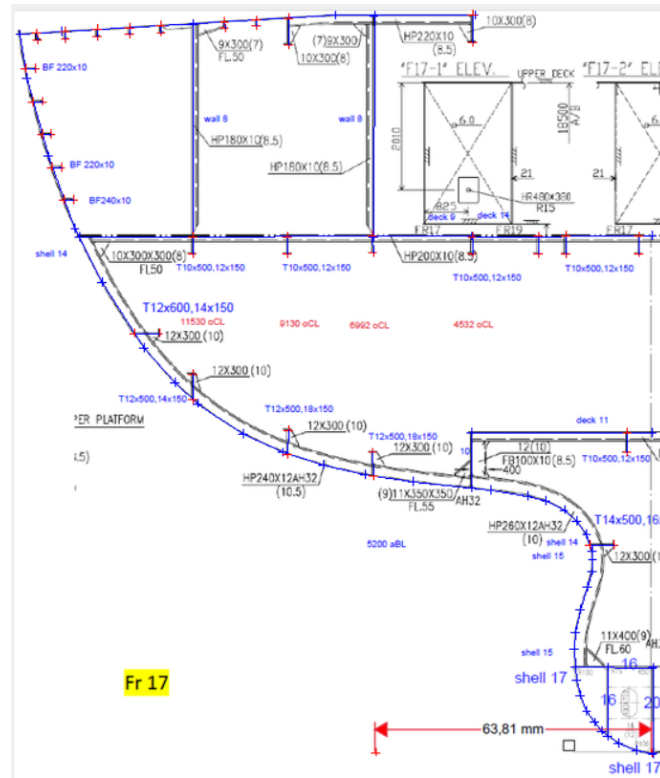


Figure 38: Process of measurement

For the sake of completeness, hull deflection calculations for the case study ship will be presented below:

Measuring process has been done for 15 frames of engine room and stern length and linear interpolation was used to find the values of the rest frames. Frames measured are marked in the following figure:

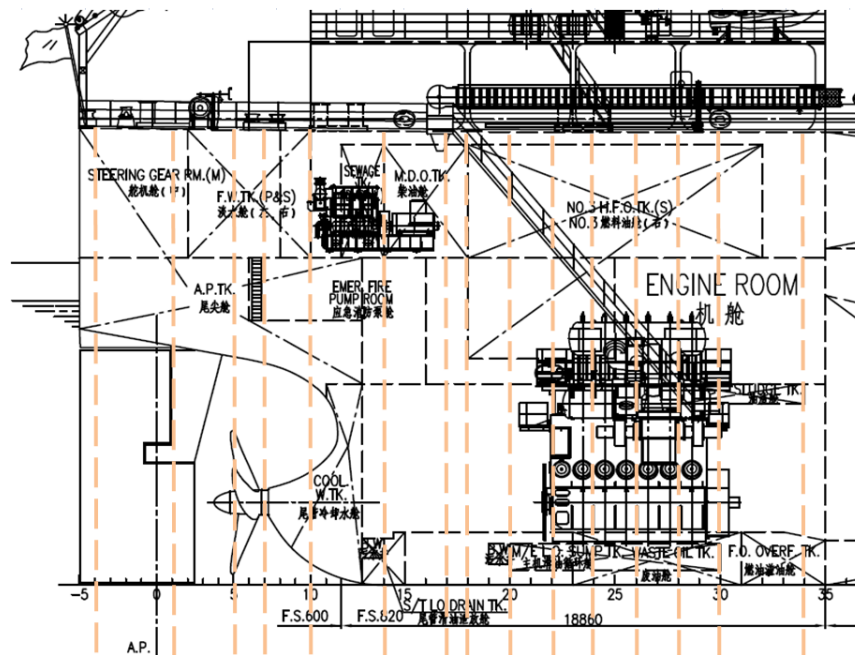


Figure 39: Profile view of engine room of case study ship and frames measured



Second moment of area and shear area are in (Figure 40), (Figure 41).

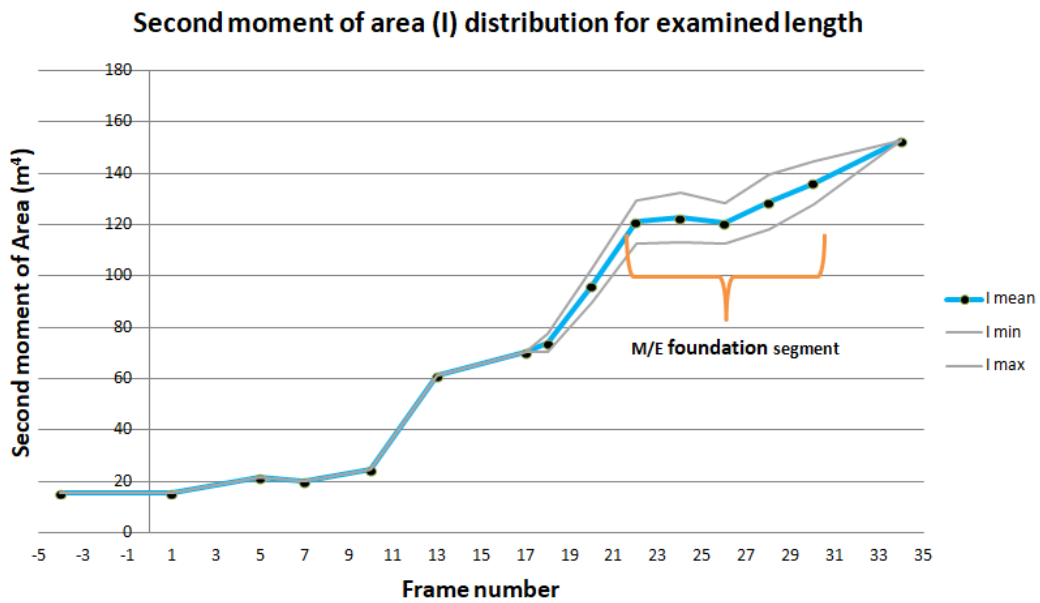


Figure 40: Measured second moment of area

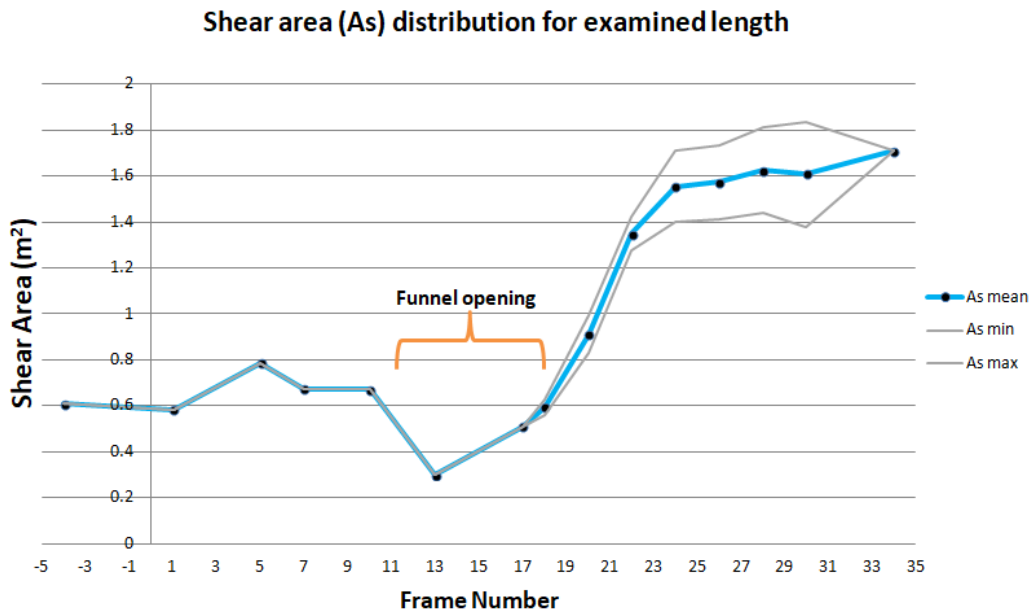


Figure 41: Measured shear area

The increase in shear area diagram at engine's position is due to foundation plates and stiffeners which have a significant thickness there for accommodating the forces and vibrations of engine weight and operation. Also the lower values in frames 11 to 16 are due to the opening for the funnel in decks. Moreover, given that 1D method cannot provide the exact inertia values, in order to reduce uncertainty, the minimum possible and higher possible values of I and As were measured (min, max). This differentiation is attributed to the existence of tanks, openings and structural members extended to few frames, whose their exact contribution to sectional

properties of a frame can only be quantified by a full 3D FEM model. For this reason hull deflection curves are produced for: minimum, maximum and mean values of I and As.

Shear force distribution from Loading manual is in (Figure 42) and its first derivative in (Figure 43). Examined loading conditions were selected according to a paper which studied the effect of hull deflections in shaft alignment for the same type of vessel.

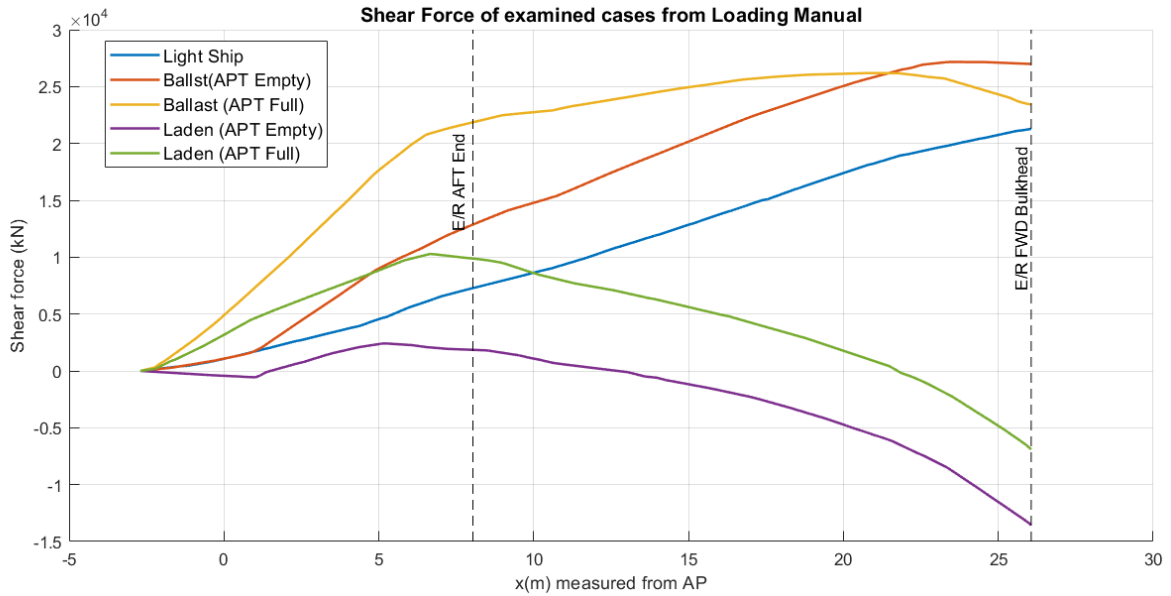


Figure 42: Shear Force points from Loading Manual interpolated by spline

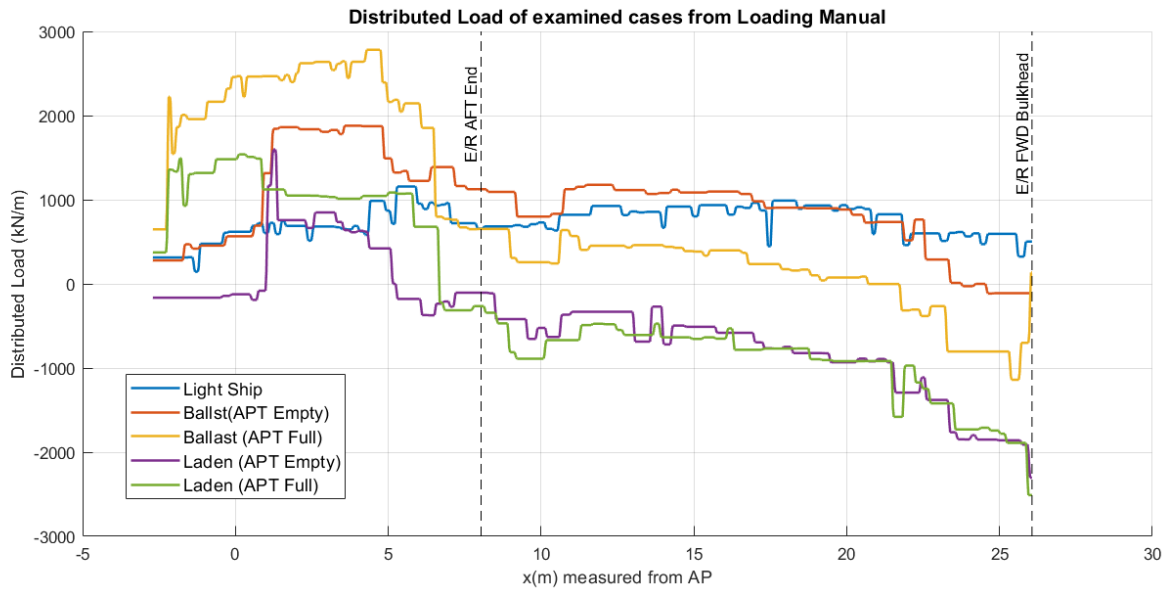


Figure 43: First derivative of shear force spline giving distributed load

For min, mean and max values, curves like the following were created. For I mean and As mean calculated curves are:

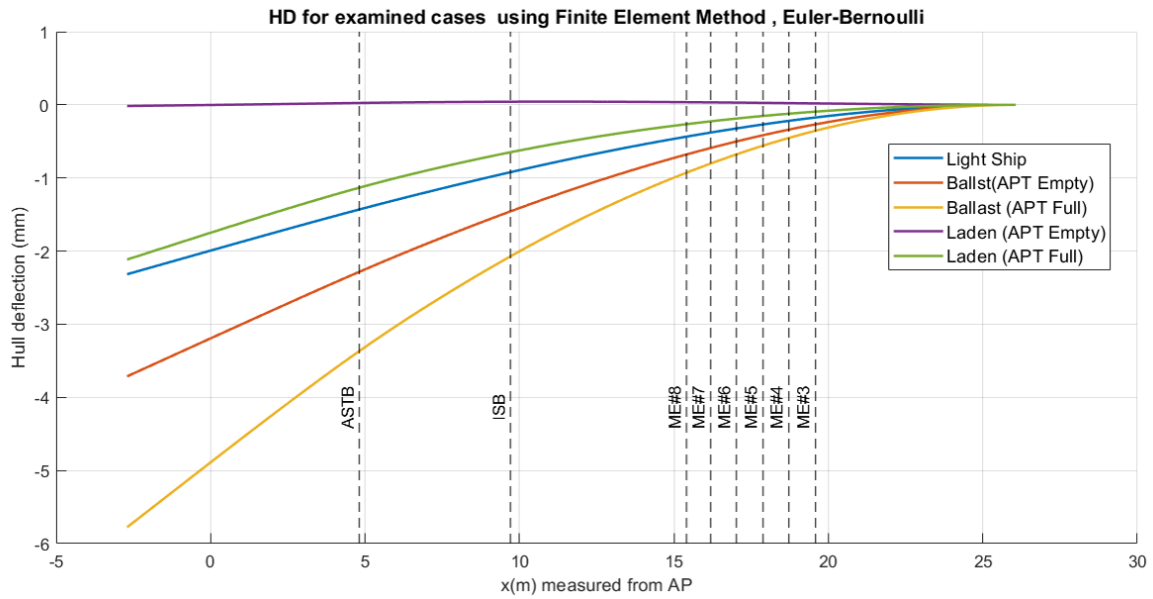


Figure 44: Hull deflection curves with Euler-Bernoulli method

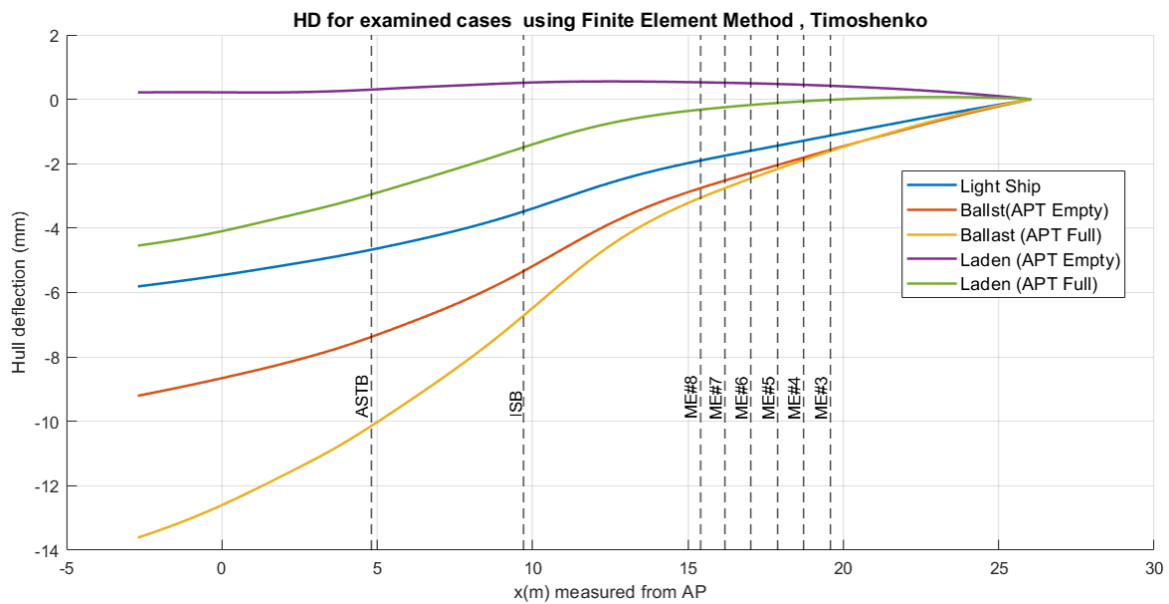


Figure 45: Hull deflection curves with Timoshenko method

From the Loading Condition, only two will be analyzed which develop the highest deflection values (Ballast APT Full) and (Laden APT Empty). In SAC plan of case study ship it is not clear in which condition the final alignment was done and no data are included regarding hull deflection and the subsequent bearing offsets. So in this thesis final alignment of case study ship is considered to have been finalized in lightship condition<sup>15</sup> and maximum & minimum hull deflection will be relative to that condition. In the following two diagrams can be observed the differences between min, mean and max calculation of I and As.

<sup>15</sup> In Chapter 3 is described a typical installation process

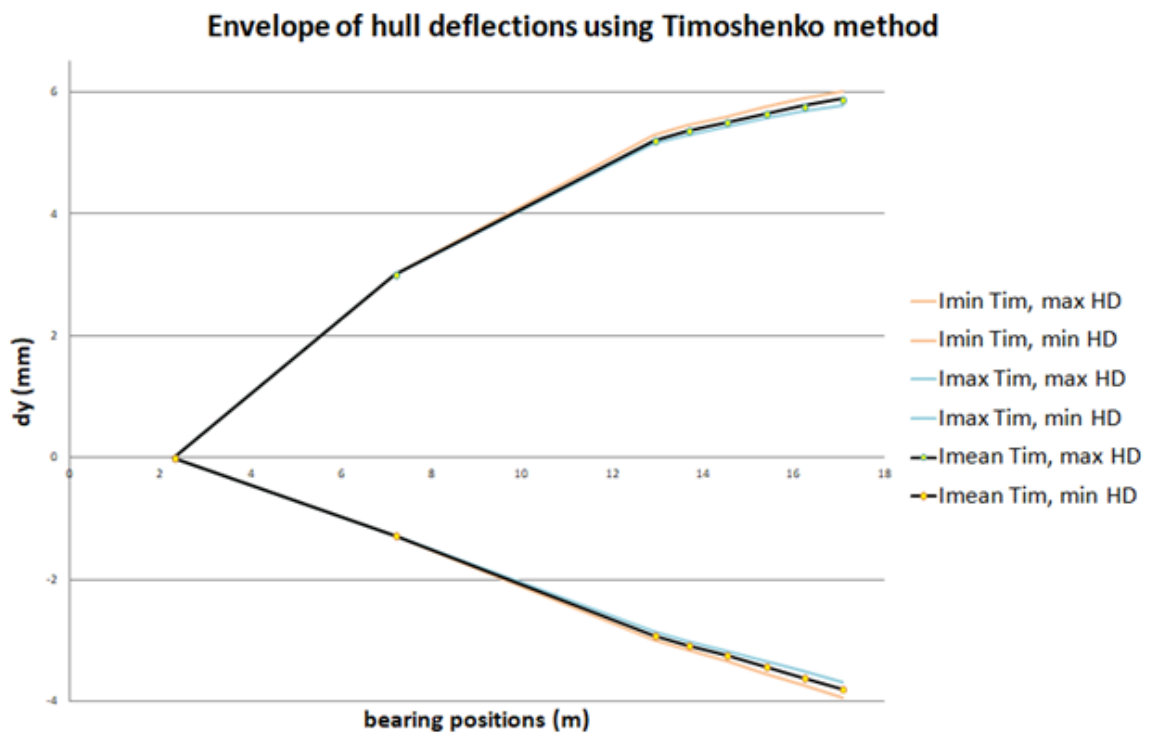
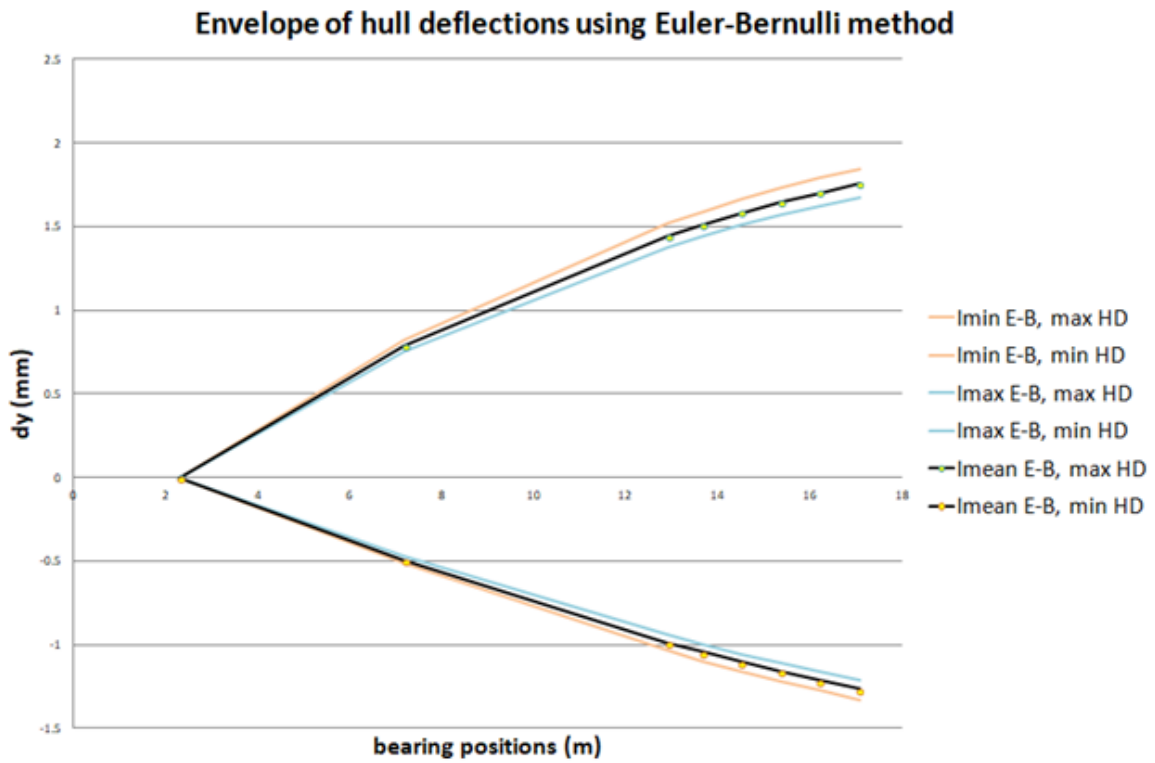


Figure 46: Relative hull deflections for I min, mean, max with Euler-Bernoulli method (up) and with Timoshenko method (down)

The above sets reveal that minimum and maximum values of HD are very close, so from now and on results from mean values will be kept.

I mean values will be used and compared with 2 available hull deflection sets from similar ships:  
 Ship 1: [5], Ship 2 : [8]

Calculated hull deflections compared to available sets



Figure 47: Calculated hull deflections envelope compared to available data

Based on the diagrams above, it is evident that the Euler-Bernoulli method computes lower hull deflection values, whereas the Timoshenko method computes higher values. Uncertainty regarding which method more accurately reflects reality cannot be eliminated and for this reason two scenarios will be examined, one for each method. **It should be noted that 1D FEM methods provide rough estimations rather than exact values. The purpose of using these methods is to compare the results against the concept of intermediate bearing actuation.**

Table 8: Relative and initial bearing offsets for examining intermediate bearing actuation

Bearing offsets	Euler – Bernoulli		Timoshenko		Initial Offsets <sup>16</sup> No HD – SAC plan
	Min	Max	Min	Max	
ASTB	0.000	0.000	0.000	0.000	0
ISB	-1.163	0.116	-1.952	2.331	-0.67
M/E #8	-2.906	-0.476	-4.839	3.284	-1.92
M/E #7	-2.964	-0.407	-5.001	3.433	-1.92
M/E #6	-3.023	-0.339	-5.173	3.579	-1.92
M/E #5	-3.082	-0.274	-5.353	3.718	-1.92
M/E #4	-3.134	-0.217	-5.532	3.842	-1.92
M/E #3	-3.184	-0.165	-5.722	3.959	-1.92

<sup>16</sup> Hull deflections are considered to be zero and are the values of SAC plan

Relative bearing offsets (as to initial offsets) are initial offsets plus relative hull deflection value at this position (examined condition minus lightship condition). The above values which are going to be examined, are visualized in (Figure 48).

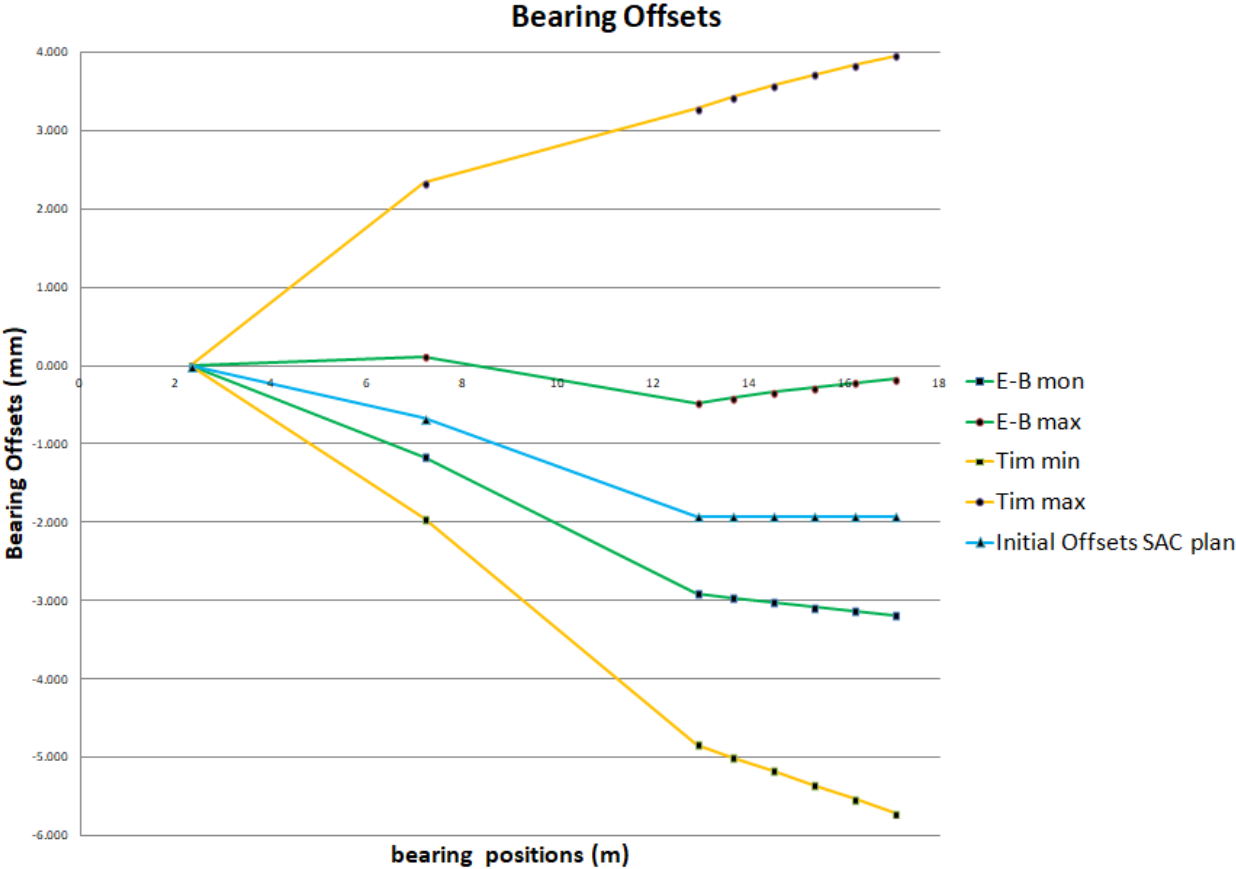


Figure 48: Relative and initial bearing offsets

## 6) Case study

### 6.1) Principal particulars of the studied vessel and operational conditions

The case study ship for examining the implementation of intermediate bearing movement is a typical Supramax Bulk Carrier built in 2013. Vessel's particulars and shafting description are presented below.

**Table 9: Principal particulars of the case study vessel**

Type	56582 t DWT class bulk carrier
Length OA	189.99 m
Length BP	185 m
Breadth (moulded)	32.26 m
Depth (moulded)	18 m
Design Draft	12.8 m
Service Speed	14 kn
Main Engine	Type: MAN B&W 6S50MC-C7
	MCR: 8500 kW at 115 rpm
	NCR: 7225 kW at 108.9 rpm
Propeller	Type: Fixed pitch propeller
	Number of Blades: 4
	Material: Ni-Al-Bronze Cu3
	Diameter: 6000 mm
	Mass in air 14755 kg
	Pitch at 0.7R : 4544.90 mm
	Pitch (mean): 4524.35 mm
	Skew angle: 24.3 deg
	Expanded area ratio: 0.5
	Direction of rotation: Right handed
	With propeller boss cap fin

The shafting system particulars of the studied vessel can be found in the following table:

**Table 10: Shafting particulars of the case study vessel**

Total length of shaft	17062 mm
Weight of shaft	36361 kg
Density of shaft material	7850 kg/m <sup>3</sup>
Modulus of elasticity	210 GPa
Shear modulus	81 GPa
<b>Propeller Shaft</b>	
Length	6507 mm
Diameter (at bearing region)	510 mm
Number of bearings	1
• Aft Stern Tube Bearing (ASTB)	
Length (effective)	1020 mm
Diameter	510 mm
Max permissible mean pressure	0.829 MPa
Max permissible load	431.4 kN
<b>Intermediate Shaft</b>	
Length	6006 mm

Diameter (at bearing region)	430 mm
Number of bearings	1
• Intermediate Shaft Bearing (ISB)	
Length	280 mm
Diameter	430 mm
Max permissible mean pressure	0.8 MPa
Max permissible load	96.3 kN
<b>Main Engine Shaft</b>	
Length	4549 mm
Diameter until crankshaft	600 mm
Diameter of equivalent crankshaft model	324 mm
Number of bearings before crankshaft	2
Number of crankshaft bearings modeled	4
• Aft most M/E Bearing (M/E #8)	
Length	541 mm
Diameter	600 mm
Max permissible load	291 kN
Min permissible load	0 kN
• M/E Bearing 7 (M/E #7)	
Length	289 mm + 227 mm
Diameter	600 mm, 324 mm
Max permissible load	291 kN
Min permissible load	14.55 kN
• M/E Bearings 6, 5, 4 (M/E #6 - #4)	
Length	454 mm
Diameter	324 mm
Max permissible load	291 kN
Min permissible load	14.55 kN
• M/E Bearing 3 (M/E #3)	
Length	228 mm
Diameter	324 mm
Max permissible load	291 kN
Min permissible load	14.55 kN

**Table 11: Longitudinal position and vertical offsets of bearings**

Description	Node number	Distance from aft end (m)	Vertical offset	
			Cold Condition (mm)	Hot Condition (mm)
ASTB	6 (Static condition) 7 (Dynamic condition)	2.137 2.307	0.00	0.00
ISB	17	7.192	-0.67	-0.67
M/E #8 Bearing	26	12.907	-2.16	-1.92
M/E #7 Bearing	31	13.662	-2.16	-1.92
M/E #6 Bearing	35	14.512	-2.16	-1.92
M/E #5 Bearing	39	15.362	-2.16	-1.92
M/E #4 Bearing	43	16.212	-2.16	-1.92
M/E #3 Bearing	47	17.062	-2.16	-1.92



As cold condition is that of 20°C and hot is that of 55°C which is the normal running temperature.

In vessel's booklet there are 5 cases examined. Four of them are during static condition, where propeller is not rotating and one dynamic condition in which there is a moment excited on the propeller node, modeling thrust vertical eccentricity. Actually that dynamic state is a quasi-static approach of the shafting system during sea-going condition. Examined conditions are can be found in the following table:

**Table 12: Operating conditions analyzed in booklet**

Operating Conditions			
Condition	Temperature	Immersion	Thrust Moment
1	Cold	50 %	0
2	Cold	100 %	0
3	Hot	100 %	0
4	Hot	100 %	-105.873 kNm
5	Cold	75 %	0

Propeller thrust moment **Mz** acts on the vertical plane and her value is considered as a percentage of the torque transmitted to propeller shaft, while main engine operates in MCR condition. That percentage is 15%. The calculation is:

$$Q_{MCR} = \frac{\text{power}}{\text{angular velocity}} = \frac{8500 \text{ kW}}{115 \cdot 2\pi/60} = 705.82 \text{ kNm}$$

$$Mz = -15\% \cdot Q_{MCR} = -105.873 \text{ kNm}$$

A negative Mz sign indicates that the considered point of thrust force application is located above propeller disc center and consequently tends to lift propeller cantilever upwards.

## 6.2) Input data for Shaft Alignment Tool

### 6.2.1) Segment properties

The method to assess and validate bearing loads in the shafting system relies on 1D beam theory. Following the appropriate segmentation of the shaft into segments, their geometrical and material characteristics are input into the Shaft Alignment Tool for a detailed shafting analysis. The shaft is discretized with 47 beam elements and a total of 48 nodes. The following table contains all the necessary information for the analysis.

**Table 13: Geometric data of the propulsion shaft of case study vessel**

Segment Number	Right node distance from aft end (m)	Length (m)	Diameter (mm)	Inertia (m <sup>4</sup> )	Mass (kg)	Load Distribution (N/m)	Young Elasticity (N/m <sup>2</sup> )
1	0.197	0.197	0.370	0.00092	145.0942	-7225.25	2.1E+11
2	0.395	0.198	0.370	0.00092	145.8307	-7225.25	2.1E+11
3	0.965	0.57	0.456	0.00212	637.6563	-10974.4	2.1E+11
4	1.475	0.51	0.485	0.00272	645.4073	-12414.6	2.1E+11
5	1.967	0.492	0.510	0.00332	703.545	-14028	2.1E+11

6	2.137	0.17	0.510	0.00332	243.0948	-14028	2.1E+11
7	2.987	0.85	0.510	0.00332	1215.474	-14028	2.1E+11
8	3.067	0.08	0.510	0.00332	114.3976	-14028	2.1E+11
9	5.697	2.63	0.500	0.00307	3614.789	-13483.3	2.1E+11
10	6.031	0.334	0.513	0.0034	483.248	-14193.6	2.1E+11
11	6.207	0.176	0.500	0.00307	271.2768	-15120.6	2.1E+11
12	6.407	0.2	0.500	0.00307	308.2691	-15120.6	2.1E+11
13	6.507	0.1	0.900	0.03221	499.3955	-48990.7	2.1E+11
14	6.607	0.1	0.900	0.03221	499.3955	-48990.7	2.1E+11
15	6.952	0.345	0.420	0.00153	375.213	-10669.1	2.1E+11
16	7.043	0.091	0.430	0.00168	103.7381	-11183.2	2.1E+11
17	7.183	0.14	0.430	0.00168	159.5971	-11183.2	2.1E+11
18	7.323	0.14	0.430	0.00168	159.5971	-11183.2	2.1E+11
19	7.499	0.176	0.430	0.00168	200.6364	-11183.2	2.1E+11
20	7.999	0.5	0.420	0.00153	543.787	-10669.1	2.1E+11
21	11.404	3.405	0.420	0.00153	3703.189	-10669.1	2.1E+11
22	12.404	1	0.420	0.00153	1087.574	-10669.1	2.1E+11
23	12.504	0.1	0.900	0.03221	499.3955	-48990.7	2.1E+11
24	12.569	0.065	0.900	0.03221	324.6071	-48990.7	2.1E+11
25	12.611	0.042	1.060	0.06197	290.9517	-67958	2.1E+11
26	12.898	0.287	0.600	0.00636	637.0054	-21773.6	2.1E+11
27	13.152	0.254	0.600	0.00636	563.7609	-21773.6	2.1E+11
28	13.258	0.106	1.100	0.07187	790.7708	-73183.6	2.1E+11
29	13.29	0.032	1.100	0.07187	238.7233	-73183.6	2.1E+11
30	13.364	0.074	1.100	0.07187	552.0475	-73183.6	2.1E+11
31	13.653	0.289	0.600	0.00636	641.4445	-21773.6	2.1E+11
32	13.88	0.227	0.324	0.00054	0	0	2.1E+11
33	14.078	0.198	0.324	0.00054	0	0	2.1E+11
34	14.276	0.198	0.324	0.00054	0	0	2.1E+11
35	14.503	0.227	0.324	0.00054	0	0	2.1E+11
36	14.73	0.227	0.324	0.00054	0	0	2.1E+11
37	14.928	0.198	0.324	0.00054	0	0	2.1E+11
38	15.126	0.198	0.324	0.00054	0	0	2.1E+11
39	15.353	0.227	0.324	0.00054	0	0	2.1E+11
40	15.58	0.227	0.324	0.00054	0	0	2.1E+11
41	15.778	0.198	0.324	0.00054	0	0	2.1E+11
42	15.976	0.198	0.324	0.00054	0	0	2.1E+11
43	16.203	0.227	0.324	0.00054	0	0	2.1E+11
44	16.43	0.227	0.324	0.00054	0	0	2.1E+11
45	16.628	0.198	0.324	0.00054	0	0	2.1E+11
46	16.826	0.198	0.324	0.00054	0	0	2.1E+11
47	17.053	0.227	0.324	0.00054	0	0	2.1E+11

The above segment characteristics derive from the SAC plan. Inertia  $I$  and load distribution  $q$  of each segment is calculated as:

$$I = \pi \cdot \frac{D^4}{64}, \text{ where } D \text{ is diameter of the segment}$$

$$q = \frac{\text{segment mass}}{\text{segment length}}$$

According to engine manufacturer, segments 32 to 47 should be considered as weightless for the shaft alignment calculation. Moreover the table above represents the static condition, since in dynamic condition node 7 is moved forward by 170 mm (that distance equals to 1/3 of bearing's length). This means that during dynamic analysis length of segment 6 increases by 170 mm and length of segment 7 decreases by the same amount.

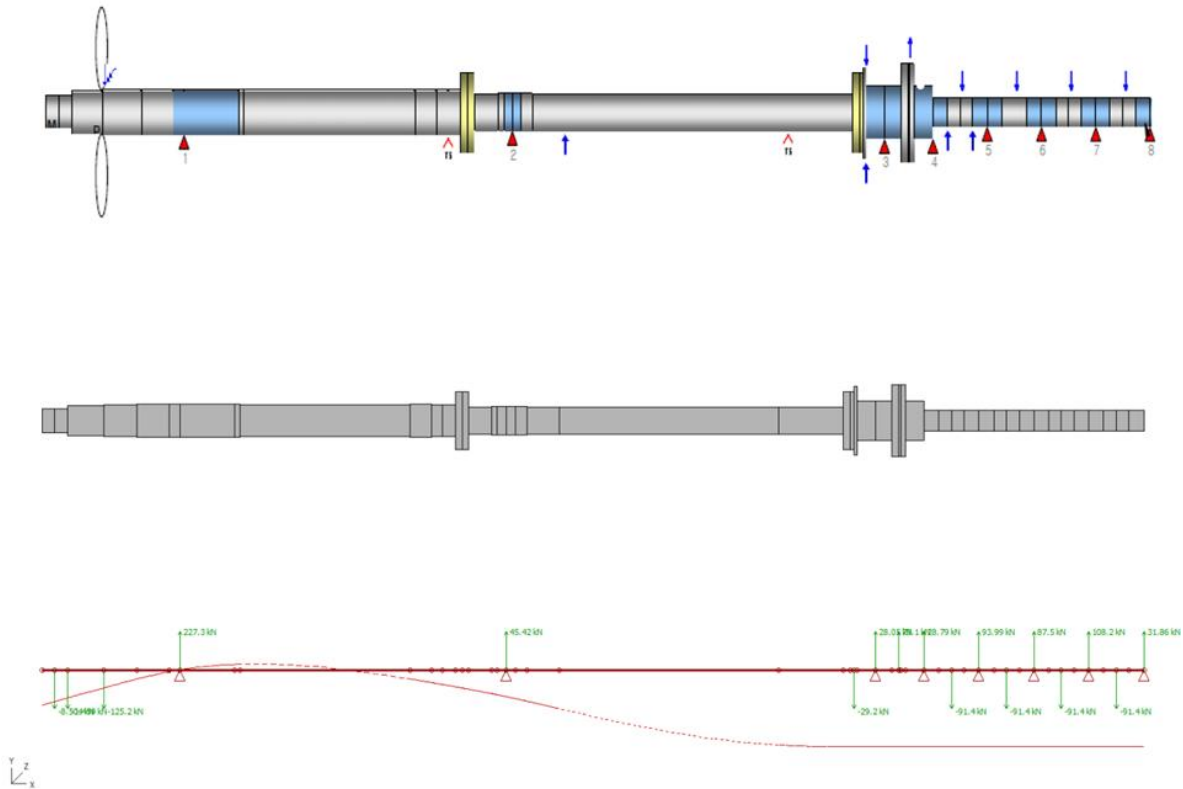


Figure 49: Case study shaft equivalent 1D FEM model and shaft deflection curve for static condition

## 6.2.2) External Loads

### Propeller load

The scenarios for propeller immersion are 3: fully immersed (100%), half immersed(50%) and immersed by 75% for the static condition. By this approach the vertical load applied to the propeller load is different for each scenario due to the effect of buoyancy. The calculation of that load is:

$$\text{Vertical load} = \text{Propeller weight in air} - \text{Buoyant force of immersed part}$$

where:

$$\text{Buoyant force of immersed part} = \text{Water density} \cdot \text{Volume of immersed part}$$

**Table 14: Propeller vertical load for immersion conditions**

Item	Node	Mass in air (kg)	Buoyancy in full immersion condition (kg)	Force in immersion conditions (N)		
				100%	75%	50%
Propeller	4	14755	1990	125224.7	130110	134985.6

In the SAC plan PBCF and Nut have the same vertical load for all immersion conditions (buoyancy effect for them is neglected), for this reason will be the same in this analysis.

**Rest of external loads**

**Table 15: Rest of vertical loads**

Description	Vertical Load (N)	Node	Distance from aft end (m)
Propeller Cap & Nut	8503.995	2	0.197
Propeller Boss Cap Fin	1458.943	3	0.395
Turning Wheel	-29204	25	12.587
Chain Force minus Mass of chain wheel	79100	29	13.267
Moving Mass including Crankthrow	-91400	34	14.087
		38	14.937
		42	15.787
		46	16.637

**6.3) Shaft Alignment Booklet compared to Shaft Alignment Tool Software (NTUA)**

**6.3.1) Influence factors**

**Table 16: Comparison of influence factors (1/2)**

kN/mm	ASTB				ISB			
	NTUA	Booklet	Difference	%	NTUA	Booklet	Difference	%
ASTB	5.386	5.381	0.005	0.09	-12.917	-12.942	0.025	-0.19
ISB	-12.917	-12.942	0.025	-0.19	37.154	37.345	-0.191	-0.51
M/E #8 Bearing	28.640	28.997	-0.357	-1.25	-121.847	-123.525	1.678	-1.38
M/E #7 Bearing	-21.222	-21.685	0.463	-2.18	98.131	100.274	-2.143	-2.18
M/E #6 Bearing	0.136	0.304	-0.168	-123.53	-0.63	-1.409	0.779	-55.28

**Table 17: Comparison of influence factors (2/2)**

kN/mm	M/E #8 Bearing				M/E #7 Bearing			
	NTUA	Booklet	Difference	%	NTUA	Booklet	Difference	%
ASTB	28.640	28.997	-0.357	-1.25	-21.222	-21.685	0.463	-2.18
ISB	-121.847	-123.525	1.678	-1.38	98.131	100.274	-2.143	-2.18
M/E #8 Bearing	1272.54	1305.796	-33.256	-2.61	-1894.27	-1960.567	66.297	-3.50
M/E #7 Bearing	-1894.27	-1960.569	66.299	-3.50	3567.65	3714.162	-146.512	-4.11
M/E #6 Bearing	865.016	916.162	-51.146	-5.91	-2387.94	-2516.33	128.39	-5.38

### 6.3.2) Bearing reactions

Moreover, detailed comparison will take place for two conditions:

- Static Hot 100% Immersion (condition 3)
- Dynamic Hot 100% Immersion (condition 4)

**Table 18: Comparison of bearing reaction forces**

Condition	Bearing Reaction Force (kN)							
	Static Hot 100% Immersion				Dynamic Hot 100% Immersion			
	Bearing	NTUA	Booklet	Difference	%	NTUA	Booklet	Difference
ASTB	227.285	230.213	-2.928	-1.29	210.905	213.931	-3.026	-1.43
ISB	45.416	44.562	0.854	1.88	65.338	64.402	0.936	1.43
M/E #8 Bearing	28.052	28.047	0.005	0.02	14.582	14.403	0.179	1.23
M/E #7 Bearing	28.792	28.351	0.441	1.53	38.773	38.555	0.218	0.56
M/E #6 Bearing	93.985	94.133	-0.148	-0.16	93.921	93.989	-0.068	-0.07
M/E #5 Bearing	87.500	87.157	0.343	0.39	87.513	87.207	0.306	0.35
M/E #4 Bearing	108.205	108.572	-0.367	-0.34	108.202	108.565	-0.363	-0.34
M/E #3 Bearing	31.864	31.716	0.148	0.46	31.865	31.717	0.148	0.46

### 6.3.3) Shaft slope at ASTB

Bearing shaft slope at ASTB is an important parameter that has to be checked for potential slope boring machining. Since neither angle was exceeding 0.3 mrad no slope boring was needed.

**Table 19: Comparison of shaft slope**

Condition	Shaft Slope (mrad)							
	Static Hot 100% Immersion				Dynamic Hot 100% Immersion			
	Bearing	NTUA	Booklet	Difference	%	NTUA	Booklet	Difference
ASTB	0.2659	0.2720	-0.0061	-2.42	0.0801	0.0879	-0.0078	-8.87

**Since calculated results approach SAC plan's values with minor differences, the present model can be utilized for the further simulations.**

Besides from the calculations above, one more diagram could be produced to provide additional information about the shafting system. A diagram from which could be known the acceptable range of propeller hydrodynamic loads (lateral forces and vertical bending moments) could give to the designer higher confidence if the expected loads lied in the center of this diagram, or could alert him if these are located near the boundaries. It is proposed by [25], called **Allowable Propeller Loads Diagram** and for the case study ship is the following:



#### 6.4) Need for intermediate bearing actuation

Now the concept of intermediate bearing actuation is being considered for the aforementioned vessel and the study focuses on analyzing how the shafting system responds to a range of propeller hydrodynamic loads without and with a specific type of actuation. As it was mentioned in paragraph 4.2 exact calculation of propeller hydrodynamic loads during straight ahead course and maneuvering at any draft can be done through CFD analysis or experiments in towing tank, both being expensive and time-consuming tasks.

Shaft alignment calculation plan of case study vessel neglects hull deflections and examines only one running condition. Therefore three ballast drafts conditions without hull deflection effect will also be studied in which propeller moment  $M_z$  alters from its designed value. Moreover minimum and maximum hull deflections have been calculated through 1D FEM method, so these two sets of offsets are also going to be examined for a range of  $M_z$ . Summarizing, behavior of shafting system will be examined for the following scenarios:

- Offsets from SAC plan (shipyard calculation) for running condition:
  - a) designed draft
  - b) partially immersed propeller (1)
  - c) partially immersed propeller (2)
  - d) partially immersed propeller (3)
  
- Offsets from calculated hull deflections with Timoshenko (1) and Euler-Bernoulli (2) method for running condition:
  - e 1,2) hull deflection (max)
  - f 1,2) hull deflection (min)

For the Ballast Conditions, certain assumptions are necessary to address the costly and time-consuming numerical calculations, as well as potential tank model tests. These assumptions serve to establish the problem's boundaries and capture the trends in the shafting system.

### 6.4 a) Designed draft running condition

To address the challenge of expansive CFD calculations, the impact of hydrodynamic loads on shaft alignment will be simulated by a vertical bending moment series application at the propeller node, modeling propeller-wake interaction. These moments are considered to be a percentage of torsional torque transmitted through the shaft when the main engine is operating at Maximum Continuous Rating (MCR) condition. More precisely, the specified range is within  $\pm 30\%$  of  $Q_{MCR}$ <sup>18</sup>. The values for the bending moment  $M_z$  in the case study vessel are provided in the following table.

**Table 20: Limits of propeller hydrodynamic load range**

Torsional torque of M/E during MCR	$Q_{MCR}$	705.82 kNm
Limits of bending moment range	+30% $Q_{MCR}$ ( $M_{z_{max}}$ )	211.746 kNm
	-30% $Q_{MCR}$ ( $M_{z_{min}}$ )	-211.746 kNm

By applying intervals of 25%  $M_{z_{max}}$  into the initial design like in figure (Figure 51), the shafting system exhibits the behavior depicted in the following diagram:

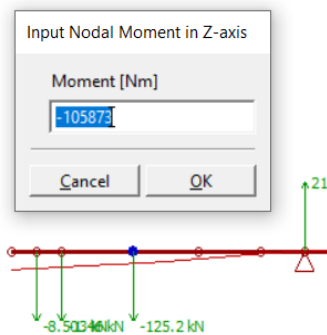


**Figure 51: Application of  $M_z$  in Shaft Alignment Tool**



<sup>18</sup> That range was explained in paragraph 4.2



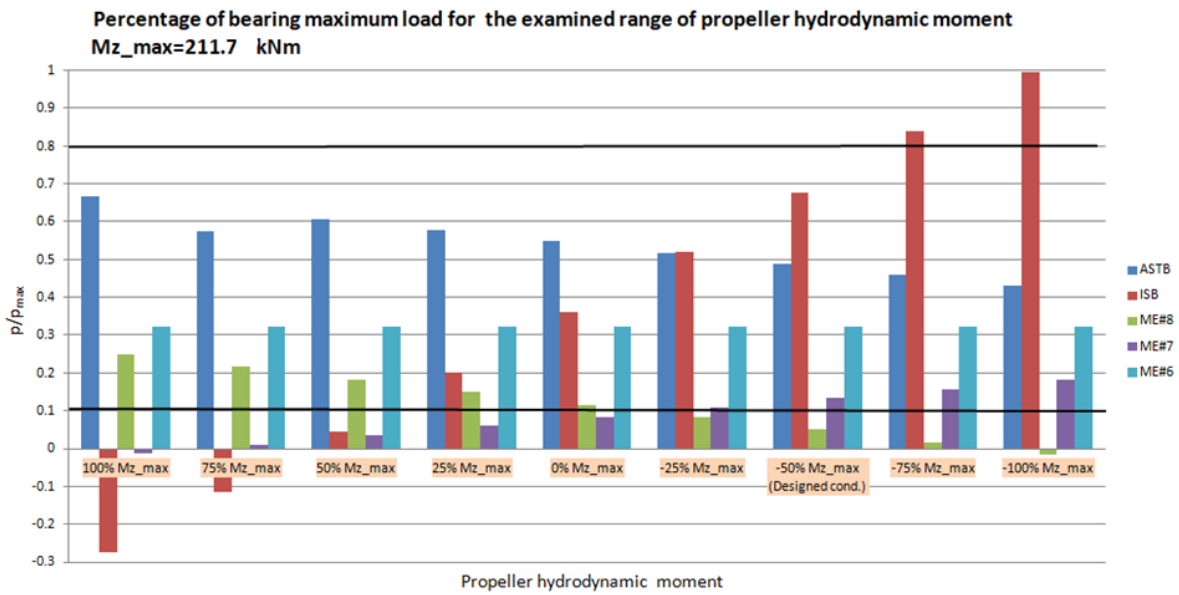


**Figure 52: Behavior of shafting system under examined propeller hydrodynamic load range**

The diagram above illustrates how deviations in Mz from its designed value affect the loads on various bearings. When Mz becomes more negative (elevating the propeller further), the load on the ISB exceeds 80% of its maximum allowable value, while ME#8 bearing becomes unloaded and even reaches a negative value. Conversely, as Mz becomes more positive (pushing the cantilever beam downwards), the ISB and ME#7 bearing become unloaded<sup>19</sup>. The loads on main engine bearings ME#6 to ME#3 remain constant at values of 0.30, 0.37, and 0.11, respectively, and thus are not all represented in the diagram. Additionally, the rate at which a column changes height depends on the maximum allowable load of the bearing.

<sup>19</sup> Consequences of bearing unloading and overloading are described in Chapter 4.1

## 6.4 b,c,d) Partially immersed propeller running conditions

Investigating partially submerged propeller conditions reveals two primary impacts on the shafting system. Firstly, with a portion of the propeller disc above the waterline, the buoyancy force decreases as less volume is submerged, affecting the overall dynamics. Secondly, the hydrodynamic forces exerted by the propeller change, both in magnitude and point of application, compared to the design draft running condition. Consequently, the thrust magnitude and point of application must be evaluated for these scenarios.

From the Typical Loading Manual two specific conditions will be examined, in which propeller is not fully immersed. Those are **Docking condition with 10% Bunker, Normal Ballast at Midway Before Ballast** and **an additional condition of  $T_M=4.8$  m** (not from Loading Manual). Their key characteristics are enlisted in the following table:

**Table 21: Ballast conditions from Loading - Unloading Sequence booklet**

Conditions examined	$T_A$ Draft (m)	$T_M$ Draft (m)	$T_F$ Draft (m)	Trim (m)	Displacement (t)	Propeller Immersion	Immersed propeller diam.
Docking 10% Bunker	3.536	3.476	3.416	-0.12	16200.75	3.927 %	3.235/6
condition of $T_M=4.8$ m	4.8	4.8	4.8	0	23009.80	25.0 %	4.5/6
Normal Ballast at Midway Before Ballast	6.245	5.825	5.406	-0.838	28277.79	49.076 %	5.944/6

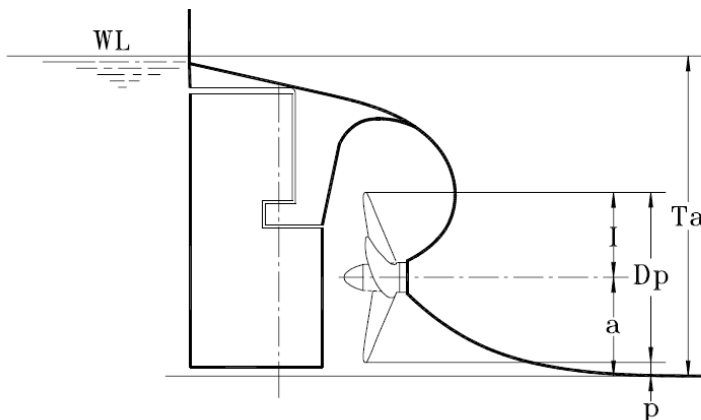
The propeller immersion percentage is defined as:

$$T_A \text{ draft} - \text{Height of shaft above bottom line} / \text{Propeller diameter}$$

where,

height of shaft above bottom line = 3.3 m

propeller diameter = 6.0 mm



Propeller Immersion Ratio:

$$I / D_p = (T_a - a) / D_p$$

Where:

$T_a$ : Draft at A.P. (m)

$a$ : Height of shaft above B.L. (m)

$a = 3.30$  m

$D_p$ : Propeller Diameter (m)

$D_p = 6.00$  m

**Figure 53: Convention of propeller immersion ratio**

For the condition above, vessel's speed will be considered to be 12 kn. This speed is quite high for such draughts. According to myshiptracking.com, ship's average speed is 12 kn. So this decision is made so as to be in the safe side, capturing an extreme condition. In Appendix A, thrust force and application point (eccentricity) are calculated for the above 3 conditions using simplified

assumptions for the latter. The resistance force equals to propeller thrust for each condition. The results are:

**Table 22: Results of Appendix A**

$T_M$ Draft (m)	Thrust Force (kN)	Eccentricity (mm)
3.476	206.8	1147
4.8	231.4	513
5.825	269.8	16

The propeller's vertical load still needs to be calculated, which is equal to the propeller's mass force in air minus the buoyancy of the immersed volume. Additionally, the moment  $M_z$  is calculated as the product of the thrust force and the eccentricity. It's important to note that a positive sign for  $M_z$  indicates that the propeller shaft cantilever is being pushed downwards.

**Table 23: Conditions for ballast simulations**

$T_M$ Draft (m)	Immersion	Propeller weight force in air (kN)	Buoyancy force (kN)	Vertical load (kN)	$M_z$ (kNm)
3.476	3.927%	144.746	10.525	134.220	237.199
4.8	25.0 %		14.636	130.111	118.708
5.825	49.076%		19.339	125.406	43.168

Condition of  $T_M=5.825m$  was very similar to condition of design draft, as propeller is almost fully immersed and maximum  $M_z$  is less than 211.7 kNm. Therefore, that condition practically appertains to Design Draft running condition (6.4a). In diagrams below can be seen the behavior of the shafting system for ballast conditions, where it can be seen that for  $T_M=3.476m$  when  $M_z$  reached the maximum positive values, ISB unloads as well as ME#6 bearing.

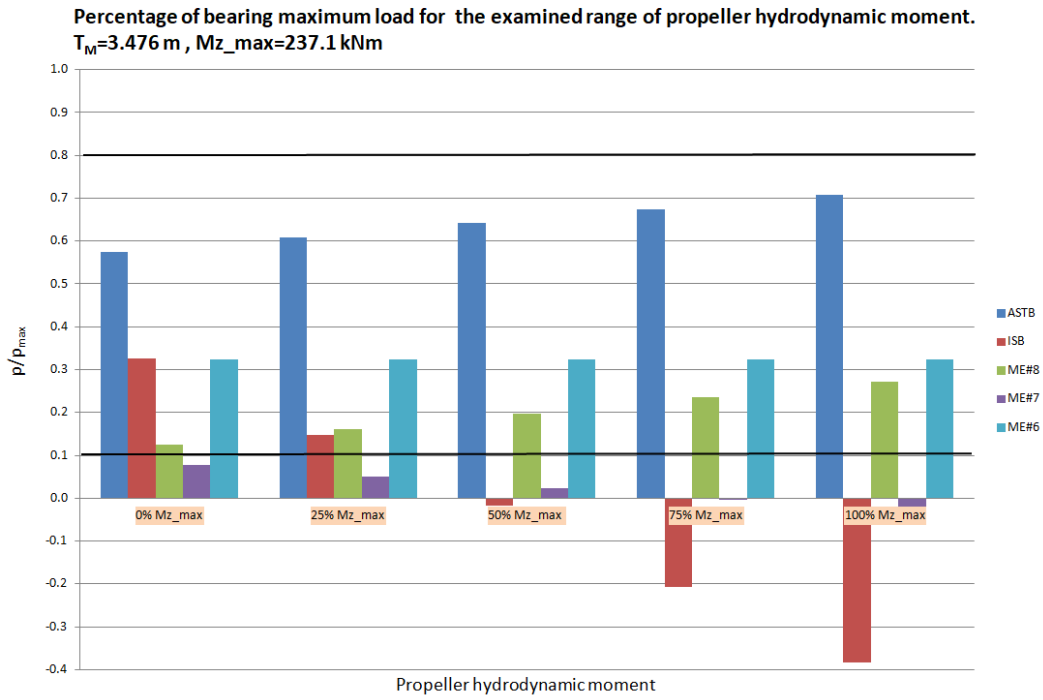


Figure 54: Behavior of shafting system under examined propeller hydrodynamic load range,  
 $T_M=3.476 \text{ m}$

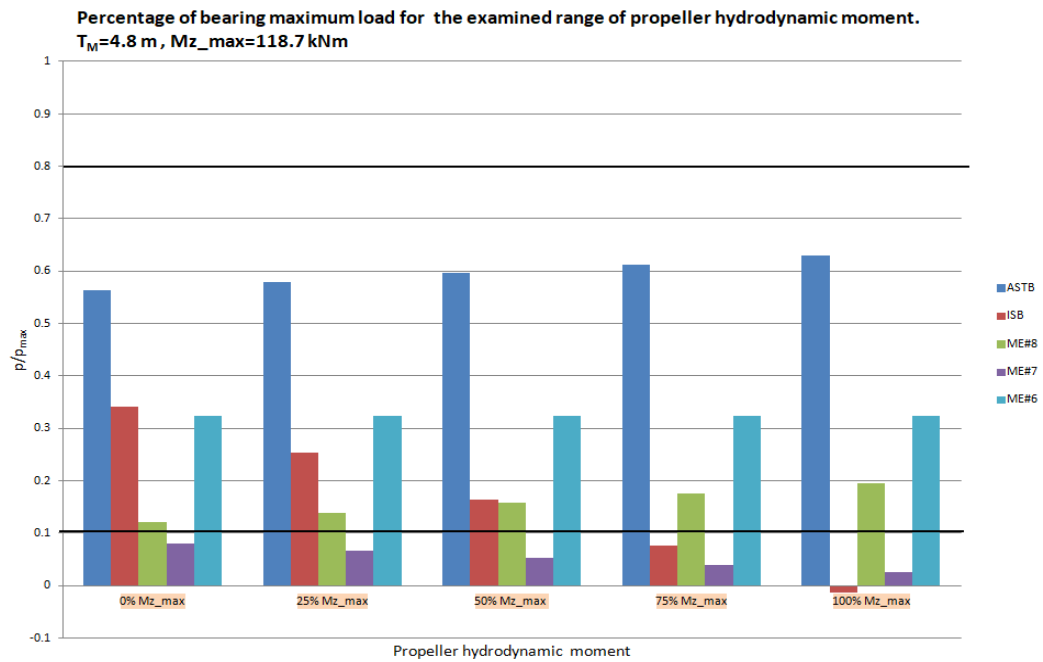


Figure 55: Behavior of shafting system under examined propeller hydrodynamic load range,  
 $T_M=4.8 \text{ m}$

## 6.4 e,f) Hull deflection max & min during running conditions

The same propeller hydrodynamic bending moment range as in 6.4a will be applied to check the behavior of shafting system ships, when specific loading conditions cause minimum and maximum hull deflections. As it was stated in Chapter 5.3.4, the uncertainty of the most suitable method (E-B or Timoshenko) has to be addressed by examining both of them.

### Euler Bernoulli method's results

**Table 24: Bearing Offsets calculated with Euler-Bernoulli method**

Relative Bearing Offsets (mm)	Euler – Bernoulli	
	Min	Max
Bearing position		
ASTB	0.000	0.000
ISB	-1.163	0.116
M/E #8	-2.906	-0.476
M/E #7	-2.964	-0.407
M/E #6	-3.023	-0.339
M/E #5	-3.082	-0.274
M/E #4	-3.134	-0.217
M/E #3	-3.184	-0.165

Corresponding shaft lines for the aforementioned offsets with designed  $M_z$  (-105.8 kNm) are the following:

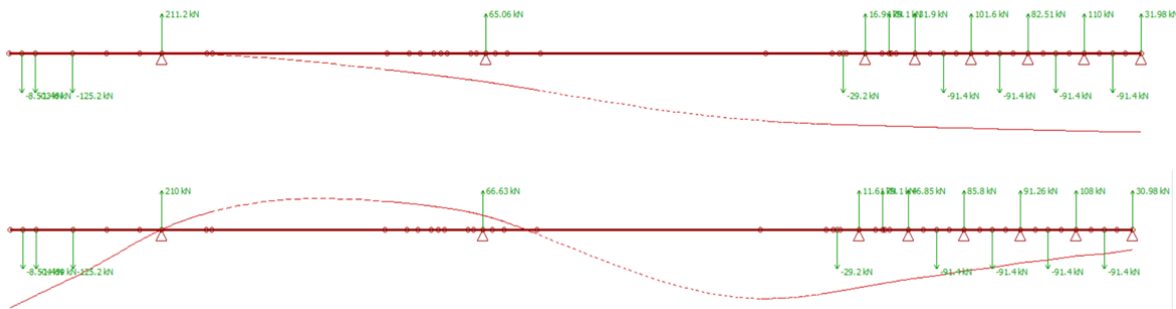


**Figure 56: Shaft lines (running condition) for Euler-Bernoulli method's HD, min (up) max (bottom)**

In diagrams below it can be seen that shafting systems' behavior is similar to the designed condition and has the same pattern. Again there are  $M_z$  values which result in overloading or unloading of specific bearings.

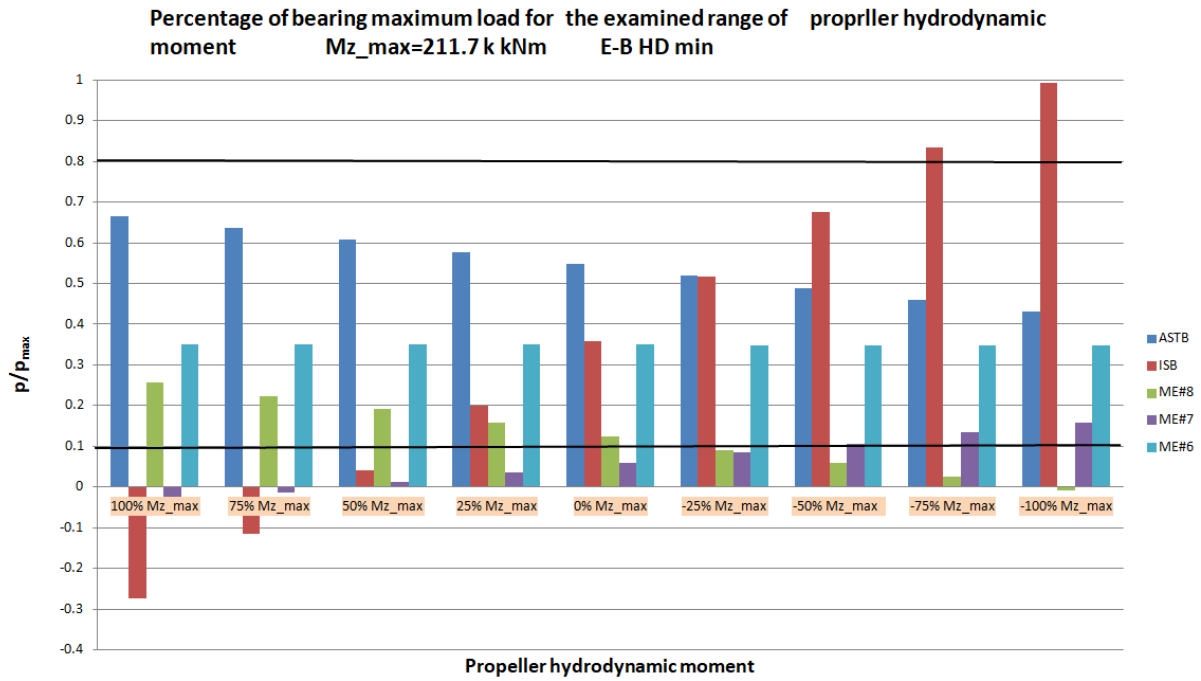


Figure 57: Behavior of shafting system under examined propeller hydrodynamic load range for HD min calculated with E-B method

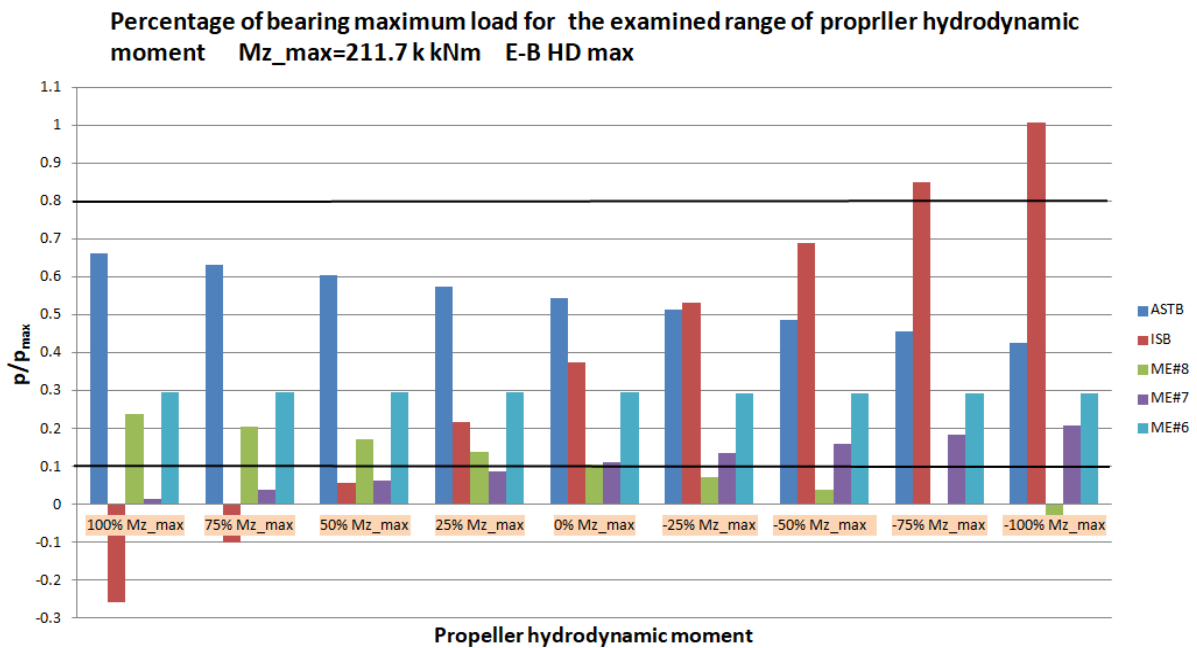


Figure 58: Behavior of shafting system under examined propeller hydrodynamic load range for HD max calculated with E-B method

## Timoshenko method's results

The same propeller hydrodynamic bending moment range as in 6.4a) will be applied to check the behavior of shafting system ships loading causes minimum and maximum hull deflections

**Table 25: Relative Bearing Offsets calculated with Timoshenko method**

Relative Bearing Offsets (mm)	Timoshenko	
	Min	Max
Bearing position		
ASTB	0.000	0.000
ISB	-1.952	2.331
M/E #8	-4.839	3.284
M/E #7	-5.001	3.433
M/E #6	-5.173	3.579
M/E #5	-5.353	3.718
M/E #4	-5.532	3.842
M/E #3	-5.722	3.959

Corresponding shaft lines for the aforementioned offsets with designed  $M_z$  (-105.8 kNm) are the following:

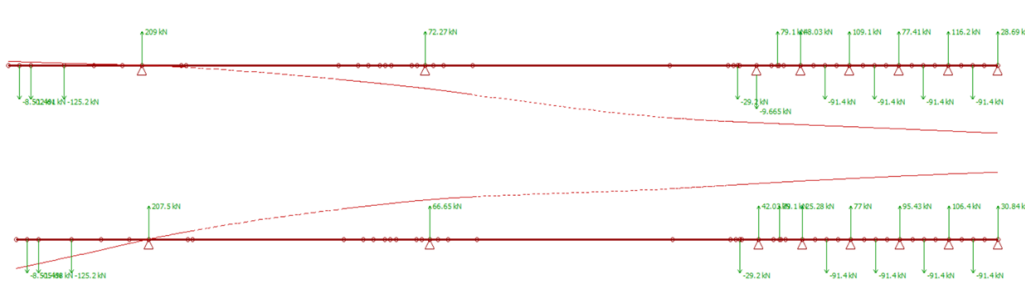


**Figure 59: Shaft lines (running condition) for Timoshenko method's HD, min (up) max (bottom)**

**Percentage of bearing maximum load for the examined range of propeller hydrodynamic moment  $M_{z\_max}=211.7$  kNm Tim HD min**

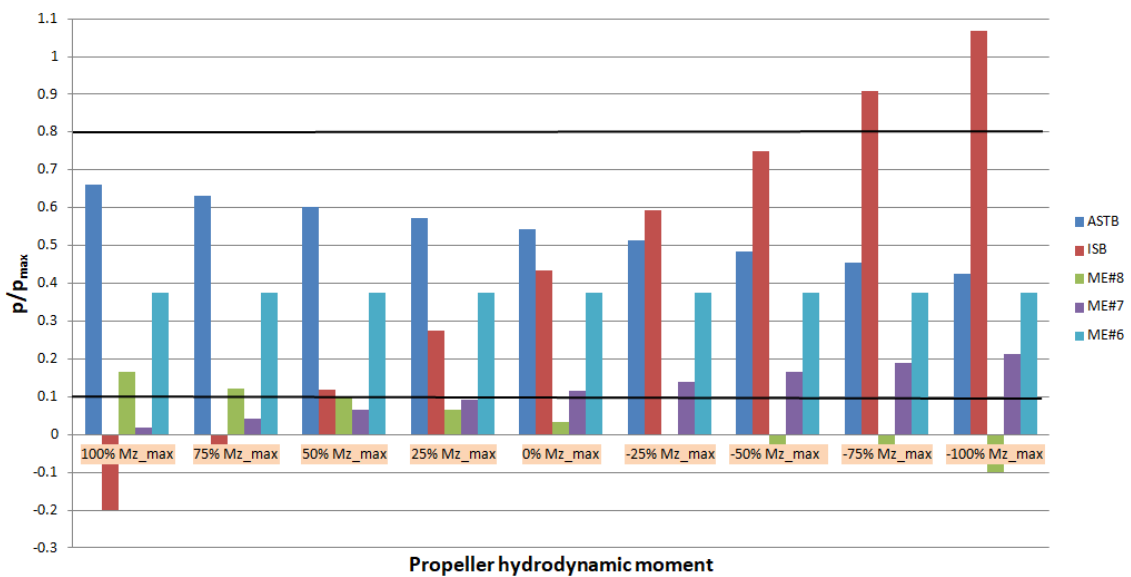


**Figure 60: Behavior of shafting system under examined propeller hydrodynamic load range for HD min calculated with Timoshenko method**

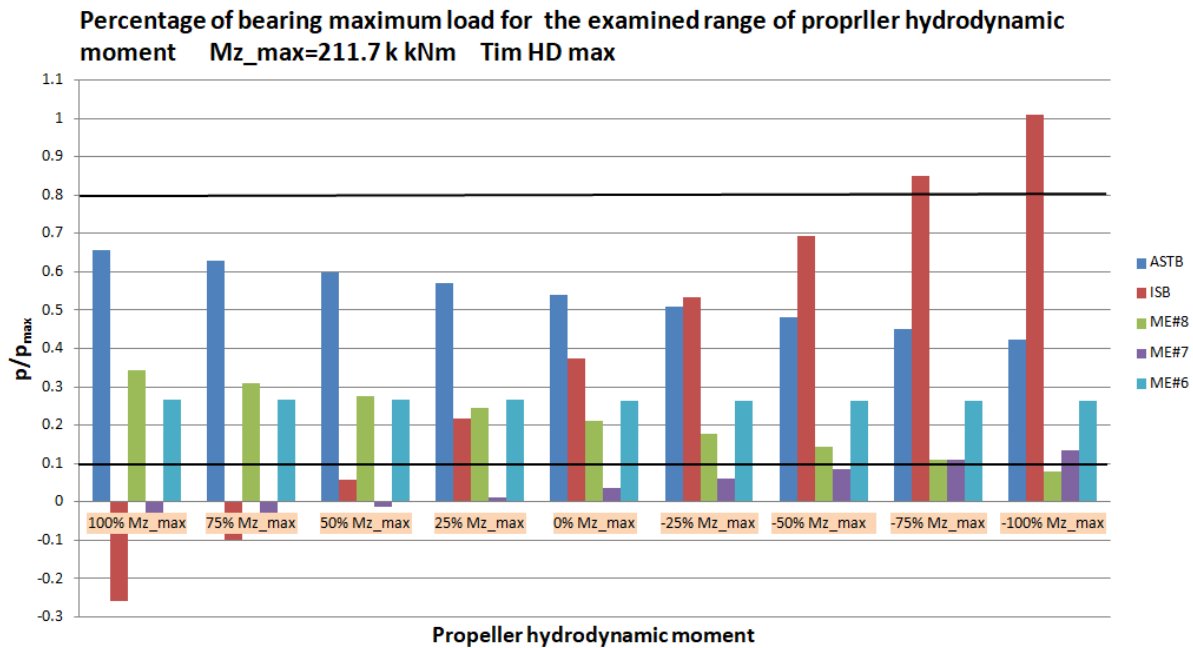


**Figure 61: Behavior of shafting system under examined propeller hydrodynamic load range for HD max calculated with Timoshenko method**

Having captured the behavior of the shafting system for all cases, it is evident that bearings become excessively overloaded (e.g. ISB almost 1.1 for Tim max) or unloaded (e.g. ISB -0.4 for  $T_M=3.476 \text{ m}$ ). Also the trend of load for some of the bearings is monotonically increasing while for others monotonically decreasing. The only affected bearings are ASTB, ISB and two aft most main engine bearings (ME#8, ME#7). That was also observed in Smart Bearing Sensor paper (Chapter 4.2.3) which also had ASTB, one ISB and main engine bearings. Regarding the designed condition (6.4a) the unloading of ISB was observed when the  $Mz=121 \text{ kNm}$  equal to 17.1 % of shaft torque when M/E operates at MCR, while in Smart Bearing Sensor paper at 32%.

## 6.5) Implementation of intermediate bearing actuation

### 6.5.1) Search for ISB line of movement

The previously discussed cases of unfavorable reaction forces suggest the introduction of intermediate bearing actuation. This approach ensures that, across the entire range of specified propeller bending moments, all bearings remain loaded as closely as possible to their acceptable values. Notably, ISB controls load distribution between the aft most 2 or 3 of the main engine (for the case study ship the 2).

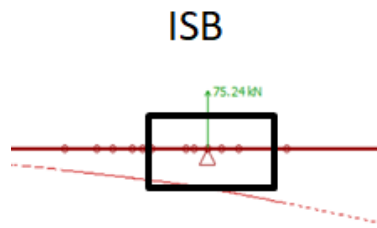
First, it is essential to define potential movements. The longitudinal and vertical movements of the intermediate bearing can be incorporated. However, within the context of 1D beam theory, rotation is determined to be inadequate for simulating the actual phenomenon. Applying a node rotation in the model is equivalent to imposing a bending moment at that node. In practice, a pair of forces should be applied to the shaft, with one force originating from the lower part of the bearing and the other from the top. Over time, the contact region would be eliminated due to friction, resulting in no further application of moments and debris in the lubricant oil. Therefore, only longitudinal and vertical movements will be applied.




**So longitudinal and vertical movements will only be applied.** In order to find out which are the optimal positions for every Mz load on propeller node for each scenario, an algorithm was used and corresponding diagrams were created. For each Mz moment, a range of possible longitudinal and vertical positions is examined from which optimal sub-regions will be visible, where reactions are acceptable and from all of these diagrams the line of movement will be found.

The scenario in which the algorithm will be applied is for the set of offsets from SAC plan for running condition, meaning the support of ASTB lies in L/3 from bearing's aft end. The selected line will afterwards be tested for the rest scenarios and then it can be determined whether is suitable for the shafting system.



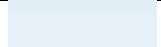
In the 1D model, ISB movement is applied by increasing and reducing finite segments from both sides of the supporting node, keeping the sum of their lengths constant. In the following diagrams, the x-coordinate represents the length of the left segment, and the y-coordinate represents the absolute offset of the ISB. A rectangle-shaped area (**Figure 62**) was selected for examination, considering the geometric limitation of the flange between the propeller and intermediate shaft, left of the ISB.



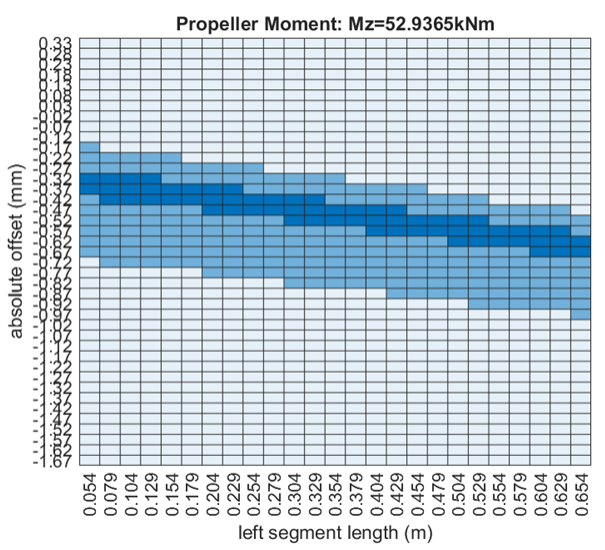
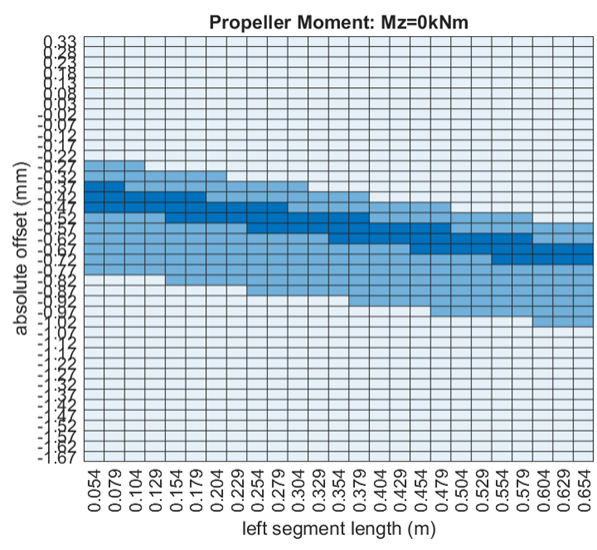
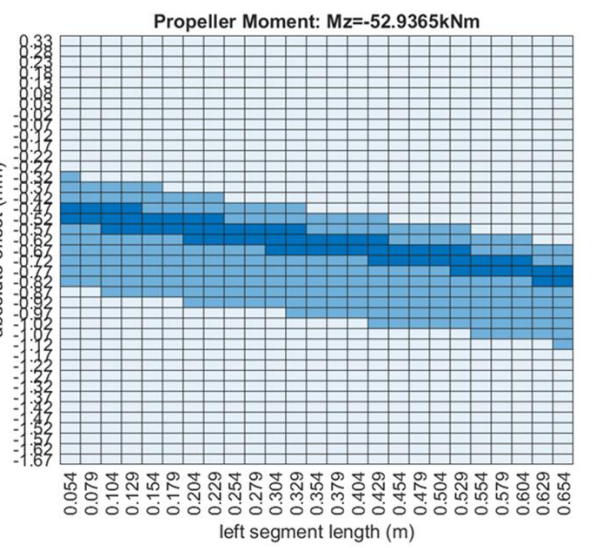
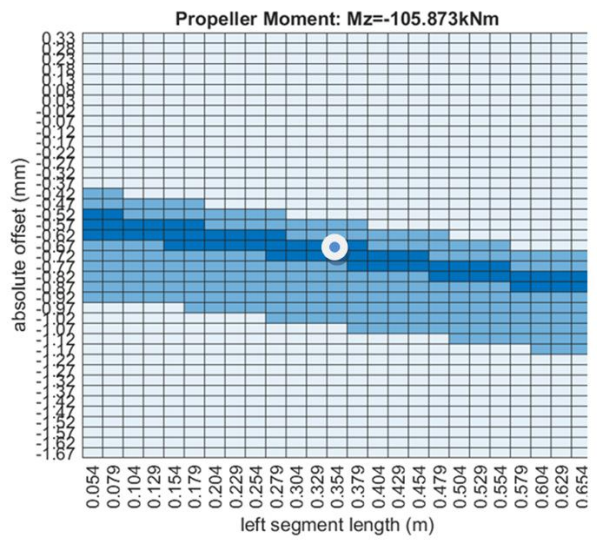
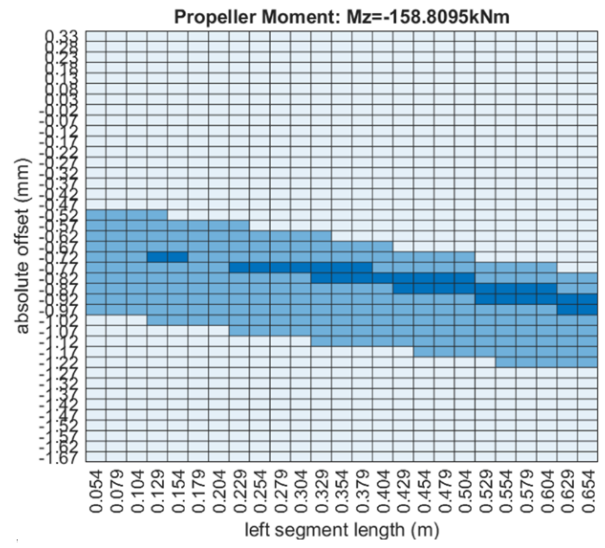
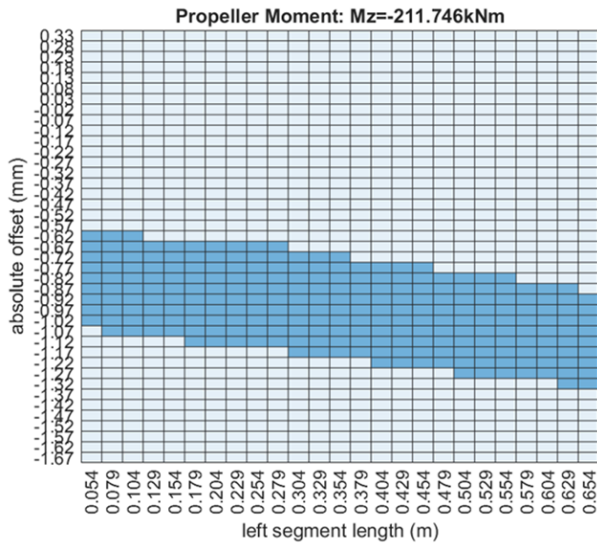
**Figure 62: Selected area for examination**

The designed condition from SAC plan is shown with: 

**Table 26: Legend for following diagrams**

Condition of shafting system	Color on diagram	Criterion <sup>20</sup> for $p/p_{max}$	
		For all bearings except ME#8	For ME#8
Acceptable		$0.1 < p/p_{max} < 0.8$	$0.04 < p/p_{max} < 0.8$
Marginal		$0 < p/p_{max} < 0.1 \vee 0.8 < p/p_{max} < 1$	$0 < p/p_{max} < 0.04 \vee 0.8 < p/p_{max} < 1$
Not Acceptable		$p/p_{max} < 0 \vee p/p_{max} > 1$	

<sup>20</sup> In ABS [20] it is stated that : “An alignment condition is acceptable as long as the bearing reactions remain positive under all service drafts, and no bearing is unloaded. In general, any positive static load is therefore acceptable. For practical reasons and to prevent unloading or overloading of the bearings due to unaccounted for disturbances, it is preferred at least 10% of the allowable bearing load is desired on each bearing and measured bearing reactions may not exceed 80% of the manufacturer’s maximum allowable load. So in a case in which all bearing reactions are greater or equal to 10% of their respective maximum allowable load limits and less than 80% of their maximum allowable load limits, it is considered as **Acceptable**. In a case in which all bearing reactions are positive and not exceed their respective maximum allowable load limits and at least one bearing reaction is less than 10% of its respective maximum allowable load limit or greater than 80% of its respective maximum allowable load limit, it is considered as **Marginal**. And in a case in which at least one bearing reaction is negative or exceeds its respective maximum allowable load limit, then the scenario belongs to **Not Acceptable**. In this study the minimum **acceptable criterions of ME#8 is lowered**, since engine manufacturer allows for zero loading and in shipyards SAC, during dynamic condition, attains value of  $p/p_{max}=0.044$ .”



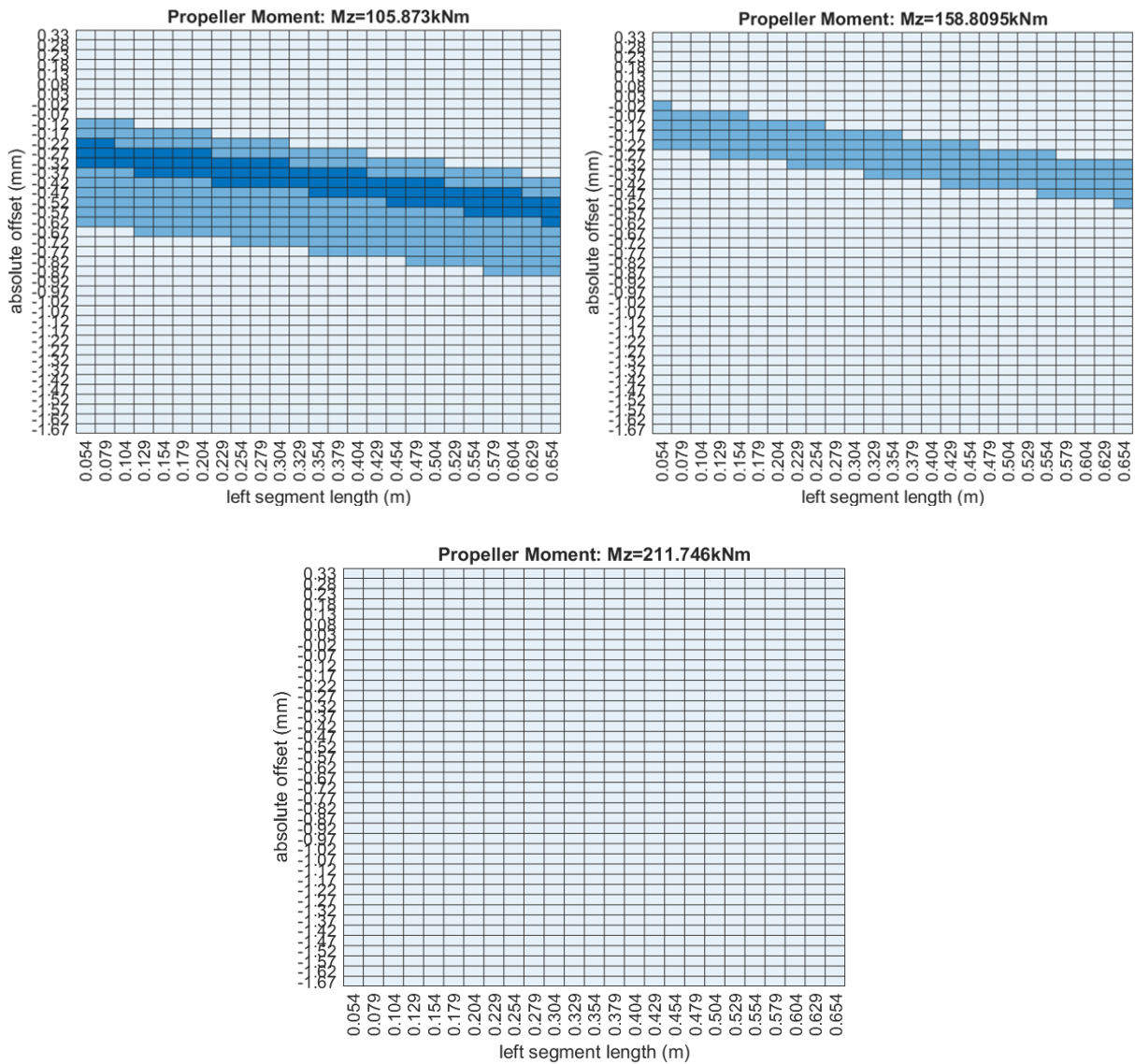


**Figure 63: Possible positions of ISB for different Mz for achieving acceptable reaction forces**

The line of movement should pass from original point of ISB (that of SAC plan) to prevent the need for checking reactions under different immersion conditions of the SAC plan. Moreover in order for the shafting system to remain in acceptable condition, the line should pass from an Acceptable region of each diagram, if feasible. Through an iterative process, the most suitable line for ISB translation was derived:

$$y = -5x + 1.1 \quad \text{x: left segment length (m)} \quad \text{y: ISB absolute offset (mm)}$$



**Figure 64: Plotted line of movement (Slope has been exaggerated for clarity)**

Then all cases were tested with ISB positions given by equation above, so diagrams like (**Figure 65**) were created to visualize the optimal positions of ISB for each case. Green color is for ISB position on the line which give acceptable loading for the shafting system, while orange is for marginal loading.

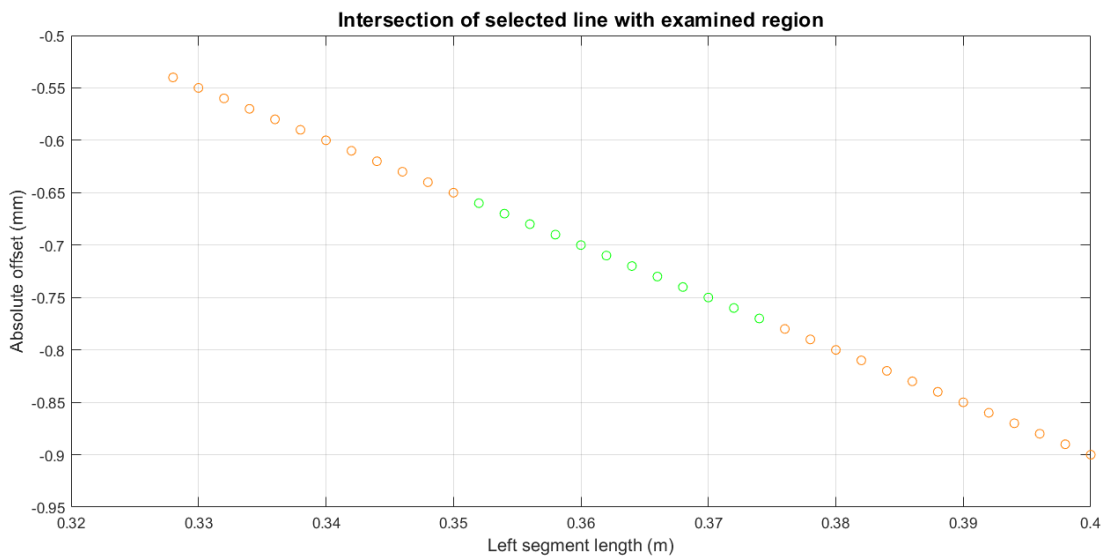


**Figure 65: Intersection of selected line with examined region, showing all acceptable and marginal positions**

From diagram where  $M_z=211.746$  kNm it is evident that no possible ISB position provides a marginal or acceptable condition for the shafting system. One influencing factor is the assumption of supporting point of ASTB, set at  $L/3$  (according to SAC plan) since it is a running condition. However this practice is quite conservative, as when propeller shaft is pushed downwards, supporting point is moved to the aft region of bearing (edge loading).

To determine a more realistic ASTB supporting point for this scenario, the software described in chapter 5.2 will be used to recalculate the loads and misalignment angle.

## 6.5.2) Application of ISB line of movement

a) Designed draft running condition (6.4a), shaft lines for each case are in (Figure 66)

Percentage of bearing maximum load for the examined range of propeller hydrodynamic moment  $Mz_{max}=211.7$  k kNm with ISB actuation

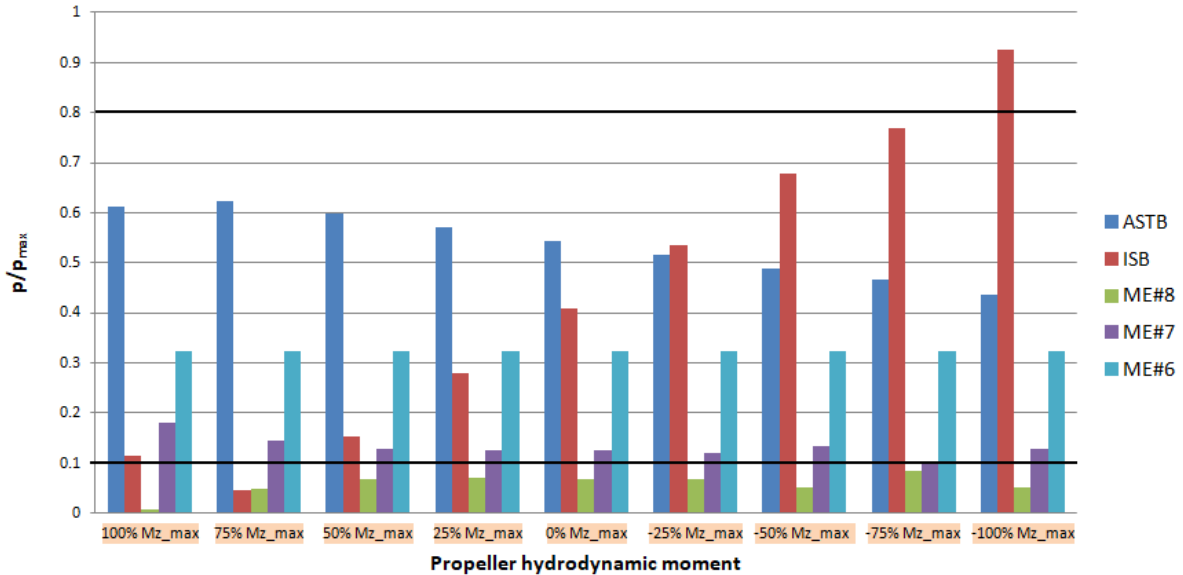


Figure 66: Behavior of shafting system under examined propeller hydrodynamic load range with ISB actuation

For  $Mz=211.746$  kNm Reynolds solver the exact supporting point is calculated by an iterative process. Given an initial ASTB reaction force and misalignment angle to the solver, supporting position is calculated and then follows the same procedure. After 3 iterations position point value has converged. The process below concluded that actual supporting point position of ASTB is at 7.84%L rather than at 33.3%L (L/3).

Table 27: Actual supporting position of ASTB for  $Mz=211.746$  kNm, iterative process

ISB position (0.238, -0.09)	Initially	1 <sup>st</sup> iter	2 <sup>nd</sup> iter	3 <sup>d</sup> iter
Supporting point from left end (m)	0.34	0.040	0.086	0.080
ASTB Reaction force (kN)	280.137	262.3	264.951	264.6
Misalignment angle (mrad)	0.941	0.868	0.880	0.843

Bearing final forces for $Mz=211.746$ (kNm) ISB position (0.238, -0.09)	Reaction force (kN)	
	Initially (Without Reynolds solver)	Finally (With Reynolds solver)
ASTB	280.1	264.6
ISB	-6.174	10.91
M/E #8 Bearing	7.81	2.019
M/E #7 Bearing	47.87	52.17
M/E #6 Bearing	93.86	93.83
M/E #5 Bearing	87.53	87.53
M/E #4 Bearing	108.2	108.2
M/E #3 Bearing	31.87	31.87
Supporting point from left end (m)	0.34 (33.3% $L_{ASTB}$ )	0.08 (7.84% $L_{ASTB}$ )
Misalignment angle (mrad)	0.941	0.843

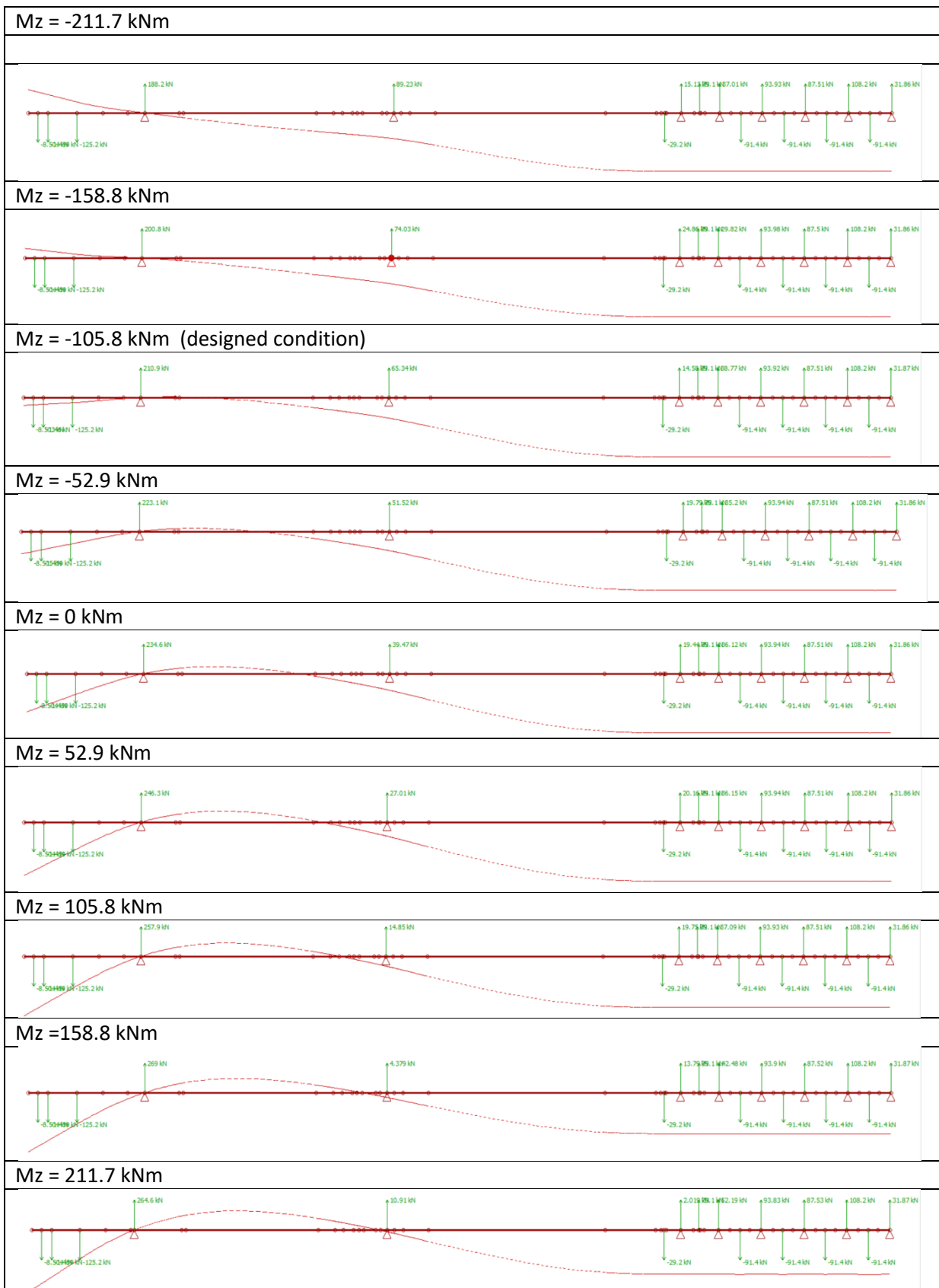
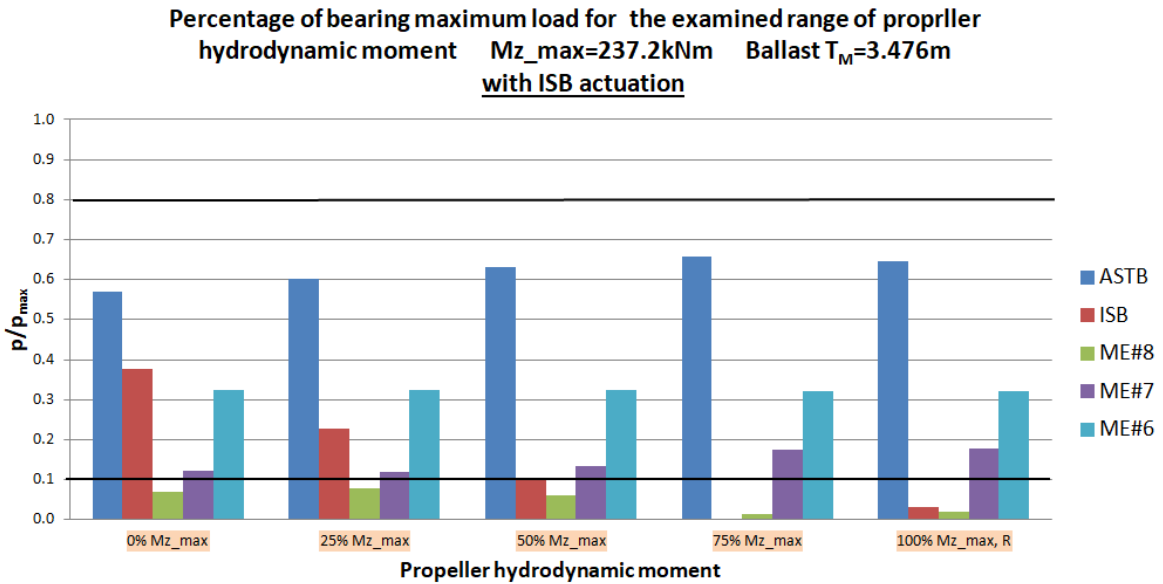


Figure 67: Shaft lines cases for varying propeller loads, while ISB placed optimally for each case on selected line

**b) Partially immersed propeller  $T_M=3.476$  (6.4b)**

Reynolds solver was used for  $Mz=237.2$  kNm and supporting position of ASTB was found to be at 3.23%L



**Figure 68: Behavior of shafting system under examined propeller hydrodynamic load range with ISB actuation  $T_M=3.476$  m**

**c) Partially immersed propeller  $T_M=4.8$  (6.4c)**

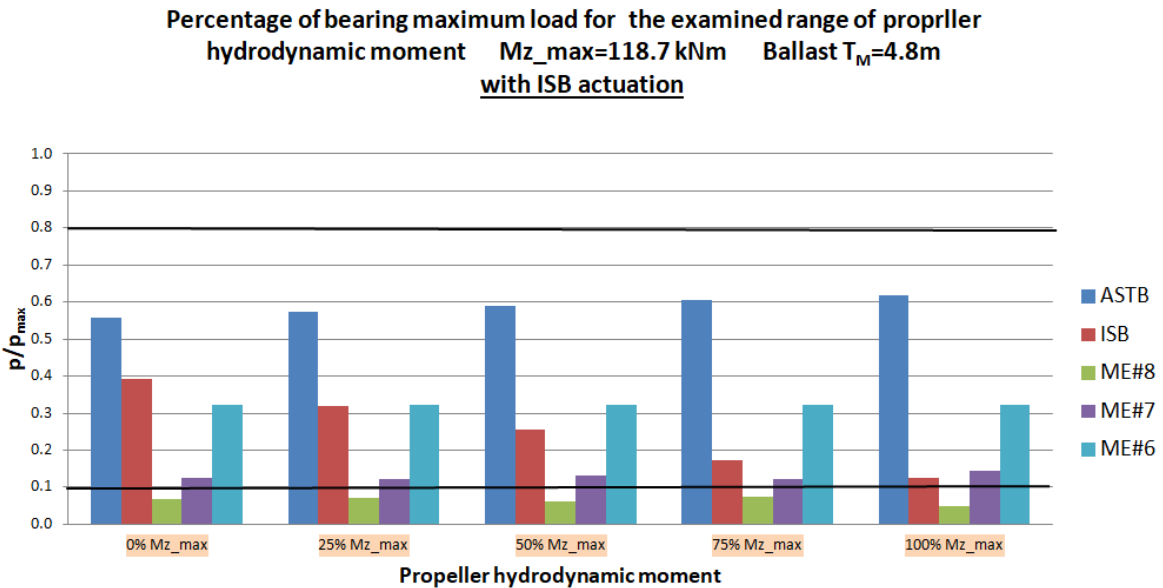


**Figure 69: Behavior of shafting system under examined propeller hydrodynamic load range with ISB actuation,  $T_M=4.8$  m**

**d) Partially immersed propeller  $T_M=5.825$  (6.4.d)**

For  $T_M=5.825$  propeller is almost completely immersed and the  $M_z$  moment lies in the range of 211.7 kNm. For this reason this case is practically examined within case (6.4a).

For hull deflection scenario results of Timoshenko method will presented here while of E-B method are only listed in Appendix B.

**e1) Hull deflection max Tim (6.4e)**

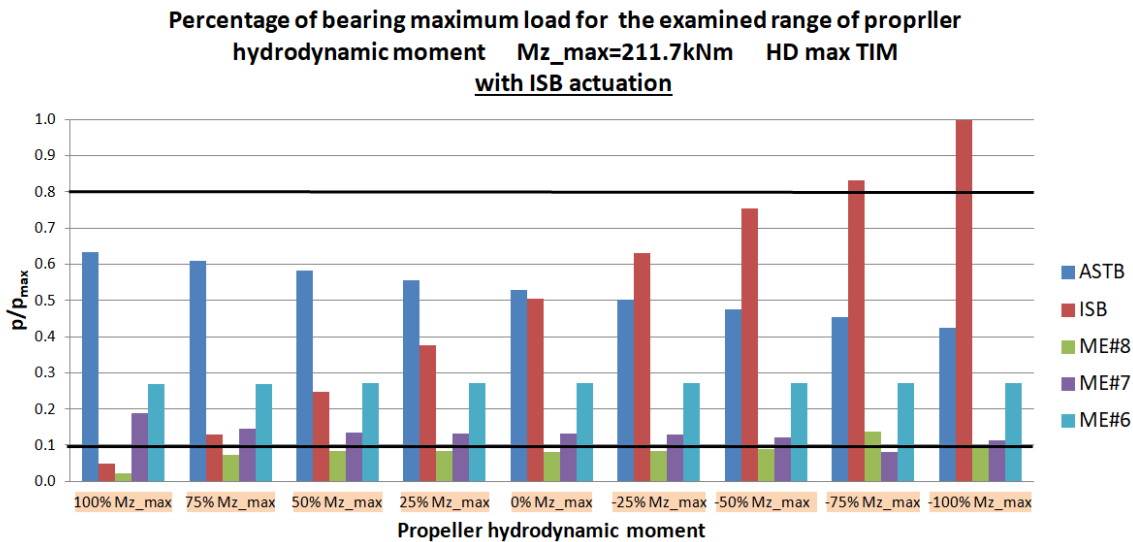


**Figure 70: Behavior of shafting system under examined propeller hydrodynamic load range with ISB actuation, HD max with Timoshenko method**

**f1) Hull deflection min Tim (6.4.f)**

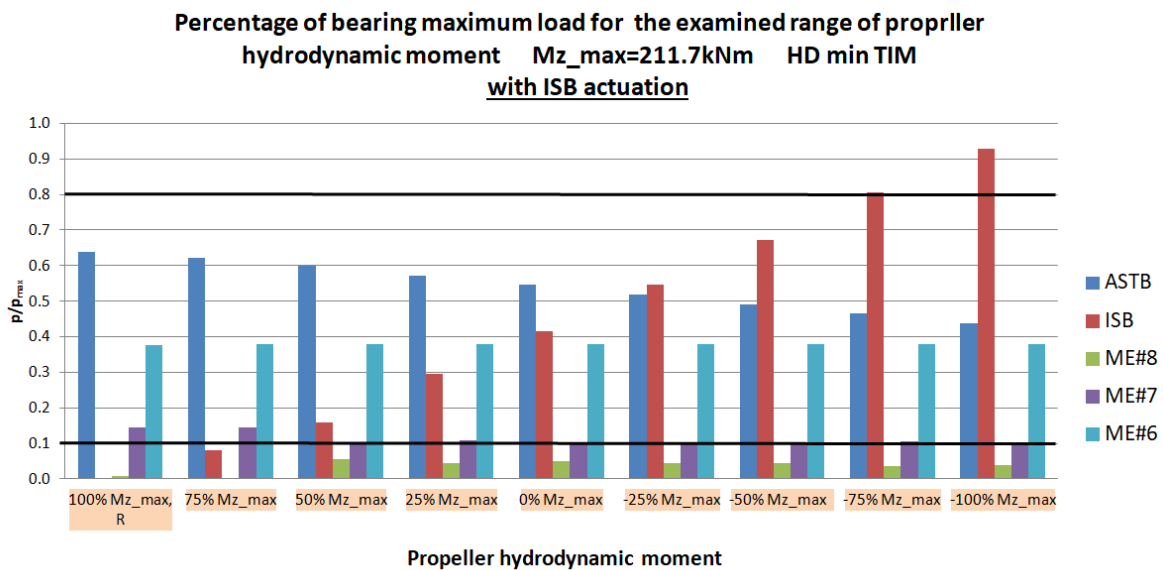


**Figure 71: Behavior of shafting system under examined propeller hydrodynamic load range with ISB actuation, HD min with Timoshenko method**



The letter "R" next to the  $M_z$  percentage indicates that the Reynolds solver was utilized to calculate the actual supporting position of ASTB for that specific bending moment. Without this calculation, no possible ASTB position would yield an acceptable or marginal condition for that  $M_z$ . Appendix B presents all cases with reactions without ISB actuation, with ISB actuation, and the optimal position on the selected line of movement for each  $M_z$ .

### 6.5.3) Extend of line of movement

Having examined all those conditions and defined the positions of ISB on the line of movement for all of them, the total length on that line can be found:

**Table 28: Length on line of movement for each condition**

Condition	Range (left segment length) (m)
a) Designed draft	0.238 – 0.390
b) Ballast $T_M=3.476m$	0.230 – 0.326
c) Ballast $T_M=4.8m$	0.278 – 0.326
e1) HD max Tim	<b>0.216</b> – 0.360
f1) HD min Tim	0.270 – <b>0.434</b>
e2) HD max E-B	0.250 – 0.400
f2) HD min E-B	0.250 – 0.410
<b>Extreme values</b>	<b>0.216 – 0.434</b>

**So, the total length on line of movement is 218 mm, resulting in a total ISB vertical offset of 1.09 mm.** With all assumption taken into account, shafting system will work in acceptable and marginal conditions. The purpose of this thesis was to investigate the feasibility, motion of actuation and the advantages of ISB movement.

## 6.6) Possible ISB actuation applications

### 6.6.1) ASTB temperature rise

During ship operation, instances of ASTB temperature rise typically indicate a compromise in the hydrodynamic lubricant film over a portion of the bearing. Alarm limits for oil-lubricated, whitemetal-lined journal bearings are generally set around 65°C, with slow-down recommended at 70°C, and an immediate stop at 75°C. If temperatures increase by more than 5°C per minute at any time, the system should be stopped. Causes may include transient increases in shaft load during heavy maneuvering, heavy ship motions, poor alignment between the bearing and shaft journal, or lubricant degradation (e.g., water contamination due to seal leakage). Bearing problems often involve multiple contributory factors [22]. Continuing operation under these conditions can exacerbate the situation, causing deformation and detachment of the white metal and increasing friction [41]. A potential reaction measure in the event of ASTB heating is to maintain the shaft at the highest speed that still allows for a decreasing bearing temperature towards the typical operating condition. Normalization of the stern-tube bearing temperature may take several hours, but the shaft should not be stopped.

In the case of an urgent ASTB bearing temperature increase, the situation will be addressed using a 1D model of the shaft by attempting to unload the bearing as much as possible with optimal ISB positioning on the selected line of movement. The aim is to increase the load on the other bearings. By placing the ISB at each point on the line of movement (and beyond), the following diagram is produced:

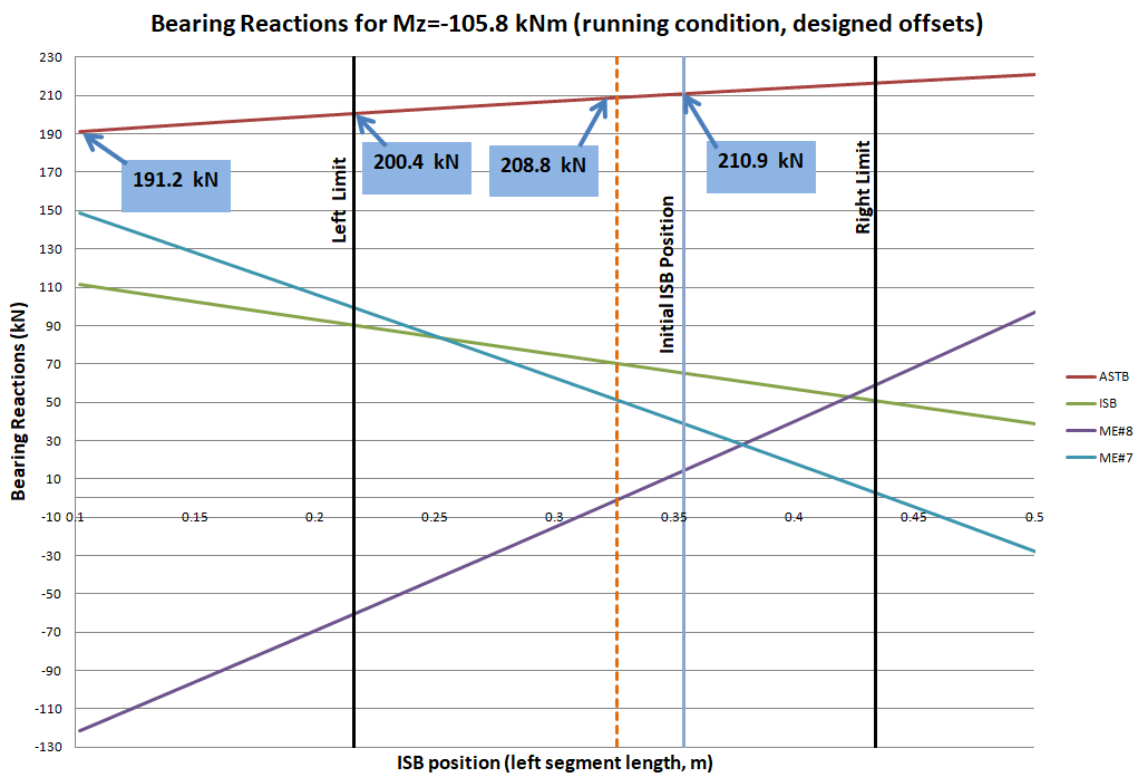


Figure 72: Reaction forces while ISB moves on line of movement

In (Figure 72), it's evident that at the initial position of ISB, the reaction force of ASTB is 210.9 kN. As ISB moves to the left, just before unloading ME#8, the ASTB load reduces to 208.8 kN (a reduction of 2.1 kN). Further leftward movement of ISB to the end of the line of movement results in an ASTB reaction force of 200.4 kN (a reduction of 10.3 kN), but with ME#8 experiencing negative load. If ISB is moved beyond the left end of the line of movement, the ASTB reaction force could reach 191.2 kN (a reduction of 19.7 kN). However, during this unloading process, ISB and ME#7 become more heavily loaded, and near the left end, ISB starts to become overloaded.

Adjusting ISB to the left of its initial position leads to a decrease in ASTB load. The extent of this reduction depends on the decision to unload the ME#8 bearing or not. Nonetheless, every effort to unload ASTB could synergistically decrease ASTB temperature in case of an alarm. Additionally, starboard turns should be avoided as they push the propeller cantilever downwards, thereby increasing ASTB reaction force. Moreover, a reduction in speed would likely increase ASTB load, as the bending moment during straight ahead courses lifts the propeller cantilever.

**6.6.2) Optimal static positioning depending the loading condition**

If ISB was to be optimally positioned, in a static way, before departure given the loading condition the following position on the line of movement could be selected for each case:

Laden (aft peak tank empty) → Hull deflection max

Lightship → Initial offsets

Ballast (aft peak tank full) → Hull deflection min

The selected positions for each case while  $M_z = -105.8 \text{ kNm}$ , using Timoshenko method are:

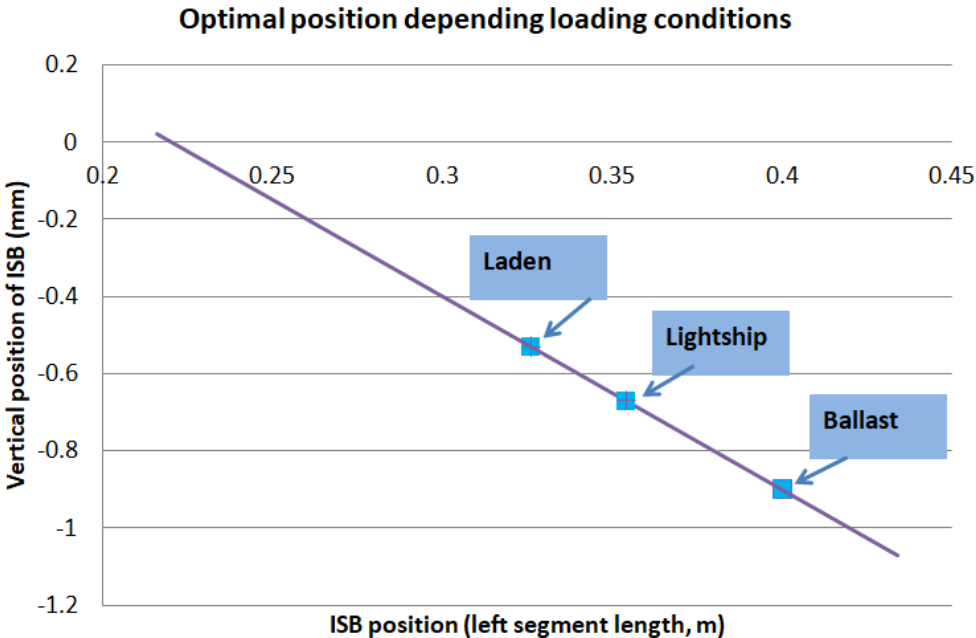


Figure 73: ISB optimal placement prior to departure depending the loading condition

Having one calculated hull deflection values for all loading conditions a diagram like the above could be produced, so as to ISB would be optimally placed prior to departure.

## 6.7) Concept design of actuation mechanism for simulations on a scaled Test-rig

Laboratory of Marine Technology is equipped with a testing rig for shaft alignment [1]. On that rig different alignment configurations can be examined, shaft deflection and bearing reactions can be measured.

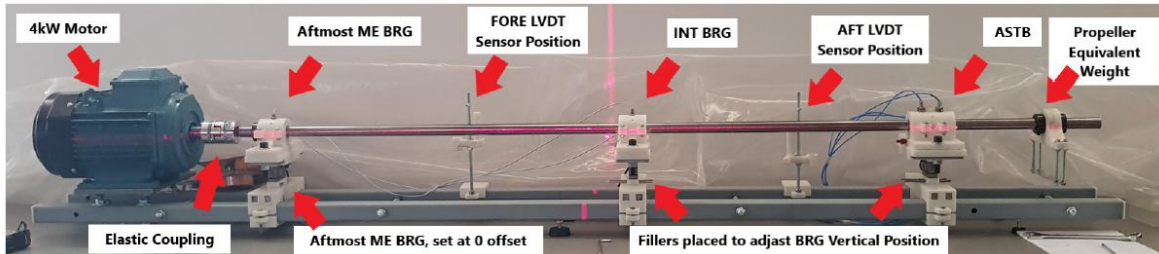


Figure 74: Scaled Test-rig [1]

ISB actuation could be possible by inserting a base and an actuation mechanism below that bearing. A proposal for that configuration is the following:

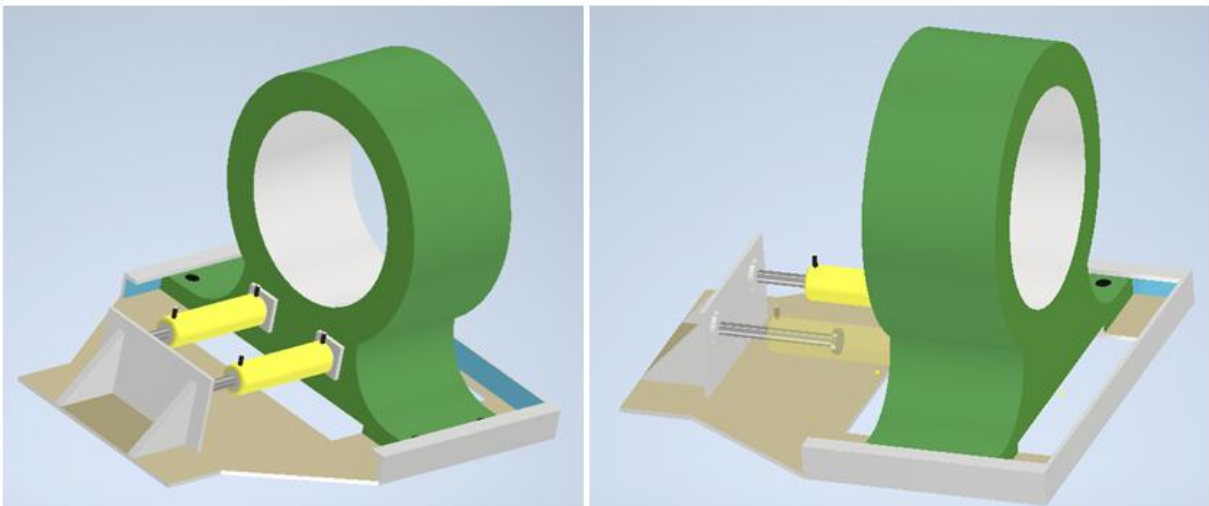
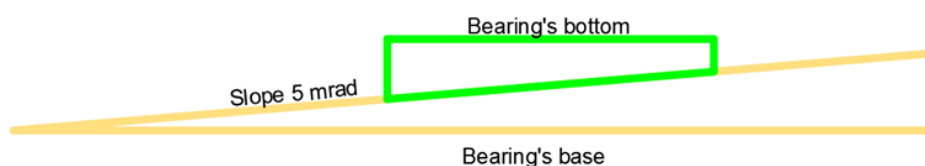


Figure 75: Proposed configuration for ISB actuation for the testing rig

Bearing's position will be governed by the two hydraulic cylinders, whose function could be controlled by a PID controller. These cylinders have inside a rod and by using a high pressure oil pumping system, its position can be changed by increasing pressure in one side of the cylinder, which is inserted through the two inlets. Regarding the surface of the base, a low frictional coefficient has to be established to reduce required actuation force. The surface of the base has the found slope of 5 mm and bearing's base will have the same force so as to bearing's axis remains horizontal, causing vertical movement. A sketch of the base-bearing contact will be given bellow:



Slope has been exaggerated for clarity. As hydraulic cylinder expands, bearing moves closer to the ATSB and its offset gets increased.

## 7) Conclusions and future work suggestions

### Conclusions

The present study thoroughly examines the behavior of the shafting system in a Supramax Bulk Carrier under various operational conditions. The impact of propeller hydrodynamic loads on the shafting system was modeled using a range of vertical bending moments applied to the propeller node. This range, influenced by the shaft torque at maximum continuous rating (MCR) of the main engines, was based on literature suggested by classification societies. Notably, there is no universal method for calculating these loads, and even computational fluid dynamics (CFD) models may fail during transient conditions.

Moreover NTUA SAC plan database was examined in order to evaluate the way shipyards account for these moments and key findings were enlisted which can be used in future shaft alignment calculations for ships with similar particulars, increasing calculation's robustness as one more condition can be examined. Additionally, since SAC plan of case study ship did not include hull deflections, 1D method for calculating them was utilized. Specifically second moment of area and shear area of several frames of engine room and stern construction were measured and external loading distribution was extracted from loading manual for specific conditions. Then Euler-Bernoulli and Timoshenko methods were both used to calculate minimum and maximum hull deflections which were selected to be studied.

Hydrodynamic loads on the propeller during ballast conditions, where the propeller was partially immersed, were calculated as the product of thrust force and vertical thrust eccentricity. These propeller bending moments led to bearing unloading and overloading, specifically affecting the ASTB, ISB, ME#8, and ME#7 bearings. For all conditions and the selected range of vertical bending moments, the optimal position of the ISB was determined on a chosen line of movement to ensure no bearing had a negative load and the shafting condition was acceptable. In rare cases where the propeller cantilever was pushed downward, no ISB position met the objective, and a Reynolds solver was used to accurately estimate the support point in the ASTB bearing.

The key finding of the thesis is that a longitudinal movement of 218 mm with a slope of -5 mrad could significantly contribute to shafting systems' robustness for running conditions.

## Future Work Suggestions

- Enhance accuracy of the present study by completing the following sub-projects:
  1. Calculation of propeller hydrodynamic loads with CFD method for several ships during straight ahead course, maneuvering and for partially immersed propeller condition.
  2. Improving 1D method for hull deflection estimation by selecting which parts of a frame section contribute and by which extend. Maybe do comparisons between a 3D FEM and 1D FEM by examining specific construction parts (e.g. engine foundation, tanks, openings).
  3. Construction of the shafting model utilizing Fluid Structure Interaction (FSI) for modeling shaft-bearing interaction.
  4. Gather, evaluate and thoroughly write down methodologies and practices of aforementioned works. (CFD, 3D FEM, FSI models).
- Expand and test the operation of ISB actuation by experiments in NTUA testing rig with the following objectives:
  - 1 Run experiments in testing rig, by applying different moments through weight adjustments at propeller position and create the mechanism of ISB actuation.
  - 2 Creation of PID controller for ISB actuation with inputs to be shafting line deflection (with strain gauges methods and proximity probes) or bearing loads (i.e. load cells).
  - 3 Investigate the relation of ISB actuation in vibration characteristics of the system.
  - 4 Implement ISB actuation in a ship with more than one ISB bearings (e.g. containership), which possibly operates in a more extended hull deflection envelope.
  - 5 Study the shaft- ISB interaction during movement and calculate maximum required actuation force.

## Literature - References

- [1] Assistant Professor Principal Investigator: Christos Papadopoulos, "Intelligent adaptive-controllable alignment in marine propulsion systems for performance optimization and failure prevention," Cooperative Organizations: NTUA, ABS, RINA, STARBULK, [2415 – i-MARINE], 2021.
- [2] "MARINE ENGINEERING DESIGN," 1 January 2008. [Online]. Available: [https://me5001.blogspot.com/2008/01/marine-engineering-design.html?\\_sm\\_au\\_=iVV03Ff3kTWdVnVjctQQFK3qWK4TJ](https://me5001.blogspot.com/2008/01/marine-engineering-design.html?_sm_au_=iVV03Ff3kTWdVnVjctQQFK3qWK4TJ).
- [3] A. Ursolov, Y. Batrak and W. Tarelko, "Application of the optimization methods to the search of marine propulsion shafting global equilibrium in running conditions," *Polish Maritime Research*, 2019.
- [4] Y. Batrak, R. Batrak and D. Berin, "Computer application for shaft alignment design," *International Conference on Computer Application in Shipbuilding*, 2013 Busan Korea.
- [5] Jae-ung Lee, "Application of strain gauge method for investigating influence of ship shaft movement by hydrodynamic propeller forces on shaft alignment," ELSEVIER, June 2018.
- [6] American Bureau of Shipping (ABS), "Cutsheet: Enhanced Shaft Alignment (ESA)," [Online].
- [7] Minxiong Chen, "Some Concerns on Shaft Alignment Onboard Ship," Rules & Technology Center, China Classification Society (CCS), Shanghai, China.
- [8] Chris Leontopoulos, Charalampos Mouzakis, and Michail Petrolekas, "Smart Bearing Sensor," *Journal of Ship Production and Design*, Vol. 36, No. 1,, February 2020.
- [9] L. Jae-ung, J. Byongug and A. Tae-Hyun, "Investigation on effective support point of single stern tube bearing for marine propulsion shaft alignment," *Marine Structures ELSEVIER*, 17 1 2019.
- [10] American Bureau of Shipping (ABS), Guide for Enhanced Shaft Alignment, 2022.
- [11] Tae-goo Lee, Gi-su Song, Ji-nam Kim, Jin-suk Lee and Hyoung-gil Park, Samsung Heavy Industries Co., Ltd., "Effect of Propeller Eccentric forces on the Bearing Loads of the Complicated shafting system for Large Container Ships," *Fifth International Symposium on Marine Propulsors*, 2017.
- [12] "DNV GL tackles shaft bearing challenges," 7 June 2018. [Online]. Available: <https://www.dnv.com/expert-story/maritime-impact/DNV-GL-tackles-shaft-bearing-challenges>.
- [13] Bjørn Johan Vartdal, Tormod Gjestland, Terje Ingvar Arvidsen, "Lateral Propeller Forces and their Effects on Shaft Bearings," *First International Symposium on Marine Propulsors smp'09 Trondheim, Norway, June 2009*, Det Norske Veritas (DNV), Oslo, Norway.
- [14] Quang Dao Vuong, Byongug Jeong, Jae-Ung Lee, Ji-Woong Lee, "Changes in Propeller Shaft Behavior by Fluctuating Propeller Forces during Ship Turning," *MDPI*, April 2022.



- [15] Mitsubishi Heavy Industries Ltd., "Reliability improvement of stern tube bearing considering propeller thrust forces during ship turning," Sep. 2007.
- [16] (Dr-Ing), Dipl-Ing, C. Gurr, Lloyd, Germanische, AG, & H., Rulfs, (Prof and Dr-Ing), "Influence of transient operating conditions on propeller shaft bearings," *Journal of Marine Engineering & Technology*, 2014.
- [17] L. Vassilopoulos, Associate, Member, Maritech, Inc, Belmont and Massachusetts, "The Influence of Propeller Mean Loads on Propulsion Shaft Alignment," *SNAME Propellers Symposium*, 1978.
- [18] "A guide to shaft alignment". *Engineers, Royal Belgian Institute of Marine*.
- [19] C. Andreaw and R. Ville, "Determination of hydrodynamic propeller forces and moments from measured deformations of line shafting," Bureau Veritas HYDRODYNAMICS TECHNICAL BULLETIN , 2006.
- [20] American Bureau of Shipping (ABS), Guidance notes on Propulsion Shafting Alignment, 2019.
- [21] Class NK Nippon Kaiji Kyokai, Guidelines on shafting alignment, 2006.
- [22] Brabon Engineering Services - Troubleshooting problems on rotating machinery, [Online]. Available: <https://brabon.org/propeller-shaft-alignment-bearing-load/>.
- [23] Yang-Gon Kim, Ue-Kan Kim, Jin-Suk Sun: "Study on shaft alignment of propulsion shafting system depending on single reaction force supporting position of aft stern tube bearing," *Journal of Marine Science and Technology* , 24 March 2021.
- [24] Det Norske Veritas (DNV), "Rules and Standards Explorer".
- [25] Y. Batrak, R. Batrak and D. Berin, "Computer application for shaft alignment design," *Intellectual Maritime Technologies Ukraine*, 2013.
- [26] Wärtsilä, "Engine Alignment Procedure & measurements at shipyard," 2010.
- [27] "Riviera," Investigating an uptick in shaft bearing failures, February 2019. [Online]. Available: <https://www.rivieramm.com/opinion/opinion/investigating-an-uptick-in-shaft-bearing-failures-21806>.
- [28] Dr Yuriy Batrak, "Lateral vibration prediction issues".
- [29] John Balaouras, Svend Leo Larsen, Gard, "Increase in stern tube damages - a concerning new trend?," 12 October 2023. [Online]. Available: <https://www.gard.no/web/articles?documentId=36102314>.
- [30] Royal Belgian Institute of Marine Engineers, "A guide to shaft alignment".
- [31] DNV, "Incomplete Propeller Immersion - Risk of propeller shaft bearing damage," *TECHNICAL AND REGULATORY NEWS*, 12 January 2017.

- [32] Rossopoulos Georgios Nikitas, "Tribological Study of the Stern Tube Bearing of Marine Vessels," *NTUA Diploma Thesis*, March 2018.
- [33] Total Shaft Solutions, "An Introduction to Bearing Failure," [www.osborne-engineering.com](http://www.osborne-engineering.com).
- [34] Ertuğrul Durak, Yasar Sevik, "Investigation of fretting wear in journal bearings," *Industrial Lubrication and Tribology*, 13 June 2016.
- [35] Rheinmetall, "Damage to engine bearing: Corrosion".
- [36] "Chief Engineer's Log," What you need to know about vessel propeller immersion and stern tube cooling, 2022. [Online]. Available: <https://chiefengineerlog.com/category/vessel-propulsion/propeller/>.
- [37] H. Jaengsoo, P. Jongyeul, P. Gyukpo, K. Jaehun, K. Jaeheon, S. Jeonghwa and R. Shin Hyung, "Propulsion Performance Analysis of a Partially Submerged Propeller," *SNAME Maritime Convention*, September 2023.
- [38] L. RAPTIS, "Software development for the solution of hydrodynamic lubrication problems in main bearings of marine Diesel engines," *Diploma Thesis*, March 2014.
- [39] D. Batrak, "How to estimate bearings displacements due to hull deflections," Intellectual Maritime Technologies, January 2020. [Online]. Available: <https://shaftsoftware.com/how-to-estimate-bearings-displacements/>.
- [40] Anastasios Dardamanis, "Development of model for the calculation of ship hull deflection, with application to the optimal alignment of propulsion shafting system," *NTUA Diploma Thesis*, July 2022.
- [41] C. Jallal, "Solving shaft line issues on tankers," Riviera, 2020.
- [42] H. O. Kristensen, "Prediction of Resistance and Propulsion Power of Ships," Technical University of Denmark, 2017.
- [43] Royal Belgian Institute of Marine Engineers, "Preventing shaft bearing damage".
- [44] Hongjun Yang · Yuxin Zhang · Liping Lu Shanghai Merchant Ship Design and Research Institute, "Numerical investigation of after stern tube bearing during ship turning maneuver," *Journal of Marine Science and Technology*, April 2019.

## Appendix A: Case study ship, resistance calculation for propeller partially immersion conditions

In order to estimate the needed thrust for those ballast conditions, a statistical method will be utilized. It is a variant of FORMDATA method, called Prediction of Resistance and Propulsion Power of Ships by Hans Otto Kristensen [42] which requires the following parameters

**Table 29: Input parameters for resistance calculation method**

Design values	L, B, T, Δ, V, S
Calculated values (using design values)	C <sub>B</sub> , C <sub>p</sub> , M, Fn, Rn
Environmental constants:	Water density, temperature, kinematic viscosity

Resistance values will be calculated for speed of 12 kn, for T<sub>M</sub>: 3.476 m, 4.8 m and 5.825 m. For those drafts the design values are:

**Table 30: Hydrostatic characteristics of vessel for examined drafts**

Parameters	V=12 kn = 6.1728 m/s			
T <sub>M</sub> Draught(m)	3.476	3.85	4.8	5.825
Displacement (m <sup>3</sup> )	15744	17614.6	22361.3	27480
Wetted surface (m <sup>2</sup> )	5630	5787.8	6175.5	6600
L <sub>wl</sub> (m)	182.61	182.63	180.63	179.95
C <sub>p</sub>	0.77	0.78	0.78	0.8
Rn	9.469E+08	9.470E+08	9.366E+08	9.33E+08
Fn	0.1449			
ρ <sub>sw</sub> (t/m <sup>3</sup> )	1.026			
t (°C)	15			
ν (m <sup>2</sup> /s)	1.1904E-06			

The total resistance coefficient, C<sub>T</sub>, of a ship can be defined by:

$$C_T = C_F + C_A + C_{AA} + C_R = \frac{R_T}{\frac{1}{2} \rho \cdot S \cdot V^2}$$

### Frictional Resistance Coefficient

The frictional resistance coefficient, C<sub>F</sub>, in accordance with the ITTC-57 formula is defined by:

$$C_F = \frac{0.075}{(\log Rn - 2)^2} = \frac{R_F}{0.5 \cdot \rho \cdot S \cdot V^2}$$

Where

$$Rn = \frac{V \cdot L_{wl}}{\nu}$$

ν: is the kinematic viscosity of water

### Incremental Resistance Coefficient

The frictional resistance coefficient is related to the surface roughness of the hull. The  $C_A$  value can be estimated as:

$$10^3 \cdot C_A = \max(-0.1; 0.5 \cdot \log(\Delta) - 0.1 \cdot (\log(\Delta))^2)$$

### Air Resistance Coefficient

Air resistance caused by the movement of the ship through the air for the displacement category the studied vessel belongs is:

$$C_{AA} \cdot 10^3 = 0.07$$

### Residual Resistance Coefficient

The residual resistance coefficient,  $C_R$ , is defined as the total resistance coefficient minus the friction resistance coefficient,

$$C_R = C_T - C_F$$

At this point it has to be mentioned that the followed method works for  $M \in [4.5, 7]$ . The  $M$  for draft = 3.476 m gives  $M=7.2$  and for this reason resistance value will be calculated for draft=3.85 m where  $M=7.0$  and will be corrected by the Admiralty coefficient **(A)**. **That coefficient** is a constant number, valid for a given ship and is useful when simple ship estimations are needed, given there are data available for one propulsion condition. The quantities used in the coefficient are: propulsion power **(P)**, ship speed **(V)** and displacement **(Δ)**. Thus, the Admiralty coefficient is defined as follows:

$$CAD = \frac{\Delta^{2/3} \cdot V^3}{P}$$

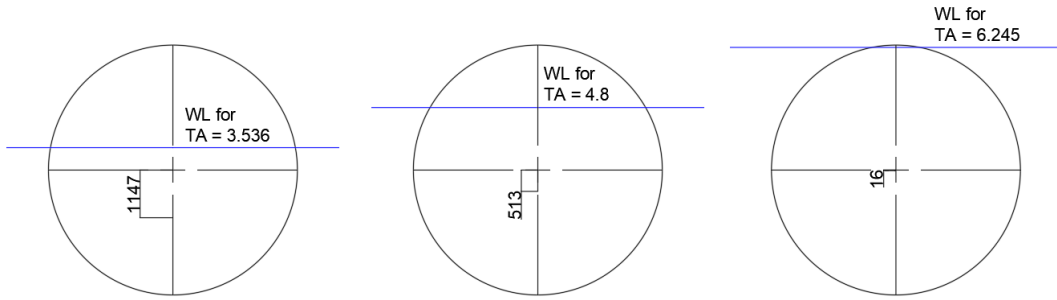
**Table 31: Resistance components and EHP force**

Draft (m)	3.85	4.8	5.825
M	7.0	6.41	5.96
$C_F$	1.541E-03	1.543E-03	1.544E-03
$C_A$	0.320E-03	0.282E-03	0.249E-03
$C_{AA}$	0.070E-03	0.070E-03	0.070E-03
$C_{R,uncorrected}$	0.423E-03	0.479E-03	0.557E-03
$C_{R,correction \text{ for } B/T \neq 2.5}$	0.0032E-03	0.0032E-03	0.0032E-03
$C_{R,correction \text{ for Bulb}}$	-0.3318E-03	-0.3318E-03	-0.3318E-03
$C_T$	2.025E-03	2.045E-03	2.091E-03
$R_T$ (kN)	222.8	231.4	269.8

Now using the CAD between drafts 3.536 and 3.85, the resistance for draft=3.536 is:

$$R_T = 206.8 \text{ kN}$$

Now remains to calculate the point of thrust application. As eccentricity will be defined the distance of propeller's submerged part centroid from the center of the cap. This simplification has been done since there were no available formulas in the bibliography to predict thrust eccentricity for a partially immersed propeller working behind the ship.



So the wanted values are:

**Table 32: Values for Mz calculation**

$T_M$ Draft (m)	Resistance force (kN)	Eccentricity (mm)
3.476	206.8	1147
4.8	231.4	513
5.825	269.8	16

## Appendix B: Tables of bearings loading ( $p/p_{max}$ ), without and with ISB actuation for each examined scenario

Equation of selected line for cases that take into account hull deflection has been appropriately expressed.

a) Designed ( $y=-5x+1.1$ )

Mz 211.7kN m	Without ISB actuation								With ISB actuation								Optimal position	
	ASTB	ISB	ME#8	ME#7	ME#6	ME#5	ME#4	ME#3	ASTB	ISB	ME#8	ME#7	ME#6	ME#5	ME#4	ME#3	x (m)	y (mm)
100%, R	0.666	-0.273	0.249	-0.014	0.324	0.301	0.372	0.109	0.613	0.113	0.007	0.179	0.322	0.301	0.372	0.110	0.238	-0.09
75%	0.574	-0.115	0.216	0.010	0.324	0.301	0.372	0.109	0.623	0.045	0.047	0.146	0.323	0.301	0.372	0.110	0.266	-0.230
50%	0.607	0.044	0.183	0.035	0.323	0.301	0.372	0.109	0.598	0.154	0.068	0.127	0.323	0.301	0.372	0.110	0.294	-0.370
25%	0.577	0.202	0.150	0.060	0.323	0.301	0.372	0.109	0.571	0.280	0.069	0.124	0.323	0.301	0.372	0.110	0.312	-0.460
0%	0.548	0.361	0.116	0.084	0.323	0.301	0.372	0.109	0.544	0.410	0.067	0.124	0.323	0.301	0.372	0.110	0.328	-0.540
-25%	0.518	0.519	0.083	0.109	0.323	0.301	0.372	0.109	0.517	0.535	0.068	0.121	0.323	0.301	0.372	0.110	0.346	-0.630
-50% (D.C.)	0.489	0.678	0.050	0.133	0.323	0.301	0.372	0.110	0.489	0.678	0.050	0.133	0.323	0.301	0.372	0.110	0.354	-0.670
-75%	0.459	0.839	0.017	0.158	0.323	0.301	0.372	0.110	0.466	0.769	0.085	0.102	0.323	0.301	0.372	0.110	0.390	-0.850
-100%	0.430	0.995	0.016	0.182	0.322	0.301	0.372	0.110	0.436	0.926	0.052	0.127	0.323	0.301	0.372	0.110	0.390	-0.850

b) Ballast  $T_M=3.476m$  ( $y=-5x+1.1$ )

Mz 237.1 kNm	Without ISB actuation								With ISB actuation								Optimal position	
	ASTB	ISB	ME#8	ME#7	ME#6	ME#5	ME#4	ME#3	ASTB	ISB	ME#8	ME#7	ME#6	ME#5	ME#4	ME#3	x (m)	y (mm)
100%	0.575	0.326	0.124	0.078	0.323	0.301	0.372	0.109	0.646	0.032	0.018	0.177	0.322	0.301	0.372	0.110	0.23	-0.05
75%	0.608	0.148	0.161	0.051	0.323	0.301	0.372	0.109	0.658	0.002	0.014	0.174	0.322	0.301	0.372	0.110	0.238	-0.09
50%	0.641	-0.017	0.198	0.023	0.323	0.301	0.372	0.109	0.631	0.101	0.060	0.134	0.323	0.301	0.372	0.110	0.282	-0.31
25%	0.674	-0.206	0.235	-0.004	0.324	0.301	0.372	0.109	0.602	0.229	0.077	0.119	0.323	0.301	0.372	0.110	0.31	-0.45
0%	0.707	-0.384	0.273	-0.032	0.324	0.324	0.301	0.372	0.571	0.377	0.071	0.122	0.323	0.301	0.372	0.110	0.326	-0.53

c) Ballast  $T_M=4.8m$  ( $y=-5x+1.1$ )

Mz 118.7 kNm	Without ISB actuation								With ISB actuation								Optimal position	
	ASTB	ISB	ME#8	ME#7	ME#6	ME#5	ME#4	ME#3	ASTB	ISB	ME#8	ME#7	ME#6	ME#5	ME#4	ME#3	x (m)	y (mm)
100%	0.563	0.342	0.121	0.081	0.323	0.301	0.372	0.109	0.618	0.125	0.049	0.143	0.323	0.301	0.372	0.110	0.278	-0.29
75%	0.579	0.253	0.139	0.067	0.323	0.301	0.372	0.109	0.604	0.174	0.073	0.123	0.323	0.301	0.372	0.110	0.3	-0.4
50%	0.596	0.165	0.158	0.054	0.323	0.301	0.371	0.109	0.588	0.256	0.062	0.131	0.323	0.301	0.372	0.110	0.304	-0.42
25%	0.612	0.076	0.176	0.040	0.323	0.301	0.372	0.109	0.574	0.320	0.070	0.123	0.323	0.301	0.372	0.110	0.318	-0.49
0%	0.629	-0.013	0.195	0.026	0.323	0.301	0.372	0.109	0.558	0.394	0.067	0.124	0.323	0.301	0.372	0.110	0.326	-0.53

e1) HD max Tim ( $y=-5x+4.101$ )

Mz 211.7kN m	Without ISB actuation								With ISB actuation								Optimal position	
	ASTB	ISB	ME#8	ME#7	ME#6	ME#5	ME#4	ME#3	ASTB	ISB	ME#8	ME#7	ME#6	ME#5	ME#4	ME#3	x (m)	y (mm)
100%	0.658	-0.258	0.343	-0.061	0.266	0.328	0.366	0.106	0.633	0.050	0.022	0.189	0.270	0.343	0.345	0.113	0.216	3.021
75%	0.628	-0.100	0.310	-0.036	0.265	0.328	0.366	0.106	0.610	0.129	0.074	0.145	0.270	0.343	0.345	0.113	0.242	2.891
50%	0.599	0.059	0.277	-0.011	0.265	0.328	0.366	0.106	0.583	0.249	0.084	0.135	0.270	0.343	0.345	0.113	0.262	2.791
25%	0.569	0.217	0.244	0.013	0.265	0.328	0.366	0.106	0.556	0.375	0.085	0.131	0.270	0.343	0.345	0.113	0.278	2.711
0%	0.540	0.375	0.211	0.038	0.265	0.328	0.366	0.106	0.529	0.506	0.082	0.132	0.270	0.343	0.345	0.113	0.292	2.641
-25%	0.510	0.534	0.178	0.062	0.265	0.328	0.366	0.106	0.502	0.631	0.083	0.129	0.270	0.343	0.345	0.113	0.308	2.561
-50%	0.481	0.692	0.144	0.087	0.265	0.328	0.366	0.106	0.476	0.753	0.089	0.122	0.270	0.343	0.345	0.113	0.326	2.471
-75%	0.452	0.850	0.111	0.111	0.264	0.328	0.365	0.106	0.453	0.831	0.137	0.081	0.270	0.343	0.345	0.113	0.358	2.311
-100%	0.422	1.009	0.078	0.136	0.264	0.328	0.365	0.106	0.423	0.997	0.095	0.113	0.270	0.343	0.345	0.113	0.36	2.301

f1) HD min Tim ( $y=-5x-0.182$ )

Mz	Without ISB actuation									With ISB actuation									Optimal position	
	ASTB	ISB	ME#8	ME#7	ME#6	ME#5	ME#4	ME#3	ASTB	ISB	ME#8	ME#7	ME#6	ME#5	ME#4	ME#3	x (m)	y(mm)		
211.7kN m																				
100% R	0.661	-0.200	0.166	0.018	0.376	0.266	0.399	0.099	0.639	0.001	0.007	0.145	0.375	0.266	0.399	0.099	0.27	-1.532		
75%	0.632	-0.041	0.122	0.042	0.376	0.266	0.399	0.099	0.622	0.080	0.003	0.145	0.378	0.267	0.396	0.100	0.284	-1.602		
50%	0.602	0.117	0.099	0.067	0.376	0.266	0.399	0.102	0.599	0.158	0.056	0.100	0.378	0.267	0.396	0.100	0.332	-1.842		
25%	0.573	0.275	0.066	0.091	0.376	0.266	0.399	0.099	0.571	0.296	0.044	0.108	0.378	0.267	0.396	0.100	0.344	-1.902		
0%	0.544	0.434	0.033	0.116	0.375	0.266	0.399	0.099	0.545	0.416	0.050	0.101	0.378	0.267	0.396	0.100	0.366	-2.012		
-25%	0.514	0.592	0.000	0.140	0.375	0.266	0.399	0.099	0.518	0.546	0.045	0.102	0.378	0.267	0.396	0.100	0.382	-2.092		
-50%	0.484	0.750	-0.033	0.165	0.375	0.266	0.399	0.099	0.492	0.673	0.044	0.101	0.378	0.267	0.396	0.100	0.4	-2.182		
-75%	0.455	0.909	-0.066	0.190	0.375	0.266	0.399	0.099	0.465	0.805	0.035	0.105	0.378	0.267	0.396	0.100	0.414	-2.252		
-100%	0.426	1.067	-0.100	0.214	0.375	0.266	0.399	0.099	0.439	0.927	0.038	0.101	0.378	0.267	0.396	0.100	0.434	-2.352		

e2) HD max E-B ( $y=-5x+1.866$ )

Mz	Without ISB actuation									With ISB actuation									Optimal position	
	ASTB	ISB	ME#8	ME#7	ME#6	ME#5	ME#4	ME#3	ASTB	ISB	ME#8	ME#7	ME#6	ME#5	ME#4	ME#3	x (m)	y(mm)		
211.7kN m																				
100%	0.664	-0.258	0.239	0.014	0.296	0.313	0.371	0.106	0.606	0.135	0.021	0.187	0.295	0.314	0.371	0.106	0.250	0.616		
75%	0.634	-0.100	0.206	0.038	0.296	0.313	0.371	0.106	0.619	0.090	0.003	0.208	0.267	0.366	0.323	0.123	0.254	0.596		
50%	0.604	0.059	0.173	0.063	0.295	0.314	0.371	0.106	0.598	0.145	0.080	0.144	0.267	0.366	0.323	0.123	0.31	0.336		
25%	0.575	0.217	0.139	0.087	0.295	0.314	0.371	0.106	0.571	0.266	0.086	0.137	0.267	0.366	0.323	0.123	0.33	0.236		
0%	0.546	0.375	0.106	0.112	0.295	0.314	0.371	0.106	0.544	0.394	0.085	0.136	0.267	0.366	0.323	0.123	0.346	0.156		
-25%	0.516	0.534	0.073	0.136	0.295	0.314	0.371	0.106	0.517	0.522	0.083	0.135	0.267	0.366	0.323	0.123	0.362	0.076		
-50%	0.487	0.692	0.040	0.161	0.295	0.314	0.371	0.106	0.491	0.649	0.081	0.134	0.267	0.366	0.323	0.123	0.378	-0.004		
-75%	0.457	0.850	0.004	0.186	0.295	0.314	0.371	0.106	0.465	0.768	0.088	0.127	0.267	0.366	0.323	0.123	0.398	-0.104		
-100%	0.428	1.008	0.026	0.210	0.295	0.314	0.371	0.106	0.436	0.922	0.058	0.149	0.267	0.366	0.323	0.123	0.4	-0.114		

f2) HD min E-B ( $y=-5x+0.607$ )

Mz	Without ISB actuation									With ISB actuation									Optimal position	
	ASTB	ISB	ME#8	ME#7	ME#6	ME#5	ME#4	ME#3	ASTB	ISB	ME#8	ME#7	ME#6	ME#5	ME#4	ME#3	x (m)	y(mm)		
211.7 kNm																				
100%	0.666	-0.274	0.257	-0.038	0.350	0.283	0.378	0.110	0.625	0.037	0.055	0.124	0.349	0.284	0.378	0.110	0.25	-0.643		
75%	0.637	-0.116	0.224	-0.013	0.350	0.283	0.378	0.110	0.622	0.067	0.004	0.189	0.327	0.279	0.385	0.108	0.256	-0.673		
50%	0.607	0.042	0.191	0.011	0.349	0.283	0.378	0.110	0.600	0.131	0.072	0.133	0.328	0.279	0.385	0.108	0.31	-0.943		
25%	0.578	0.200	0.158	0.036	0.349	0.283	0.378	0.110	0.573	0.258	0.072	0.130	0.328	0.279	0.385	0.108	0.328	-1.033		
0%	0.548	0.359	0.125	0.060	0.349	0.283	0.378	0.110	0.547	0.380	0.077	0.125	0.328	0.279	0.385	0.108	0.348	-1.133		
-25%	0.519	0.517	0.091	0.085	0.349	0.284	0.378	0.110	0.520	0.509	0.073	0.125	0.328	0.279	0.385	0.108	0.364	-1.213		
-50%	0.490	0.675	0.058	0.107	0.349	0.284	0.378	0.110	0.493	0.634	0.074	0.122	0.328	0.279	0.385	0.108	0.382	-1.303		
-75%	0.460	0.834	0.025	0.134	0.349	0.284	0.378	0.110	0.466	0.767	0.066	0.126	0.328	0.279	0.385	0.108	0.396	-1.373		
-100%	0.430	0.992	-0.008	0.159	0.349	0.284	0.378	0.110	0.440	0.898	0.059	0.130	0.328	0.279	0.385	0.108	0.41	-1.443		